INTERNAL MOTIONS IN BIOMOLECULES STUDIED BY NMR SPECTROSCOPY: AN APPLICATION TO MAJOR URINARY PROTEIN-I AND ITS COMPLEX WITH 2-METHOXY-3-ISOBUTYLPYRAZINE

THÈSE N^{O} 3489 (2006)

PRÉSENTÉE LE 17 MARS 2006

À LA FACULTÉ SCIENCES DE BASE

Laboratoire de résonnance magnétique biomoléculaire

SECTION DE CHIMIE ET GÉNIE CHIMIQUE

ÉCOLE POLYTECHNIQUE FÉDÉRALE DE LAUSANNE

POUR L'OBTENTION DU GRADE DE DOCTEUR ÈS SCIENCES

PAR

Chiara PERAZZOLO

Laurea in chimica, Università degli studi di Padova, Italie
et de nationalité italienne

acceptée sur proposition du jury:

Prof. M. Mutter, président du jury
Prof. G. Bodenhausen, directeur de thèse
Prof. S. Homans, rapporteur
Prof. A. Merbach, rapporteur
Prof. V. Sklenar, rapporteur

ÉCOLE POLYTECHNIQUE
FÉDÉRALE DE LAUSANNE

Lausanne, EPFL
2006

Thesis advisor

Prof. Geoffrey Bodenhausen

Author

Chiara Perazzolo

Internal Motions in Biomolecules Studied by NMR Spectroscopy: an Application to Major Urinary Protein I and its Complex with 2-Methoxy-3-Isobutylpyrazine

Abstract

Since many biological processes occur on the μs to ms time scale, internal dynamics on that time scale is believed to be related to biological functionality. The characterization of internal dynamics is thus an important issue to improve our understanding of the biological activity of macromolecules, such as proteins, RNA and DNA fragments. Solution NMR spectroscopy, in particular relaxation measurements, is well suited for the determination of exchange rates on that slow time scale.

The formation of a small pheromone-protein complex is associated with some kind of internal rearrangements, necessary to accomodate the ligand. In this work, we are interested in the changes in internal dynamic upon the binding of a model odorant molecule, the 2-methoxy-3-isobutylpyrazine, to Major Urinary Protein I, MUP I. The study of the internal dynamics of both apo- and holo-MUP I has been carried out with the goal of monitoring the differences between the two states of the protein. In fact, impressive changes in chemical shifts are present between the two forms, indicating that some internal rearrangements have taken place.

New and more classical experiments have been applied to MUP I in order to gain

insight into the different types of motions that occurs at different time scales. The presence of chemical exchange has been identified in apo-MUP I using the classical Carr-Purcell-Meiboom-Gill experiment on single quantum ^{15}N magnetisation. Surprisly, in holo-MUP I no presence of chemical exchange has been found, so in which time scale are the dynamics which leads to the release of the ligand in the environnment? Slow motions (ms-μs) in both apo- and holo-MUP I have been found using a new experiment, which highlight the presence of correlated motions in the backbone of proteins.

Key words: *Chemical exchange, Chemical shift anisotropy (CSA), Chemical shift modulation (CSM), Correlation time (τ_c), Dipole-dipole (DD), Dynamics (slow/fast), Isothermal Titration Calorimetry (ITC), Relaxation, Relaxation dispersion.*

Sommario

Dato che molti processi biologici avvengono nell'intervallo che va dai micro ai millisecondi, si presuppone che la dinamica interna, in questo intervallo di tempi, sia legata alle funzioni biologiche. La caratterizzazione della dinamica interna diventa così di fondamentale importanza per la comprensione delle attività biologiche delle macromolecule, quali proteine, RNA e frammenti di DNA. La risonanza magnetica nucleare, NMR, ed in particolare la misura del rilassamento degli spin, ben si presta per la determinazione delle velocità dei moti presenti in questa scala di tempi.

In particolare, la formazione di complessi tra una proteina e un feromone é associata a riarrangiamenti interni, necessari per il posizionamento del ligante. In questo lavoro, siamo interessati ai cambiamenti di dinamica interna a seguito della formazione del complesso tra la Proteina Urinaria Maggiore I, MUP I, e la 2-metossi-3-isobutilpirazina. Lo studio della mobilità interna della MUP I nelle sue forme con e senza legante, holo e apo, é stato condotto allo scopo di individuare eventuali differenze tra le due forme. Le prime significative differenze sono state rilevate nella misura dei chemical shifts, differenze che fanno presupporre una modifica della struttura interna.

Nuovi e più classici esperimenti sono stati utilizzati per ottenere informazioni sui tipi di movimenti che avvengono in diverse scale di tempi. La presenza dello scambio chimico é stata individuata nella apo-MUP I usando l'esperimento di Carr-Purcell-Meiboom-Gill sulla magnetizzazione a singolo quanto dell'azoto, considerato un classico. Sorprendentemente, nella holo-MUP I non é stata trovata traccia dello scambio chimico, in quali scale di tempi si collocano i moti che permettono la liberazione del

legante nell'ambiente? Movimenti lenti (μs-ms), che influenzano sia il chemical shit dell'azoto e del carbonio carbonilico nello scheletro della proteina in modo correlato o anticorrelato, sono stati evidenziati attraverso l'uso di un nuovo esperimento nelle due forme della proteina.

Key words: *Chemical exchange, Chemical shift anisotropy (CSA), Chemical shift modulation (CSM), Correlation time (τ_c), Dipole-dipole (DD), Dynamics (slow/fast), Isothermal Titration Calorimetry (ITC), Relaxation, Relaxation dispersion.*

Acknowledgments

I'd like to thank professor Geoffrey Bodenhausen for giving me the possibility to start this work, for his confidence during these three years and for the interest he has always shown in my work.

I thank professor Steve W. Homans, professor André Merbach, professor Manfred Mutter and professor Vladimír Sklenář for having taken the time to read the manuscript.

J'aimerais remercier Julien Wist qui a fortement contribué à ma connaissance de la Résonance Magnétique Nucléaire et au septième chapitre de ce travail. Je ne le remercierai jamais assez de m'avoir forcé à apprendre le français !

Other thanks go to Liliya, Luisa and Mariachiara who contributed to different parts of this work.

I'd like to thank Jens Dittmer for the stimulating discussion and for the infinite summer mountain trips and winter snowboarding sections he was always ready to organise.

I thank the members of the Lausanne group, in order of appearance: Dominique Frueh, Joel Tolman, Audrey Petit, Dimitri Bytchenkoff, Julien Wist, Jens Dittmer, Liliya Vugmeyster, Sapna Ravindranathan, Karthik Gopalakrishnan, Erik Persson, Karthick Babu Saisankar Gupta, Saša Antonijević, Adonis Lupulescu, Mariachiara Verde, Nicolas Aeby, Simone Cavadini, Riddhiman Sarkar and Paul Vasos who all gave their personal touch to the nice atmosphere of the lab. Again, a special thanks to Christine, Paul, Julien, Mariachiara and Adonis for reading this manuscript.

Je remercie tout particulièrement Martial Rey qui inlassablement répare, met à jour, nous explique et nous répète, toujours et encore, tout ce que nous ignorons des ma-

chines avec lesquelles nous travaillons.

Un grazie a Mariachiara per la pazienza dimostrata nell'avermi come capo e per aver contribuito al mio buonumore. Vorrei ringraziare Christine per le numerose serate passate assieme e per avermi fatto pattinare per la prima volta in vita su un lago ghiacciato. Un ringraziamento speciale ad Anna che mi é stata vicina da sempre e che ha ascoltato pazientemente tutti i miei sfoghi.

Et finalement, j'aimerai remercier toutes les personnes que j'ai rencontrées dans le monde du tango argentin à Lausanne et en particulier à l'association *Tangofolie*, qui m'ont permis de passer des très belles soirées et ont ainsi contribué à mon bonheur.

A Jean-Marc, ad Anna e alla mia famiglia.

Contents

Chapter 1

Relaxation Theory: a Phenomenological Introduction

1.1 Basic Concepts about Relaxation

In this section an elementary introduction to relaxation will be presented. Although the definition is quite simple: "relaxation is the sum of phenomena that restores the equilibrium in a perturbed system", the NMR theory that describes it is very complex. Due to the fundamental role of relaxation in the investigation of protein dynamics, it is of crucial importance to understand, by a phenomenological description, the concepts of relaxation before analyzing it in mathematical detail.

1.1.1 Relaxation to Termal Equilibrium and Longitudinal Relaxation

In the absence of a magnetic field, the spin polarizations are uniformly distributed over all the space available; the net magnetization is zero, because the spin magnetic moments average to zero. In contrast, in presence of an external magnetic field all spins will start precessing around it. Immediately after the introduction of a spin system into a magnetic field, the net magnetization is still zero because all spins start to precess from their position at time zero, i.e. an isotropic distribution of polarizations results in a vanishing net polarization. However, each spin generates itself a small magnetic field, which will fluctuate rapidly due to thermal motions of the environment: the field experienced by each spin is the sum of the external static field and of all the tiny random fields generated by neighbouring spins. The total magnetic field felt by each spin is slightly fluctuating in time, both in amplitude and in direction: the spins will change precession angle and over a long time experience all possible orientations. As a consequence, the isotropy of the initial condition is broken and a net magnetization is built up. After a long time, the system will reach a *stable anisotropic* distribution of nuclear spins polarization; the so called *thermal equilibrium*.[1]

More generally, the energy of the spin orientations, in the presence of an external field $\mathbf{B}$, depends on the strength and orientation of both $\mathbf{B}$ and the magnetic moment of

[1] We shall remember that the equilibrium is stable but dynamic, since the same number of spins will fluctuate from the parallel to the anti-parallel orientation at each moment.

the nuclei, $\boldsymbol{\mu}$:

$$E = -\boldsymbol{\mu} \cdot \mathbf{B} \tag{1.1.1}$$

Under normal conditions, $\mathbf{B}$ is parallel to the z axis so that eq. 1.1.1 can be rewritten as:

$$E = -\gamma I_z B_0 = -m_I \hbar \gamma_I B_0 \tag{1.1.2}$$

in which B_0 is the static magnetic field and I_z the z component of the nuclear spin angular momentum, $\mathbf{I}$, γ the gyromagnetic ratio and $\hbar$ Plank's constant divided by 2π. The latter results in $\mathrm{m}_I = 2\mathbf{I}+1$ equally spaced energy levels, the Zeeman levels. For a spin with a magnetic number $1/2$, there are only two levels with energies $-\frac{1}{2}\gamma B_0$ and $\frac{1}{2}\gamma B_0$, called α and β states respectively.[2] The difference in populations between the two states is given by the Boltzmann equation:

$$\frac{N_\beta}{N_\alpha} = exp(\frac{-\Delta E}{k_B T}) = exp(-\frac{\hbar \gamma B_0}{k_B T}) \tag{1.1.3}$$

where N_i is the population of state i and k_B is the Boltzmann constant. To understand how the anisotropic field fluctuations influence the populations of state α and β, we can explore the rate of transition between them. In other words, we are interested in

[2]Note that α is the lower energy state only for nuclei with positive γ. In the present text γ is considered positive, if not specified.

the relaxation rate of population N_β, which is given by:

$$\frac{dN_\beta}{dt} = -N_\beta W_{\beta,\alpha} + N_\alpha W_{\alpha,\beta} \tag{1.1.4}$$

$W_{\beta,\alpha}$ is the probability of transition between the states β and α. Defining $N = N_\alpha + N_\beta$ and $n = N_\alpha - N_\beta$, we can rewrite eq. 1.1.4 as follow:

$$\frac{dn}{dt} = -n(W_{\alpha,\beta} + W_{\beta,\alpha}) + N(W_{\beta,\alpha} - W_{\alpha,\beta}) \tag{1.1.5}$$

At equilibrium $dn/dt = 0$, thus we can define $n_{eq} = N\frac{W_{\beta,\alpha} - W_{\alpha,\beta}}{W_{\alpha,\beta} + W_{\beta,\alpha}}$. The latter permits the substitution of N into eq. 1.1.5 to give:

$$\frac{dn}{dt} = -(n - n_{eq})(W_{\alpha,\beta} + W_{\beta,\alpha}) \tag{1.1.6}$$

The solution of the previous equation is:

$$n(t) - n_{eq} = -(n_0 - n_{eq}) exp\{(W_{\alpha,\beta} + W_{\beta,\alpha})t\} \tag{1.1.7}$$

where n_0 is equal to the difference in populations at time t=0. If we consider the introduction of an NMR tube into the spectrometer then n_0=0. The sum ($W_{\alpha\beta}$ + $W_{\beta,\alpha}$) is called the *spin-lattice relaxation rate* and represents the rate at which the populations α and β reach equilibrium.

1.1.2 Transverse Relaxation

A phenomenological explanation can be used to understand *transverse relaxation*. We shall consider a perturbation that rotates the equilibrium magnetization from the z axis to the -y axis; the net magnetization in the xy plane, or more precisely perpendicular to B_0, is called *transverse magnetization*. From a microscopic point of view, the spins, initially precessing around the +z axis, are now equally distributed around the -y axis, while the spins previously precessing around the -z axis have an analog distribution along the +y axis, with zero net magnetization along both z and x axes. Once the perturbation is removed, the spins resume their precession around the z axis. As a result, the macroscopic magnetization will rotate too. During the precession, the spins will lose their coherence due to the tiny random fields generated by neighbour spins, the same process as seen before. The loss of synchrony (fanning out) is responsible for the irreversible loss of magnetization in the plane. The rate at which this dephasing occurs is called *transverse relaxation*. In this picture, no direct spin-spin interactions have been considered, in contrast with the idea that only the latter are responsible for transverse relaxation. Of course, spin-spin interactions enhance the spin dephasing rate but it is important to state that transverse relaxation takes place every time the effective field is, even slightly, time dependent. The time dependence of the effective magnetic field is increased by the spin-spin interactions. This process occurs between two neighbouring spins with identical precession frequencies but with different magnetic quantum states and consists in the possibility for the two nuclei to exchange quantum states. At the same time, one spin flips from the excited to the ground state and a second absorbs the energy to make the opposite transition. There

is no net change in the populations of the energy states, but the average lifetime of a nucleus in the excited state will decrease.

1.1.3 Influence of Molecular Motions on Relaxation

As seen previously, relaxation is caused by fluctuations of the magnetic field experienced by each spin. These fluctuations arise from molecular motions. Each spin in a molecule generates a local magnetic field, $\mathbf{B}_{loc}$, which depends on its orientation with respect to the external magnetic field. As the molecule tumbles, the magnitude and the direction of the magnetic field felt by the spin changes, thus inducing a slightly different local magnetic field. Molecular motions cause the time-varying local field, $\mathbf{B}_{loc}$(t). The amplitude of the latter is directly related to the efficiency of relaxation. In figure 1.1.1 A and C, two examples of random fluctuations of $\mathbf{B}_{loc}$(t) along one axis are shown. The field exerted by one spin is equal to:

$$\mathbf{B}(t) = B_0 \cdot \widehat{n}_z + \mathbf{B}_{loc}(t) = B_0 \cdot \widehat{n}_z + B_{loc}(t) \cdot \widehat{n}_z + B_{loc}(t) \cdot \widehat{n}_x + B_{loc}(t) \cdot \widehat{n}_y \quad (1.1.8)$$

where $B_{loc}(t) \cdot \widehat{n}_z$ is the fluctuating longitudinal field, while $\mathrm{B}_{loc}(t) \cdot \widehat{n}_{xy}$ are the fluctuating components of the transverse fields. The longitudinal component of $\mathbf{B}_{loc}$(t) introduces a variation in the Larmor frequency ω_0, stimulating the dephasing of coherences to zero. Instead, in $B_{loc}(t) \cdot \widehat{n}_{xy}$ both frequency components close to ω_0 stimulate the equilibration of the system with the surrounding, thus being responsible for lifetime broadening of the coherences.

For an isotropic molecule, there are no preferred orientations in solution; this property plus the random nature of local fields allow one to assume that the average over time of $\mathbf{B}_{loc}$(t) is zero, $\overline{\mathbf{B}_{loc}(t)} = 0$.[3] One needs to characterize both the magnitude and the frequency at which the field $\mathbf{B}_{loc}$(t) fluctuates. Since its mean value is zero, one defines the magnitude by its mean square value, $\overline{\mathbf{B}^2_{loc}(t)}$, that is, of course, non zero. How rapidly the field fluctuates is given by the *time correlation function*, C(t), which is defined as:[4]

$$C(\tau) = \overline{\mathbf{B}_{loc}(t)\mathbf{B}_{loc}(t-\tau)} \tag{1.1.9}$$

where τ is the time interval between two successive $\mathbf{B}_{loc}$ values. For a given fluctuating field, the probability that $\mathbf{B}_{loc}$(t) has a value close to $\mathbf{B}_{loc}$(t-τ) is high if τ is smaller than the timescale of the fluctuations, and low if τ is longer than this timescale. As a consequence, the function C(τ) decreases to zero when τ increases.

Using the same intervals in τ, it is possible to compare two fields fluctuating with different velocities. The correlation function of a rapidly fluctuating field decays much faster in comparison to the correlation function that characterizes a slowly fluctuating field (see figure 1.1.1). One can try to characterize the correlation function: by definition $C(0) = \overline{\mathbf{B}^2_{loc}(t)}$ and for isotropic molecules $C(\infty) = \overline{\mathbf{B}_{loc}(t)}^2 = 0$. Moreover, one assumes a simple exponential decay for $C(\tau)$:

$$C(\tau) = \overline{\mathbf{B}^2_{loc}} exp\left\{-\tau/\tau_c\right\} \tag{1.1.10}$$

[3]The overbar means average over long times for a single spin or average at one time instead of over an ensemble of spins: the two averages are assumed to be identical.

[4]For a mathematical description of correlation functions, see eq. 2.1.15.

where the constant τ_c is the *correlation time*; small values of τ_c are associated with fast fluctuations and vice versa. The exact form of τ_c and its temperature dependence is given in chapter 7, see eq. 7.3.10.

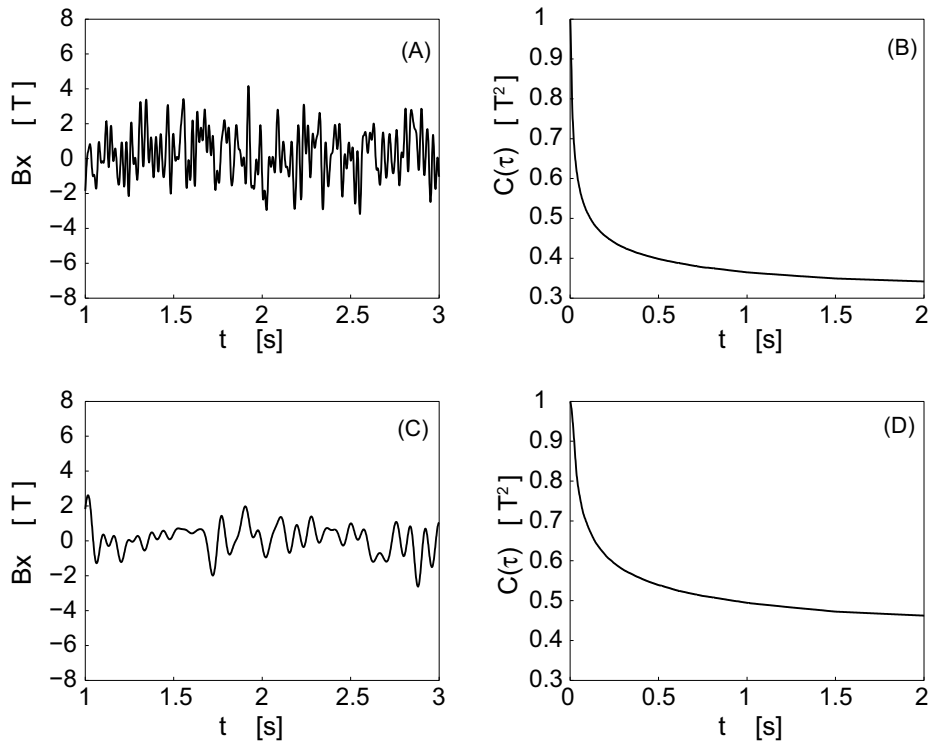

Figure 1.1.1: (A), (C), fast and slow fluctuations of the $\mathbf{B}_{loc} \cdot \widehat{n}_x$ at one spin, (B) and (D) relative time correlated functions. Note that fast fluctuating field results in a faster decaying correlated function: (A) and (B) with respect to (C) and (D).

Chapter 2

Relaxation Theory: Brief Introduction

In this chapter, I would like to give a brief introduction of the relaxation theory. The aim of the chapter is the derivation of the master equation for a spin system and the relationship between the spin system and the observables. Furthermore, the mechanisms which cause relaxation will be introduced.

2.1 The Master Equation of Relaxation

Nuclear Magnetic Resonance has been described for the fisrt time by F. Bloch and E. M. Purcell in 1946, (Bloch, 1946; Purcell et al., 1946). As soon as the studies on NMR continued, relaxation and the mechanisms behind it assumed a fundamental importance. Bloembergen is the first to formulate a relaxation theory (Bloembergen et al., 1948), followed by the work of many others, among these we shall remember Solomon, Abragam, Redfield and Wangsness. A macroscopic semiclassical theory of spin relaxation was formulated by Bloch, Redfield, and Wangsness, (Wangsness and Bloch,

1953; Redfield, 1965). In this representation, the Hamiltonian of a spin system can be written in the form:

$$\mathscr{H}(t) = \mathscr{H}_0 + \mathscr{H}_1(t) \tag{2.1.1}$$

Where $\mathscr{H}_0$ is the main time-independent Hamiltonian and $\mathscr{H}_1(t)$ is the Hamiltonian describing the random modulations that cause relaxation, with $\overline{\mathscr{H}_1(t)} = 0$.[1] The density matrix, σ, represents the ensemble-averaged state of the spin system. The system time evolution can be evaluated using the equation of motion of the density matrix:

$$\frac{d\sigma(t)}{dt} = -i\left[\mathscr{H}(t), \sigma(t)\right] \tag{2.1.2}$$

It is convenient to consider the system in the *interaction representation*, i.e. a representation where the time independent part of the Hamiltonian is removed. This frame change is equivalent to going from the laboratory to the rotating frame in the classical picture. In the new representation, any operator Q is written as:

$$\tilde{Q} = e^{-i\mathscr{H}_0 t} Q e^{i\mathscr{H}_0 t} = U^{-1} Q U \tag{2.1.3}$$

Thus using the property $e^{-A}\left[B, C\right]e^{A} = \left[e^{-A}Be^{A}, e^{-A}Ce^{A}\right]$, eq. 2.1.2 becomes:

$$\frac{d\tilde{\sigma}(t)}{dt} = -i\left[\tilde{\mathscr{H}}_1(t), \tilde{\sigma}(t)\right] \tag{2.1.4}$$

[1] The Hamiltonians used in this text are written in units of the Plank constant $\hbar$.

Analytically, it is impossible to solve eq. 2.1.4; an approximated solution is possible by expansion of $\tilde{\sigma}(t)$ up to the second order and by successive integration:

$$\tilde{\sigma}(t) = \tilde{\sigma}(0) - i\int_0^t \left[\tilde{\mathscr{H}}_1(t'), \tilde{\sigma}(0)\right] dt' - \int_0^t \int_0^{t'} \left[\tilde{\mathscr{H}}_1(t'), \left[\tilde{\mathscr{H}}_1(t''), \tilde{\sigma}(0)\right]\right] dt'' \, dt' \quad (2.1.5)$$

Whence, taking the time derivative and introducing a new variable $\tau = t - t'$ one obtains:

$$\frac{d\tilde{\sigma}}{dt} = -i\left[\tilde{\mathscr{H}}_1(t), \tilde{\sigma}(0)\right] - \int_0^t \left[\tilde{\mathscr{H}}_1(t), \left[\tilde{\mathscr{H}}_1(t'), \tilde{\sigma}(0)\right]\right] dt' \quad (2.1.6)$$

$$\frac{d\tilde{\sigma}}{dt} = -i\left[\tilde{\mathscr{H}}_1(t), \tilde{\sigma}(0)\right] - \int_0^t \left[\tilde{\mathscr{H}}_1(t), \left[\tilde{\mathscr{H}}_1(t-\tau), \tilde{\sigma}(0)\right]\right] d\tau \quad (2.1.7)$$

The perturbations described by $\mathscr{H}_1(t)$ are fluctuating randomly, so for each member of the ensemble of spins S, $\mathscr{H}_1(t)$ has a different value. We are interested in the observable statistical behaviour, that is given by the ensemble average,[2] i.e. by taking the average on both sides of the last equation:

$$\frac{d}{dt}\overline{\tilde{\sigma}(t)} = -i\overline{\left[\tilde{\mathscr{H}}_1(t), \tilde{\sigma}(0)\right]} - \int_0^t \overline{\left[\tilde{\mathscr{H}}_1(t), \left[\tilde{\mathscr{H}}_1(t-\tau), \tilde{\sigma}(0)\right]\right]} \, d\tau \quad (2.1.8)$$

We will further assume that the correlation between $\mathscr{H}_1(t)$ and $\tilde{\sigma}(0)$ can safely be neglected; consequently the two operators can be averaged separately. Due to the random fluctuating nature of $\mathscr{H}_1(t)$, its mean value is zero, so the first term in the

[2] The average can also be obtained by time averaging one single member of the ensemble.

last equation can be dropped. Moreover, if one assumes the evolution of the density operator $\tilde{\sigma}(t)$ due to $\mathscr{H}_1(t)$ to be slow, it is possible to replace $\tilde{\sigma}(0)$ by $\tilde{\sigma}(t)$, and the upper limit of the integral in eq. 2.1.8 by $+\infty$ (Redfield, 1965). Eq. 2.1.8 thus becomes:

$$\frac{d}{dt}\overline{\tilde{\sigma}(t)} = -\int_0^{\infty} \overline{\left[\tilde{\mathscr{H}}_1(t), \left[\tilde{\mathscr{H}}_1(t-\tau), \tilde{\sigma}(t)\right]\right]}\, d\tau \tag{2.1.9}$$

The range of validity of the previous assumption has been discussed elsewhere (Abragam, 1961; Goldman, 1998). To further proceed, one separates the Hamiltonian in two terms: random functions of spatial variables $F_k^q(t)$, and tensor spin operators A_k^q.[3]

$$\mathscr{H}_1(t) = \sum_{q=-k}^{k} A_k^q F_k^{-q}(t) \tag{2.1.10}$$

The random functions $F_k^q(t)$ are assumed to be statistically stationary, as consequence the mean of $F_k^q(t)$ is time independent. Additionally, $A_k^{-q} \equiv A_k^{q\dagger}$ and $F_k^{-q}(t) \equiv F_k^{q*}(t)$ where the dagger and asterisk denote Hermitian and complex conjugates respectively. To proceed further the tensor operators A_k^q are expanded as sum of basis operators:

$$A_k^q = \sum_p A_{kp}^q = \sum_p c_p^q \mathscr{H}_p \tag{2.1.11}$$

With a basis satisfying the relationship:

$$\left[A_{kp}^q, \mathscr{H}_0\right] = \omega_p^q A_{kp}^q \tag{2.1.12}$$

[3]Where q stands for the order and k for the rank, the full expressions for both irreducible tensor operators and spherical harmonics are given in table 9.1.

where A^q_{kp} and ω^q_p are the eigenfunctions and eigenfrequencies of the Hamiltonian operators.

The spin operators in the interaction representation become:

$$\begin{aligned} \tilde{A}^q_{kp} &= e^{i\mathscr{H}_0 t} A^q_{kp} e^{-i\mathscr{H}_0 t} = \sum_{q,p} e^{i\omega^q_p t} A^q_{kp} \\ \tilde{A}^{q\dagger}_{kp} &= e^{i\mathscr{H}_0 t} A^{q\dagger}_{kp} e^{-i\mathscr{H}_0 t} = \sum_{p,q} e^{-i\omega^q_p t} A^{q\dagger}_{kp} \end{aligned} \tag{2.1.13}$$

where the second equation refers to the Hermitian conjugate, and the property $\omega^{-q}_p = -\omega^q_p$ has been used. We can now rewrite eq. 2.1.9, including a change in variable, $\overline{\sigma(t)} = \sigma(t)$ (or $\tilde{\sigma}(t) = \overline{\tilde{\sigma}(t)}$):

$$\frac{d}{dt}\tilde{\sigma}(t) = -\sum_{p,q} \int_0^\infty \left[\tilde{A}^{-q}_{k,p}, \left[\tilde{A}^q_{k,p}, \tilde{\sigma}(t)\right]\right] \overline{F^{-q}_k(t) F^q_k(t-\tau)} exp\left\{-i\omega^q_p \tau\right\} d\tau \tag{2.1.14}$$

The correlation function is defined as:

$$C(\tau) = \overline{F^{-q}_k(t) F^q_k(t-\tau)} \tag{2.1.15}$$

The correlation function C is such that $C(\infty) = 0$ and $C(\tau) = C(-\tau)$, and describes the probability of finding the molecule at time t in the same orientation as at time $t - \tau$, see also section 2.1.2. For isotropic tumbling the function is assumed to decay mono-exponentially with a time constant τ_c.

The spectral densities $j^q(\omega^q_p)$ are defined as the Fourier transforms of the correlation functions:

$$j^q(\omega_p^q) = \int_0^\infty C(\tau)\, exp\left\{-i\omega_p^q\tau\right\}\, d\tau = \frac{1}{2}\left[J^q(\omega_p^q) - ik^q(\omega_p^q)\right] \tag{2.1.16}$$

$$J^q(\omega_p^q) = \int_0^\infty C(\tau)\, cos(\omega_p^q\tau)\, d\tau \tag{2.1.17}$$

$$k^q(\omega_p^q) = \int_0^\infty C(\tau)\, sin(\omega_p^q\tau)\, d\tau \tag{2.1.18}$$

The term $k^q(\omega_p^q)$ results in a very small second order shift and can thus be safely neglected. The insertion of eq. 2.1.17 into eq. 2.1.14 gives the evolution of the density operator in the interaction frame:

$$\frac{d}{dt}\tilde{\sigma}(t) = -\frac{1}{2}\sum_{p,q}\left[A_{k,p}^{-q}, \left[A_{k,p}^{q}, \sigma(t)\right]\right] J^q(\omega_p^q) \tag{2.1.19}$$

Using the above equation and eq. 2.1.3 we obtain the equation of motion for the density operator in the laboratory frame:

$$\frac{d}{dt}\sigma(t) = -i\left[\mathscr{H}_0, \sigma(t)\right] - \frac{1}{2}\sum_{p,q}\left[A_{k,p}^{-q}, \left[A_{k,p}^{q}, \sigma(t)\right]\right] J^q(\omega_p^q) \tag{2.1.20}$$

Eq. 2.1.20 does not describe correctly the return to equilibrium in a magnetic field because it predicts equal populations, so one has to substitute $\sigma(t)$ with $\sigma(t) - \sigma_{eq}$, where σ_{eq} is given by:

$$\sigma_{eq} = \frac{exp\left\{-\mathscr{H}_0/k_BT\right\}}{Tr\left[exp\left\{-\mathscr{H}_0/k_BT\right\}\right]} \tag{2.1.21}$$

Finally the *master equation* of relaxation in the laboratory frame can be written:

$$\frac{d}{dt}\sigma(t) = -i\left[\mathscr{H}_0, \sigma(t) - \sigma_{eq}\right] - \frac{1}{2}\sum_{p,q}\left[A^{-q}_{k,p}, \left[A^{q}_{k,p}, \sigma(t) - \sigma_{eq}\right]\right] J^q(\omega^q_p) \qquad (2.1.22)$$

In the previous equation only one type of interaction is considered, due to the fact that only one operator $A^q_{k,p}$ is considered. Under these conditions one speaks of *auto-correlation*, AC. Generally, when two relaxation mechanisms have the same rank and transform with the same eigenfrequency ω^q_p they can interfere with each other leading to a *cross-correlation*, CC, mechanism. This is the case of dipole-dipole and chemical shift anisotropy interactions, see section 3.1.3. To distinguish the two cases, usually two more indices are added in eq. 2.1.22 that refer to the type of interactions. To account for different mechanisms interfering to each other, the master equation is rewritten as:

$$\frac{d}{dt}\sigma(t) = -i\left[\mathscr{H}_0, \sigma(t) - \sigma_{eq}\right] - \frac{1}{2}\sum_{p,q,m,n}\left[A^{-q}_{k,p,m}, \left[A^{q}_{k,p,n}, \sigma(t) - \sigma_{eq}\right]\right] J^q_{m,n}(\omega^q_p) \quad (2.1.23)$$

For sake of clarity the indices m and n will not be explicitly expressed unless needed.

2.1.1 Master Equation for Observables

The density matrix is a powerful tool for the computation of relaxation behaviour, but we are primarly interested in the behaviour of the evolution of an observable Q.[4]

[4]See the book of Cohen and Tannoudji (Cohen-Tannoudji et al., 1992) on page 227

The two quantities are related by the following relationship:

$$\langle Q \rangle(t) = Tr\left\{Q\sigma(t)\right\} \tag{2.1.24}$$

The time evolution of Q is obtained using eq. 2.1.24 and eq. 2.1.20:

$$\begin{aligned} \frac{d}{dt}\langle Q \rangle(t) &= \frac{d}{dt} Tr\left\{Q\sigma(t)\right\} = Tr\left\{Q\frac{d}{dt}\sigma(t)\right\} && (2.1.25) \\ &= -i\langle [Q, \mathscr{H}_0] \rangle(t) - \frac{1}{2}\sum_{p,q} J^q(\omega_p^q) \times \\ &\quad \left\{ \langle \left[Q, \left[A_{k,p}^{-q}, A_{k,p}^{q}\right]\right](t) \rangle - \langle \left[Q, \left[A_{k,p}^{-q}, A_{k,p}^{q}\right]\right] \rangle_{eq} \right\} && (2.1.26) \end{aligned}$$

where the property $Tr\left\{A\left[B,C\right]\right\} = Tr\left\{\left[A,B\right]C\right\}$ has been used. The observable Q is either left unchanged by the commutator and double commutators or transformed into another observable Q'. The first case is called *auto-relaxation*, AR, and the time-evolution of the observable is predicted by evaluating eq. 2.1.26 for Q. The second case is referred to as *cross-relaxation*, CR, and the correct prediction of the evolution of Q requires the evaluation of eq. 2.1.26 for both Q and Q' and more generally for all observables that are connected by the double commutators, see also section 3.1. An important feature of relaxation can be pointed out: auto-relaxation always leads to mono-exponential decays, while cross-relaxation leads to multi-exponential decays depending on the number of observables that are connected.

To better describe these effect it is convenient to reformulate eq. 2.1.26 in a complete

orthogonal basis of operators Q_i. The density operator is then given by:

$$\sigma(t) = \sum_{i=1}^{N} b_i(t) Q_i \tag{2.1.27}$$

where $N = 4^n$ for an n spin system, and $b_i(t) = \langle Q_i | \sigma(t) \rangle$. Replacing eq. 2.1.27 into eq. 2.1.26 one obtains:

$$\frac{d}{dt}\langle Q_r \rangle(t) = \frac{d}{dt} b_r(t) = \sum_s -i\Omega_{rs} b_s(t) - R_{rs}[b_s(t) - b_s^{eq}] \tag{2.1.28}$$

where R_{rs} is the relaxation matrix element that expresses the rate of interconversion between the operators Q_s and Q_r, and Ω_{rs} is the characteristic frequency of the operator Q_s. R_{rs} and Ω_{rs} are given by:

$$\Omega_{rs} = \frac{\langle Q_r | \left[\mathscr{H}_0, Q_s\right] \rangle}{\langle Q_r | Q_r \rangle} \tag{2.1.29}$$

$$R_{rs} = \frac{1}{2} \sum_{q,p} J^q(\omega_p^q) \frac{\langle Q_r | \left[A_{k,p}^{-q}, \left[A_{k,p}^{q}, Q_s\right]\right] \rangle}{\langle Q_r | Q_r \rangle} \tag{2.1.30}$$

When $r = s$, R_{rs} is an auto-relaxation rate, and when $r \neq s$, R_{rs} is a cross-relaxation rate.

2.1.2 Spectral Density Functions

The correlation function, C(t), for DD and CSA relaxation mechanisms is given by:

$$C(t) = 4\pi \langle Y_2^{*q}\left(\Phi^{lab}(0)\right) Y_2^q\left(\Phi^{lab}(t)\right) \rangle \tag{2.1.31}$$

where Φ^{lab} denotes the polar angles θ and ϕ that determines the orientation of the relevant vector in the laboratory frame. This equation can be written as the product of an overall tumbling correlation function $C_O(t)$ and an internal correlation function $C_I(t)$[5]. The overall tumbling for a spherical molecule is given by (Werbelow and Grant, 1977):

$$C_O(t) = \frac{1}{5} exp\{-6Dt\} = \frac{1}{5} exp\{-t/\tau_c\} \tag{2.1.32}$$

where D is the diffusion tensor and for a spherical molecule $D = D_x = D_y = D_z$, and the *correlation time,* τ_c, is approximately the time for the molecule to rotate by one radian (Ernst et al., 1987). The correlation time depends on molecular size, solvent viscosity and temperature,[6] but is generally in the order of nanoseconds for proteins in aqueous solution. The internal correlation function, derived in the molecular frame is given by:

$$C_I(t) = \frac{4\pi}{5} \sum_q \langle Y_2^{*q}\left(\Phi^{mol}(0)\right) Y_2^q\left(\Phi^{mol}(t)\right)\rangle = P_2(cos\,\theta) \tag{2.1.33}$$

where $P_2(cos\,\theta) = \frac{1}{2}(3\,cos^2\theta - 1)$ is the second order Legendre polynome and θ is the angle between the interactions at time 0 and t. Using these results in eq. 2.1.17 one obtains:

$$J^q(\omega_p^q) = P_2(cos\,\theta)\,\frac{2}{5}\,\frac{\tau_c}{1 + (\omega_p^q \tau_c)^2} \tag{2.1.34}$$

[5]For further details see the work of Korzhnev (Korzhnev et al., 2001)
[6]See eq. 7.3.10 in section 7.3.4.

The ensemble average of the spherical harmonic functions is independent from the order q for isotropic liquids. However the sign of the random functions depends on their order: $F_k^q = (-1)^q F_k^{*-q}$. This characteristic is reflected in the following spectral density property (Hubbard, 1969):

$$J^q(\omega_p^q) = (-1)^q J^0(\omega_p^q) \equiv (-1)^q J(\omega_p^q) \tag{2.1.35}$$

When predicting a relaxation rate, one first evaluates the spectral densities and then takes care of their sign, see eqs. 3.1.2 and 3.1.4 in section 3.1.1.

A plot of $J(\omega_p^q)$ versus ω_p^q is given in figure 2.1.1; $J(\omega_p^q)$ is relatively constant for $(\omega_p^q \tau_c)^2 \ll 1$ and begins to rapidly decrease when $(\omega_p^q \tau_c)^2 \approx 1$. If molecular motion is fast enough to give $(\omega_p^q \tau_c)^2 \ll 1$ one obtains the extreme narrowing condition where $J(\omega_p^q) \approx J(0)$, on the opposite, if $(\omega_p^q \tau_c)^2 \gg 1$, $J(\omega_p^q) \propto {\omega_p^q}^{-2}$, which is known as the slow tumbling regime.

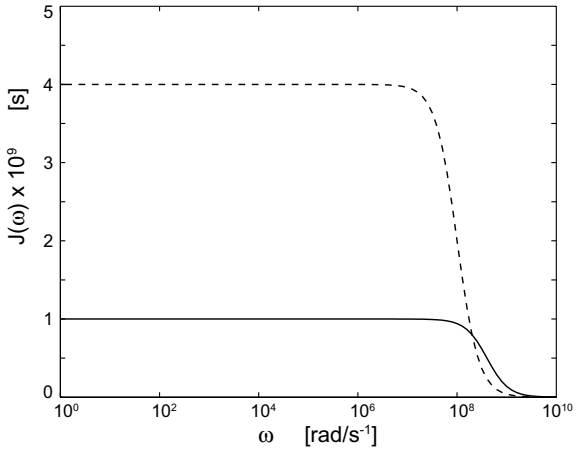

Figure 2.1.1: Spectral density functions for a molecule tumbling isotropically. Calculations were performed with τ_c= 2.5 ns, solid line, and with τ_c= 10 ns, dashed line.

Note that the previous discussion is strictly valid for spherical proteins only with independent internal and overall motions. For axially symmetric or asymmetric molecules other formulas have to be derived, but often the previous formulas are used as an approximation. In our case, both the proteins studied in this work are almost spherical: MUP I has an anisotropy $D_{\parallel}/D_{\perp}$ of about 0.91 (Žídek et al., 1999), while ubiquitin has an anisotropy $D_{\parallel}/D_{\perp}$ of about 1.14 (Tjandra et al., 1995), where $D_{\parallel}$ and $D_{\perp}$ are the principal axes of the diffusion tensors D.

2.2 Relaxation Mechanisms

In the following sections we will consider the relaxation that affects a system composed by two spins-1/2, I and S. The main sources of relaxation are the dipole-dipole interaction, DD, and the chemical shift anisotropy, CSA; both DD and CSA interactions are modulated by molecular tumbling. Cross-correlation effects can be generated between CSA of spin I (or S) and the DD of IS, or between the CSA's of spins I and S. We will first describe the ideal system of two isolated spins, but one should remember that in a real system dipole-dipole effects of neighbour spins have to be taken into account, as well as the existence of chemical exchange.

2.2.1 The Dipolar Interaction

The dipolar interaction is the easiest to understand because one can picture it classically. The energy of the interaction is given by:

$$E_{AB} = \frac{1}{\mathbf{r}_{AB}^3}\{\boldsymbol{\mu}_A \cdot \boldsymbol{\mu}_B - 3(\boldsymbol{\mu}_A \cdot \widehat{n}_{AB})(\boldsymbol{\mu}_B \cdot \widehat{n}_{AB})\} \tag{2.2.1}$$

where $\mathbf{r}_{AB}$ is the distance between the two dipoles, considered to be time independent, $\widehat{n}_{AB}$ is the unit vector along the direction between the two dipoles, $\boldsymbol{\mu}_A$ and $\boldsymbol{\mu}_B$. If we assume that the z axis is parallel to the vector $\mathbf{r}_{AB}$, only the components along z remain when computing the scalar product between the magnetisation vector and $\widehat{n}_{AB}$. In analogy with the classical picture the Hamiltonian is given by:

$$\begin{aligned} \mathscr{H}^{IS} &= \frac{\mu_0}{4\pi}\frac{\gamma_I\gamma_S\hbar}{r_{IS}^3}\{\mathbf{I}\cdot\mathbf{S} - 3(\mathbf{I}\cdot\widehat{n}_{IS})(\mathbf{S}\cdot\widehat{n}_{IS})\} \\ &= \frac{\mu_0}{4\pi}\frac{\gamma_I\gamma_S\hbar}{r_{IS}^3}\{\mathbf{I}\cdot\mathbf{S} - 3I_zS_z\} \end{aligned} \tag{2.2.2}$$

Eq. 2.2.3 simply derives from the previous by a careful definition of the z axis, as seen for the classical interaction. Because of this simplification, it is convenient to work in the laboratory frame, where the external field, B_0 is parallel to the z axis.[7] As seen previously any interaction can be written as a sum of products of irreducible tensors, A_k^q, and spherical harmonics, F_k^q, see table 9.1:

[7] As usual, the frame change is done using polar angles: $I_z^{dip} = I_z^{lab}cos\theta + I_x^{lab}sin\theta cos\phi + I_y^{lab}sin\theta sin\phi = I_z^{lab}cos\theta + 1/2sin\theta(I_+^{lab}e^{-i\phi} + I_-^{lab}e^{i\phi})$, where the suffixes dip and lab stand for dipolar and laboratory frame respectively.

$$\begin{aligned} \mathscr{H}^{IS} &= -\frac{\mu_0}{4\pi}\frac{\gamma_I\gamma_S\hbar}{r_{IS}^3}\sum_{q=-2}^{+2} F_{2,p}^{-q}(\theta,\phi)A_{2,p}^{q} \\ &= d_{IS}\sum_{q=-2}^{+2} F_{2,p}^{\prime -q}(\theta,\phi)A_{2,p}^{\prime q} \end{aligned} \tag{2.2.3}$$

where the fact that the dipole-dipole coupling is a second rank interaction has been used to reduce the summation. The choice of coefficients included in the constant d_{IS} is arbitrary, one needs only to be consistent with the definitions of the others coefficients in both the spin and spatial parts of the Hamiltonian. Usually in NMR, the modified spherical harmonics are used, that differ from the conventional functions by a factor $\sqrt{5/4\pi}$, furthermore the coefficients of the scalar and spatial terms are usually modified to simplify the calculations. The modified spherical harmonics, $F_2^{\prime q}$, and irreducible tensors operators, $A_2^{\prime q}$, which best define the dipole-dipole interactions are listed in table 2.2.1: using these functions the constant, d_{IS}, is given by:

$$d_{IS} = \sqrt{6}\frac{\mu_0}{4\pi}\frac{\hbar\gamma_I\gamma_S}{r_{IS}^3} \tag{2.2.4}$$

2.2.2 The Chemical Shift Anisotropy Interaction

Each atom possesses its local electronic environment that produces a tiny local time dependent magnetic field. This effect is called nuclear shielding and it is responsible for the difference in chemical shifts that are observed in a spectra. The magnitude and the direction of the induced field at a given nuclear site depend on the orientation of

q	p	A^{q}_{2p}	A^{-q}_{2p}=$A^{q\dagger}_{2p}$	ω^{q}_{p}
0	0	$\frac{2}{\sqrt{6}}I_zS_z$	$\frac{2}{\sqrt{6}}I_zS_z$	0
0	1	$-\frac{1}{2\sqrt{6}}I_+S_-$	$-\frac{1}{1\sqrt{6}}I_-S_+$	$\omega_I-\omega_S$
1	0	$-\frac{1}{2}I_zS_+$	$\frac{1}{2}I_zS_-$	ω_S
1	1	$-\frac{1}{2}I_+S_z$	$\frac{1}{2}I_-S_z$	ω_I
2	0	$\frac{1}{2}I_+S_+$	$\frac{1}{2}I_-S_-$	$\omega_I+\omega_S$

Table 2.2.1: Tensor operators for a DD interaction. The associated random function, F^{q}_{2}, can derived from the spherical functions, see table 9.1 (Cavanagh et al., 1996; Cohen-Tannoudji et al., 1992; Korzhnev et al., 2001).

the molecule with respect to the external field and also on the location of the nuclear spin within molecule. For this reason these shifts have been extensively studied as probes of molecular structure.[8]

The Hamiltonian describes the interaction between the external magnetic field, B_0, and the spin, I, modulated by the chemical shift tensors, σ:

$$\mathscr{H}_I^{CS} = \gamma_I \sum_{i,j} B_i \sigma_{ij} I_j \tag{2.2.5}$$

where i and j are the components in any frame. In a particular frame, the principal axis frame, PAF, the field induced by the local environment is parallel to the applied field. In this frame eq. 2.2.5 becomes:

$$\mathscr{H}_I^{CS} = \gamma_I \sum_{i} B_i \sigma_{ii} I_i \tag{2.2.6}$$

[8]A brief overview of the main conclusions can be found in section 4.2.1.

Since any arbitrary tensors can be written as sums of two axially symmetric tensors[9] with $\sigma_{zz} = \sigma_{\parallel}$ and $\sigma_{xx} = \sigma_{yy} = \sigma_{\perp}$ (Goldman, 1984), the previous equation can be rewritten as:

$$\begin{aligned} \mathscr{H}^{CS} &= \gamma \left\{ \sigma_{\parallel} B_z I_z + \sigma_{\perp} (B_x I_x + B_y I_y) \right\} && (2.2.7) \\ &= \gamma \left\{ \frac{\sigma_{\parallel} + 2\sigma_{\perp}}{3} \mathbf{B} \cdot \mathbf{I} + \frac{\sigma_{\parallel} - \sigma_{\perp}}{3} (2B_z I_z - B_x I_x - B_y I_y) \right\} && (2.2.8) \end{aligned}$$

The first term is the isotropic chemical shift, $\sigma_{iso} = (\sigma_{\parallel} + 2\sigma_{\perp})/3$, which is invariant under rotation, as a consequence it does not contribute to relaxation. The second term is the *chemical shift anisotropy* interaction, $\mathscr{H}^{CSA}$, which can be rewritten as:

$$\mathscr{H}^{CSA} = -\gamma \frac{\sigma_{\parallel} - \sigma_{\perp}}{3} (\mathbf{B} \cdot \mathbf{I} - 3B_z I_z) \qquad (2.2.9)$$

Moving from the PAF to the laboratory frame the previous equation becomes, see eq. 2.1.10:

$$\mathscr{H}^{CSA} = \gamma \frac{\sigma_{\parallel} - \sigma_{\perp}}{3} \sum_{q=-2,p}^{+2} F_{2,p}^{-q}(\theta, \phi) A_{2,p}^{q} \qquad (2.2.10)$$

In the laboratory frame, the magnetic field is parallel to the z direction, B=B_0, and

[9] This assumption holds only if one can neglige the antisymmetric part (Goldman, 1984).

the previous sum reduces to:[10]

$$\mathscr{H}^{CSA} = \gamma \frac{\sigma_{\parallel} - \sigma_{\perp}}{3} \left\{ \frac{2}{\sqrt{6}} I_z B_0 - \frac{1}{2} I_+ B_0 + \frac{1}{2} I_- B_0 \right\} \tag{2.2.11}$$

Here we clearly see that there are no second order trems in the chemical shift anisotropy Hamiltonian. Usually the $\mathscr{H}^{CSA}$ is written in a more compact form:

$$\mathscr{H}^{CSA} = c_I \sum_{q=-2,p}^{+2} F'^{q}_{k,p}(\theta, \phi) A'^{q}_{k,p} \tag{2.2.12}$$

where the constant of the CSA interaction, c_I is given by:

$$c_I = \sqrt{\frac{2}{3}} \Delta\sigma \gamma_I B_0 \tag{2.2.13}$$

As seen in the previous section, the inclusion of the external magnetic field into the constant implies a modification in the tensors operators; in this case, one must divide the CSA tensor operator by B_0. This notation is convenient for the CSA interaction, and the modified second order spherical harmonic and the spatial functions are listed in table 2.2.2.

[10] The full expressions for the irreducible tensors operators A_2^q are: $A_2^0 = \frac{1}{\sqrt{6}} \left[2B_z I_z - \frac{1}{2} \left(B_+ I_- + B_- I_+ \right) \right]$, $A_2^{\pm 1} = \pm \frac{1}{2} (B_z I_\pm + B_\pm I_z)$ and $A_2^{\pm 2} = \frac{1}{2} (B_\pm I_\pm)$. Since in the laboratory frame $B_z = B_0$ and $B_x = B_y = 0$, $B_\pm = B_x \pm i B_y = 0$, the previous equations reduce to $A_2^0 = \frac{2}{\sqrt{6}} B_0 I_z$, $A_2^{\pm 1} = \mp \frac{1}{2} B_0 I_\pm$ and $A_2^{\pm 2} = 0$.

q	p	A^{q}_{2p}	$A^{-q}_{2p}=A^{q\dagger}_{2p}$	ω^{q}_{p}
0	0	$\frac{2}{\sqrt{6}}I_z$	$\frac{2}{\sqrt{6}}I_z$	0
1	0	$-\frac{1}{2}I^{+}$	$\frac{1}{2}I^{-}$	ω_I

Table 2.2.2: Tensor operators for CSA interaction. The associated random function, F^{q}_{2}, can be derived from the spherical functions, see table 9.1 (Cavanagh et al., 1996; Cohen-Tannoudji et al., 1992; Korzhnev et al., 2001).

Chapter 3

Prediction of Relaxation Rates

3.1 Relaxation of Single Quantum Coherences

The evolution of an observable is given by eq. 2.1.30. In the last sections we derived the Hamiltonians of the CSA and DD interactions. In order to predict the relaxation rates of a given basis operator Q_i associated with an observable, a simple procedure has to be followed. First, the spin system has to be defined, i.e., the type and number of nuclei and the type and number of neighbouring spins. Second, a basis has to be chosen which allows the description of the spin system. Third, eq. 2.1.30 has to be evaluated for all interaction operators $A^q_{2,p}$ that act on a basis operator Q_r. For a correct prediction of the relaxation rate of the operator Q_r, the double commutator has to be evaluated for all interaction operators $A^q_{2,p}$ acting on Q_r, and this has to be repeated for all operators Q_s that may result from the evaluation of the double commutators.

3.1.1 Relaxation due to Chemical Shift Anisotropy

Understanding how an operator evolves under relaxation is easier if we consider a couple of examples. Let us start with the evolution of I_z under a CSA interaction; the operator Q_s in eq. 2.1.30 has to be replaced by I_z, while the sum has to run over all tensor operators for the CSA interaction, see table 2.2.2. In this particular example, the CSA interaction acts as auto-correlation auto-relaxation mechanism on I_z. As it is easier to break down the calculations in simple steps, we shall start from the calculation of the commutators.

$$\begin{aligned}
\left[A^0_{20},\left[A^0_{20},I_z\right]\right] &= \left[\frac{2}{\sqrt{6}}I_z,\left[\frac{2}{\sqrt{6}}I_z,I_z\right]\right]=0\\
\left[A^{-1}_{20},\left[A^1_{20},I_z\right]\right] &= \left[\frac{1}{2}I_-,\left[\frac{-1}{2}I_+,I_z\right]\right]=\frac{-1}{4}\left[I_-,I_+\right]=-\frac{1}{2}I_z\\
\left[A^1_{20},\left[A^{-1}_{20},I_z\right]\right] &= \left[\frac{-1}{2}I_+,\left[\frac{1}{2}I_-,I_z\right]\right]=\frac{-1}{4}\left[I_+,I_-\right]=-\frac{1}{2}I_z
\end{aligned}$$

From the previous equations one sees that the CSA interaction converts I_z into itself; therefore, since the operator basis is orthogonal, no operator cross-relaxes with I_z. As consequence, Q_r in eq. 2.1.30 can only be I_z, and we are considering an auto-relaxation mechanism (r=s).

$$-\frac{1}{2}\langle I_z|I_z\rangle=-\frac{1}{2}\langle I_z^2\rangle=-\frac{1}{2} \tag{3.1.1}$$

Using the fact that $\langle I_z|I_z\rangle$=1 and the properties of the spectral density functions, see eq. 2.1.35, one obtains from the 2.1.30 the final equation for the auto-relaxation of I_z

due to a CSA interaction:

$$R_{I_z,I_z} = \frac{1}{2}c_I^2\left\{2\frac{1}{2}J^1(\omega_I)\right\} = \frac{1}{2}c_I^2 J(\omega_I) \tag{3.1.2}$$

Let us now consider the effect of CSA interaction on I_+; the procedure is analogous to the previous.

$$\begin{aligned}
\left[A_{20}^0,\left[A_{20}^0,I_+\right]\right] &= \left[\sqrt{\frac{2}{3}}I_z,\left[\sqrt{\frac{2}{3}}I_z,I_+\right]\right] = \frac{2}{3}I_+ \\
\left[A_{20}^{-1},\left[A_{20}^1,I_+\right]\right] &= \left[\frac{1}{2}I_-,\left[\frac{-1}{2}I_+,I_+\right]\right] = 0 \\
\left[A_{20}^1,\left[A_{20}^{-1},I_+\right]\right] &= \left[\frac{-1}{2}I_+,\left[\frac{1}{2}I_-,I_+\right]\right] = \frac{1}{2}\left[I_+,I_z\right] = -\frac{1}{2}I_+
\end{aligned} \tag{3.1.3}$$

Once more only auto-relaxation mechanisms have to be taken into account; $\langle I_+|I_+\rangle = \langle I_-I_+\rangle = 2$ and the results introduced in eq. 2.1.30:

$$R_{I_+,I_+} = c_I^2\frac{1}{2}\left\{\frac{2}{3}J^0(0) - \frac{1}{2}J^{-1}(\omega_I)\right\} = \frac{1}{6}c_I^2\left\{4J(0) + 3J(\omega_I)\right\} \tag{3.1.4}$$

3.1.2 Relaxation due to Dipole-Dipole Interactions

Exactly the same procedure has to be used to calculate the evolution of both I_z and I_+ under dipole-dipole interactions. The dipole-dipole tensor operators can be found in table 2.2.1. To avoid repeating the tedious calculations, we will only give the results and highlight the new features.

$$
\begin{aligned}
\left[A^{0}_{20},\left[A^{0}_{20},I_z\right]\right] &= \left[\frac{2}{\sqrt{6}}I_z,\left[\frac{2}{\sqrt{6}}I_z,I_z\right]\right]=0\\
\left[A^{-0}_{21},\left[A^{0}_{21},I_z\right]\right] &= \left[\frac{1}{2\sqrt{6}}I_-S_+,\left[\frac{-1}{2\sqrt{6}}I_+S_-,I_z\right]\right]=\frac{1}{24}\{I_z-S_z\}\\
\left[A^{0}_{21},\left[A^{-0}_{21},I_z\right]\right] &= \left[\frac{1}{2\sqrt{6}}I_+S_-,\left[\frac{-1}{2\sqrt{6}}I_-S_+,I_z\right]\right]=\frac{1}{24}\{I_z-S_z\}\\
\left[A^{-1}_{20},\left[A^{1}_{20},I_z\right]\right] &= \left[\frac{1}{2}I_zS_-,\left[\frac{-1}{2}I_zS_+,I_z\right]\right]=0 \qquad (3.1.5)\\
\left[A^{1}_{20},\left[A^{-1}_{20},I_z\right]\right] &= \left[\frac{-1}{2}I_zS_+,\left[\frac{1}{2}I_zS_-,I_z\right]\right]=0\\
\left[A^{-1}_{21},\left[A^{1}_{21},I_z\right]\right] &= \left[\frac{1}{2}I_-S_z,\left[\frac{-1}{2}I_+S_z,I_z\right]\right]=-\frac{1}{8}I_z\\
\left[A^{1}_{21},\left[A^{-1}_{21},I_z\right]\right] &= \left[\frac{-1}{2}I_+S_z,\left[\frac{1}{2}I_-S_z,I_z\right]\right]=-\frac{1}{8}I_z\\
\left[A^{-2}_{20},\left[A^{2}_{20},I_z\right]\right] &= \left[\frac{1}{2}I_-S_-,\left[\frac{1}{2}I_+S_+,I_z\right]\right]=\frac{1}{4}\{I_z+S_z\} \qquad (3.1.6)\\
\left[A^{2}_{20},\left[A^{-2}_{20},I_z\right]\right] &= \left[\frac{-1}{2}I_+S_+,\left[\frac{1}{2}I_-S_-,I_z\right]\right]=\frac{1}{4}\{I_z+S_z\}
\end{aligned}
$$

In this case, I_z both auto-relaxes to I_z and cross-relaxes to $I_z \pm S_z$; as a consequence both auto- and cross-relaxation mechanisms have to be evaluated. This means that the three operators resulting from the above commutators have to be pre-multiplied by I_z (auto-relaxation), and by S_z (cross-relaxation), before performing the trace, leading to three equations analogous to eq. 3.1.1 for each operator that resulted from the commutators. The final relaxation rate for I_z is:

$$
\begin{aligned}
R_{I_z,I_z} &= \frac{d^2_{IS}}{24}\{J(\omega_I-\omega_S)+3J(\omega_I)+6J(\omega_I+\omega_S)\}\\
R_{I_z,S_z} &= \frac{d^2_{IS}}{24}\{-J(\omega_I-\omega_S)+6J(\omega_I+\omega_S)\} \qquad (3.1.7)
\end{aligned}
$$

in which d_{IS} is the coefficient given in eq. 2.2.4.

The same procedure has to be followed for I_+, but this operator only auto-relaxes and the final rate is:

$$R_{I_+,I_+} = \frac{d_{IS}^2}{48}\{4J(0) + J(\omega_I - \omega_S) + 3J(\omega_I) + 6J(\omega_S) + 6J(\omega_I + \omega_S)\} \qquad (3.1.8)$$

As a concluding remark, we should remember that DD and CSA are the dominant interactions leading to relaxation in a protein in solution. Thus, the evaluation of their effects on the relaxation of I_z and I_+ gives insight into the mechanisms that causes the relaxation rates R_1 and R_2 respectively.

3.1.3 Relaxation due to Cross-Correlation Effects: CSA/DD

In the last example of a relaxation rate we will consider relaxation due to the simultaneous effect of two different relaxation mechanisms; the CSA and the DD effects. In this particular case, only the parts of the Hamiltonian that have the same order and that transform with the same frequencies need to be evaluated at the same time; for the operator I_+ this results in:

$$
\begin{aligned}
\left[A_{20}^{0\,(DD)},\left[A_{20}^{0\,(CSA)},I_+\right]\right] &= \left[\sqrt{\frac{2}{3}}I_zS_z,\left[\sqrt{\frac{2}{3}}I_z,I_+\right]\right] = \frac{2}{3}I_+S_z \qquad (3.1.9)\\
\left[A_{20}^{0\,(CSA)},\left[A_{20}^{0\,(DD)},I_+\right]\right] &= \left[\sqrt{\frac{2}{3}}I_z,\left[\sqrt{\frac{2}{3}}I_zS_z,I_+\right]\right] = \frac{2}{3}I_+S_z\\
\left[A_{21}^{-0\,(DD)},\left[A_{21}^{0\,(CSA)},I_+\right]\right] &= \left[\frac{1}{2}I_-S_z,\left[-\frac{1}{2}I_+,I_+\right]\right] = 0\\
\left[A_{21}^{0\,(CSA)},\left[A_{21}^{-0\,(DD)},I_+\right]\right] &= \left[-\frac{1}{2}I_+,\left[\frac{1}{2}I_-S_z,I_+\right]\right] = \frac{1}{2}\left[I_+,I_zS_z\right] = -\frac{1}{2}I_+S_z\\
\left[A_{21}^{-0\,(DD)},\left[A_{21}^{0\,(CSA)},I_+\right]\right] &= \left[-\frac{1}{2}I_+S_z,\left[\frac{1}{2}I_-,I_+\right]\right] = \frac{1}{2}\left[I_+S_z,I_z\right] = -\frac{1}{2}I_+S_z\\
\left[A_{21}^{0\,(CSA)},\left[A_{21}^{-0\,(DD)},I_+\right]\right] &= \left[\frac{1}{2}I_-,\left[-\frac{1}{2}I_+S_z,I_+\right]\right] = 0
\end{aligned}
$$

As can be seen from the above equations not all tensor operators for the dipole-dipole interaction can interfere with those of chemical shift anisotropy, resulting in a non zero cross-correlated relaxation. Following the same steps as in the previous sections the relaxation rate for CSA/DD is given by:

$$R_{I_+,I_+S_z}^{CSA/DD} = \frac{1}{2}d_{IS}c_I\left\{\frac{2}{3}J(0)+\frac{1}{2}J(\omega_I)\right\} \qquad (3.1.10)$$

where the coefficient d_{IS} and c_I are the DD and CSA coefficients seen in eqs. 2.2.4 and 2.2.13.

3.1.4 Asymmetric Chemical Shift Anisotropy

In a recent study on ubiquitin, the CSA tensors where determined for the backbone atoms H^N, N and C', using fourteen auto- and cross-correlated relaxation rates, and

found to be asymmetric (Loth et al., 2005). Under these conditions the previous formula can only be considered as an approximation: the corrected formula for asymmetric chemical shift tensors will be given, but their derivation is beyond the scope of this work.

For asymmetric CSA tensors of spin I, the CSA/DD relaxation mechanism can be obtained by considering the cross-correlation between the dipole-dipole interaction and each of the principal components of the CSA tensor separately:

$$R_{I,IS}^{CSA/DD} = \frac{2}{3}\frac{\mu_0}{4\pi}\frac{\gamma_I^2\gamma_S}{r_{IS}^3}B_0\sum_{\xi}\sigma_{\xi}^{I}\frac{1}{2}\left(3\,cos^2\theta_{\xi,IS}-1\right)\right)\frac{2}{5}\tau_c \tag{3.1.11}$$

where σ_{ξ}^{j}, with ξ = xx, yy and zz, stands for the ξ^{th} principal component of the CSA tensors of spin I, and $\theta_{\xi,IS}$ is the angle subtended between the ξ^{th} principal axis component of the CSA and the axis of the DD interaction.

For two nuclei I and S, both having asymmetric tensor components, the cross-correlation rate is given by:

$$R_{I,S}^{CSA/CSA} = \frac{4}{9}\gamma_I\gamma_S B_0^2\sum_{\chi}\sum_{\xi}\sigma_{\xi}^{I}\,\sigma_{\chi}^{S}\frac{1}{2}\left(3\,cos^2\theta_{\xi,\chi}-1\right)\right)\frac{2}{5}\tau_c \tag{3.1.12}$$

where the symbols have a meaning analogous as before.

In the slow motion regime, $J(\omega_p) \propto \omega_p^{-2}$ and thus the high frequency components of the spectral densities can be safely neglected. If this condition does not apply, one needs to consider high frequency components. These formula will be used in the calculation of $R_{C'N}^{CSA/CSA}$ relaxation rate in chapter 7.

3.2 Relaxation Rates Affecting the Single Quantum Coherences

In the previous sections, we have considered one by one the relaxation mechanisms that can affect a spin; in this section we consider how all these mechanisms affect a spin I surrounded by two neighbouring spins X_i and X_j. As seen before, we need to evaluate the double commutators for each interaction; only when the double commutator is non zero does the relaxation mechanism considered influence the relaxation of the spin I. We will assume that the main relaxation mechanisms are the same as considered before: CSA and DD, plus so-called chemical shift modulations, CSM. This contribution arises from slow fluctuations of the isotropic parts of the chemical shifts, and its Hamiltonian is simply $\sqrt{\frac{2}{3}}I_z$. Since the isotropic part of the chemical shift is of rank zero, this interaction cannot lead to cross-correlated relaxation with CSA or DD, which are of rank two. Instead it contributes, with CSA and DD, to the auto-correlated auto-relaxation, $m = n$ and $Q_r = Q_s$ in eq. 2.1.30. For the spin I we can write:

$$R_2^{AC,AR}(I_x) = R_{I/I}^{CSA/CSA} + R_{I/I}^{CSM/CSM} + \sum_i^j R_{IX_i/IX_i}^{DD/DD} \tag{3.2.1}$$

On the other hand, cross-correlated I/IS CSA/DD can exist, along with cross-correlated IX_i/IX_j DD/DD interactions; both these mechanisms can contribute to relaxation:

$$R_2^{CC,CR}(I_x) = \sum_i^j R_{I/IX_i}^{CSA/DD} + \sum_{i,i\neq j}^j R_{IX_i/IX_j}^{DD/DD} \tag{3.2.2}$$

Where the starting operator I_x is converted into the antiphase term $2I_xX_{zi}$ by the CSA/DD interaction, and into the doubly anti-phase term $4I_xX_{zi}X_{zj}$ by the DD/DD interaction. In figure 3.2.1 a cartoon of the mechanisms affecting SQC I_x is given.

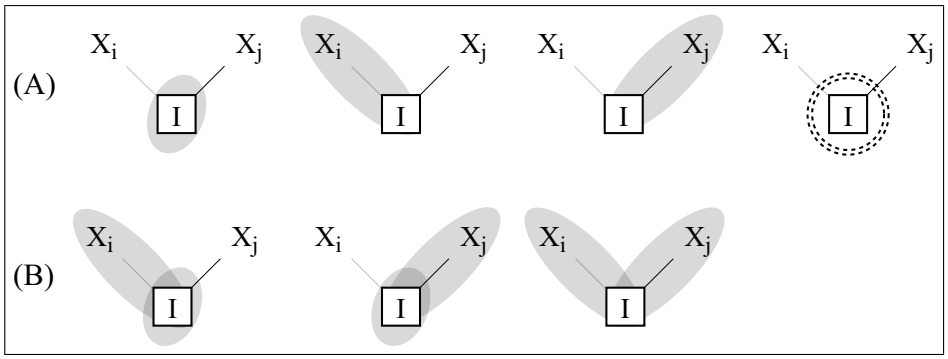

Figure 3.2.1: Relaxation mechanisms affecting the single quantum coherence of spin I. Elongated shaded ellipses, short shaded ellipses and dashed circles represent dipole-dipole (DD), chemical shift anisotropy (CSA) and chemical shift modulation (CSM) interactions. Auto-correlated mechanisms that induce auto-relaxation of the in-phase term I_x, (A). Cross-correlated mechanisms converting the in-phase term I_x into anti-phase terms $2I_xX_{zi}$, and in the doubly antiphase terms $4I_xX_{zi}X_{zj}$ (B).

3.3 Relaxation Rates Affecting the Multiple Quantum Coherence

An attractive feature of cross-correlated interference effects is their dependence on the angle subtended by the princial axes of the involved interactions. Additional interferences involving four different nuclei may affect multiple-quantum coherences (MQC) and thus enable measurements of torsion angles defining the 3-dimensional structure of a protein. The investigation of multiple-quantum relaxation also permits one to gather information about dynamic processes. Indeed, cross-correlated

relaxation rates will be scaled by fast internal dynamics. Thus, measurements of cross-correlated mechanisms affecting multiple-quantum coherences provide information about the correlation of fluctuations induced by internal dynamics.

We consider heteronuclear three-spin system involving I, S and X spins, where the double quantum coherence (DQC) ($2I_{\pm}S_{\pm}$) and the zero quantum coherence (ZQC) ($2I_{\pm}S_{\mp}$) involves the I and S spins. Using the operators of tables 2.2.2 and 2.2.1, the equations 2.2.13 and 2.2.4 into 2.1.30 allows one to determine the relaxation rates of DQC and ZQC.

$$\begin{aligned} R_2^{obs}(MQC) \propto\ & R_{I/I}^{CSA/CSA} + R_{S/S}^{CSA/CSA} + R_{I/S}^{CSA/CSA} \\ +\ & R_{I/I}^{CSM/CSM} + R_{S/S}^{CSM/CSM} + R_{I/S}^{CSM/CSM} \\ +\ & R_{I/IX}^{CSA/DD} + R_{S/SX}^{CSA/DD} \\ +\ & R_{IS/IS}^{DD/DD} + R_{IX/IX}^{DD/DD} + R_{SX/SX}^{DD/DD} \\ +\ & R_{IX/SX}^{DD/DD} \end{aligned}$$

Where the contributions for ZQC and DQC are the following:

$$
\begin{aligned}
R_{I/I}^{CSA/CSA}(ZQC) &= R_{I/I}^{CSA/CSA}(DQC) = \frac{1}{2}c_I^2\left[\frac{2}{3}J(0)+\frac{1}{2}J(\omega_I)\right] \\
R_{S/S}^{CSA/CSA}(ZQC) &= R_{S/S}^{CSA/CSA}(DQC) = \frac{1}{2}c_S^2\left[\frac{2}{3}J(0)+\frac{1}{2}J(\omega_S)\right] \\
R_{I/IX}^{CSA/DD}(ZQC) &= R_{I/IX}^{CSA/DD}(DQC) = \frac{1}{2}c_I d_{IX}\left[\frac{4}{3}J(0)+J(\omega_I)\right] \\
R_{S/SX}^{CSA/DD}(ZQC) &= R_{S/SX}^{CSA/DD}(DQC) = \frac{1}{2}c_S d_{SX}\left[\frac{4}{3}J(0)+J(\omega_S)\right] \\
R_{I/S}^{CSA/CSA}(ZQC) &= -R_{I/S}^{CSA/CSA}(DQC) = -\frac{1}{2}c_I c_S\left[\frac{4}{3}J(0)\right] \\
R_{IS/IS}^{DD/DD}(ZQC) &\neq R_{IS/IS}^{DD/DD}(DQC) \\
R_{IS/IS}^{DD/DD}(ZQC) &= \frac{1}{2}d_{IS}^2\left[\frac{1}{12}J(\omega_I-\omega_S)+\frac{1}{8}J(\omega_I)+\frac{1}{8}J(\omega_S)\right] \\
R_{IS/IS}^{DD/DD}(DQC) &= \frac{1}{2}d_{IS}^2\left[\frac{1}{2}J(\omega_I+\omega_S)+\frac{1}{8}J(\omega_I)+\frac{1}{8}J(\omega_S)\right] \\
R_{IX/IX}^{DD/DD}(ZQC) &= R_{IX/IX}^{DD/DD}(DQC) \\
&= \frac{1}{2}d_{IX}^2\left[\frac{1}{6}J(0)+\frac{1}{24}J(\omega_I-\omega_S)+\frac{1}{4}J(\omega_I+\omega_S)\frac{1}{8}J(\omega_I)+\frac{1}{4}J(\omega_S)\right] \\
R_{IX/SX}^{DD/DD}(ZQC) &= -R_{IX/SX}^{DD/DD}(DQC) = -\frac{1}{2}d_{IX}d_{SX}\left[\frac{1}{3}J(0)+\frac{1}{2}J(\omega_X)\right]
\end{aligned}
\tag{3.3.1}
$$

The two CSA/DD mechanisms in 3.3.1 convert the in-phase operators $2I_{\pm}S_{\pm}$ and $2I_{\pm}S_{\mp}$ into anti-phase operators $2I_{\pm}S_{\pm}X_z$ and $2I_{\pm}S_{\mp}X_z$ so that the double quantum commutators have to be evaluated for the anti-phase terms as well. In practice however, when designing a pulse sequence one takes care to eliminate most of unwanted relaxation mechanisms. Unfortunately this is not always possible.

As can be seen in eq. 3.3.1, the contribution from CSA/CSA I/S cross-correlation to the ZQC and DQC relaxation rates has opposite signs: by taking the difference $R_2^{obs}(\langle 2I_{\pm}S_{\pm}\rangle) - R_2^{obs}(\langle 2I_{\pm}S_{\mp}\rangle)$ it is possible to measure this interaction. This phenomenon is referred to as differential line broadening. For a three-spin system, the

following mechanisms contribute to differential line broadening:

$$R_2^{obs}(\langle 2I_{\pm}S_{\pm}\rangle) - R_2^{obs}(\langle 2I_{\pm}S_{\mp}\rangle) = R_{I/S}^{CSA/CSA} + R_{I/S}^{CSM/CSM} + R_{IS/IS}^{DD/DD} + R_{IX/SX}^{DD/DD} \tag{3.3.2}$$

The four mechanisms are not distinguishable experimentally, in fact if one decides to measure CSA/CSA I/S one must apply π pulse simultaneously to both spin I and S, otherwise such interactions will be refocused. The last three contributions in eq. 3.3.2 are affected by π pulses in the same manner as the first contribution and therefore it is not possible to separate the four contributions. In other words, any pulse sequence that enables the measurements of the cross-correlated CSA/CSA I/S relaxation rate, will be contaminated by additional contributions of eq. 3.3.2. Only numerical calculations for the system under investigation allow one to separate the contributions from unwanted mechanisms. In Chapter 7, an experiment is presented that enables the measurement of cross-correlated CSM/CSM relaxation rates for C' carbonyl and N amide nitrogen of the MUP I backbone. In this system, the contribution of both CSA/CSA and DD/DD interferences from eq. 3.3.2 are estimated by numerical computation.

Chapter 4

Major Urinary Protein I

During my thesis, I mainly worked on Major Urinary Protein I, a particular isoform of Major Urinary Proteins. In the present chapter, I will provide a brief overview of the main structural and functional characteristics of Major Urinary Proteins, and a short overview of the methodology we used to assign Major Urinary Protein I.

4.1 Structure and Function of Major Urinary Proteins

MUPs are part of the lipocalin family and are produced mainly by sexually mature male mice; female mice produce MUPs three to four time less with respect to male (Beynon and Hurst, 2004). MUPs can bind a variety of volatile pheromones that have important effects on murine physiology and behaviour, including acceleration of female puberty, pregnancy blocking and inter-male aggression. It has been shown that the main function of MUPs is to act as slow releasers by allowing the chemical

signal to persist longer in the environment.

4.1.1 Lipocalin Family

Lipocalins are usually small, 160-180 residue, extracellular proteins that bind small hydrophobic molecules. A singular characteristic is the surprisely low level of overall conservation, often below 20%, that contrasts with a high level of conservative similarity in the 3D folds. The lipocalin fold is well known (Flower, 1996; Flower et al., 2000), and is constituted by eight (or ten) strands of antiparallel β-sheets that form a β-barrel; the binding site is located in its core. The β-strands are labelled from β-A to β-I, with the adjacent loops called according, for ex. loop AB connects β-A and β-B. Between the β-H strand and the short terminal β-I strand a long α-helix is located; although its presence is conserved in the family, its length and its position relative to the axis of the β-barrel are not. The first β-A strand interacts with both β-B and β-H, thanks to a β-bulge that breaks the homogeneity of the sheet, see figure 4.1.1.

Only few residues are conserved in the whole family: Gly 17, Trp 19, Cys 64, Thr 95, Asp 96, Try 97, Arg 122, Phe 134 and Cys 157; none of these constitutes the binding site. Their function is related to structural features of MUPs. For example, Trp 19 forms the bottom of the cavity, preventing the solvent access, and together with Gly 17, plays a key role in the overall structure and stability (Yoshinori et al., 1994). Cys 64 makes a disulfide bond with Cys 157, connecting the terminal part of the molecule with its core. A similar role is played by Arg 122: its hydrogen bonds with the backbones of both Asn 16 and Gln 18 contribute to the correct positioning

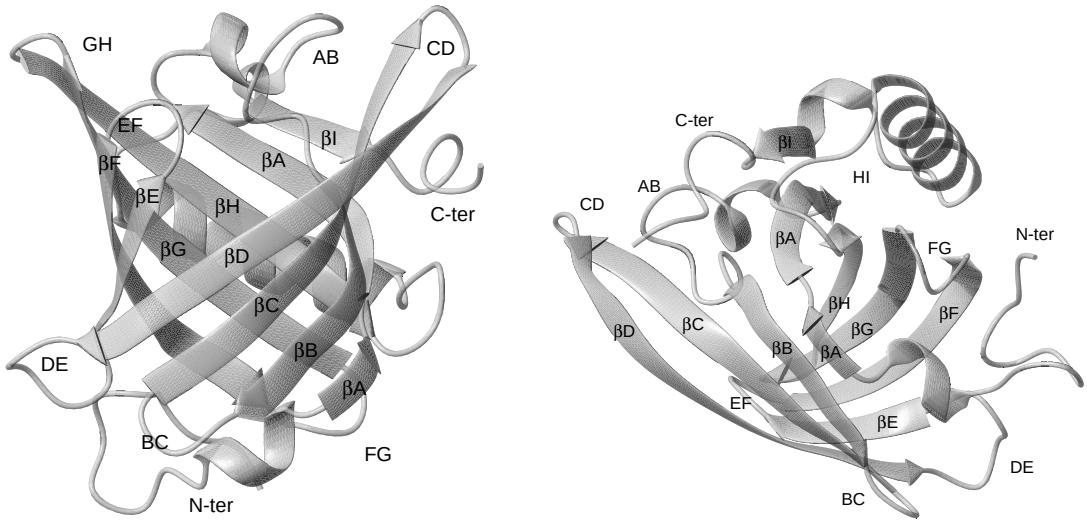

Figure 4.1.1: Two view of the Major Urinary Protein I structure, where the names of the β-strands have been indicated.

of the β-H strand. The conservation of the binding site residues is limited to their hydrophobic character. This characteristic, together with the eight- or ten-stranded scaffold, explains the ability to bind a variety of ligands (Kuser et al., 2001).

An intersting feature of the fold is the absence, in both X-ray or in NMR structures, of an evident trajectory through which the pheromone could travel to reach the binding site. As a consequence, the structure must undergo to conformational changes: the flapping of a segment, or the flexibility of the whole β-barrel could allow access to the binding site.

The residues forming the binding site, when 2-methoxy-3-isobutylpyrazine is bound, are: Phe 38, Leu 40, Leu 42, Ile 45, Leu 54, Phe 56, Met 69, Val 82, Try 84, Phe 90, Ala 103, Leu 105, Leu 116, and Tyr 120. The hydroxyl group of the latter forms an hydrogen bond with one of the nitrogens of the pyrazine ring (Bingham et al., 2004), see figure 4.1.2.

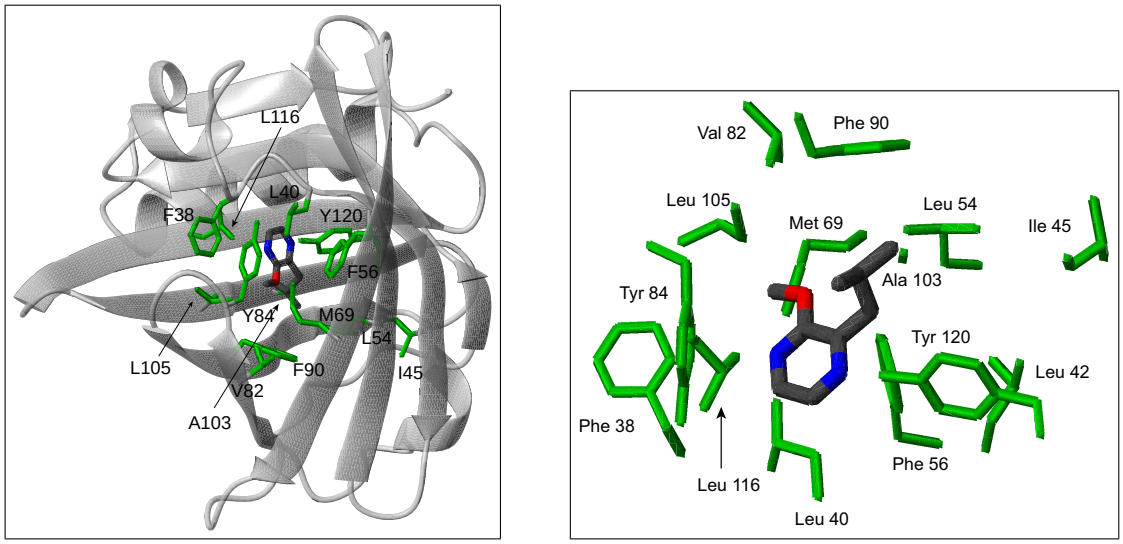

(A) (B)

Figure 4.1.2: The structure of the binding site for IBMP-MUP I-complex in the crystal structure: general view (A) and details (B).

4.1.2 Biological Role of Major Urinary Proteins

MUPs cavity is flexible and able to accommodate a variety of small hydrophobic molecules, in particular, two male pheromones, 2-*sec* butyl 4-5 dihydrothiazole and 3-4 dehydro-*exo*-brevicomin have been found in the urine of male mice and considered to be the most abundant natural pheromones, see figure 4.1.3. Both these pheromones have been proven to influence the female reproductive physiology, and to have direct effects on both female and male behaviours. These small molecules are highly volatile: their persistence in the environment is on the order of few minutes. Scent marks need to be detected by the other mice when the owner is absent; volatile molecules are necessary to attract attention but, at the same time, they need to persist long enough to be detected. A mechanism acting as slow releaser of the pheromones improves

communication among conspecifics. The presence of MUPs increases the persistence of the pheromones to several hours, decreasing the rate at which territorial marks would need to be refreshed. A mouse can thus mark a wider territory and, at the same time, decrease the danger of being caught in the same location by a predator. These advantages are balancing the dissipation of the energetically valuable protein that is synthetised only to be spread into the environment. MUPs are characterized by a huge number of isoforms that are codified in the genes, and do not result from post-translational modifications. The major changes are concentrated in the B, C and D strands of β-sheets, and the loops connecting them (Beynon et al., 2002). The urine of wild mice contains by several MUPs; the isoforms and relative concentrations being characteristic of each mouse. Beynon and co-workers (Beynon and Hurst, 2004) proved that polymorphism in MUPs is a sort of fingerprint for each mouse, allowing other mice to correctly relate to the scent of the owner. Infact, the stable composition of the urine for each individual is assured by the high resistance to degradation of these proteins and by the fact that an individual expresses the same MUPs pattern throughout his life.

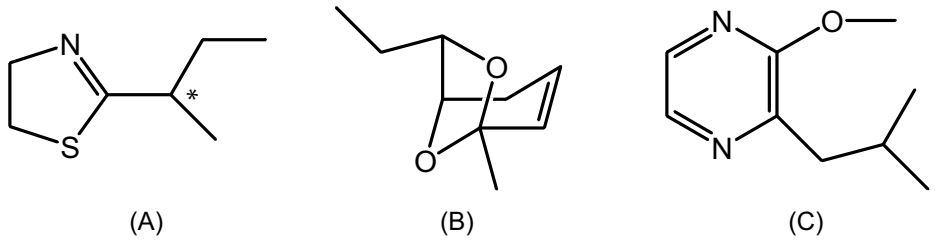

Figure 4.1.3: The structure of the two most abundant natural pheromones 2-*sec* butyl 4-5 dihydrothiazole (A), 3-4 dehydro-*exo*-brevicomin (B), and of the 2-methoxy-3-isobutylpyrazine (C).

1	E E A S S T G R N F N V E K I N G E WH T I I L A S D K R E
31	K I E D N G N F R L F L E Q I H V L E K S L V L K F H T V R
61	D E E C S E L S M V A D K T E K A G E Y S V T Y D G F N T F
91	T I P K T D Y D N F L M A H L I N E K D G E T F Q L M G L Y
121	G R E P D L S S D I K E R F A Q L C E E H G I L R E N I I D
151	L S N A N R C L Q A R E

Table 4.1.1: Secondary sequence of MUP I.

4.2 Protein Assignments: Application on Major Urinary Protein I

Although apo-MUP I has been assigned before by Abbate, (Abbate et al., 1999), a few differences in the samples called for a re-assignment of the frequencies. Our sample has been precipitated from ethanol to eliminate endogenous ligands, while in Abbate ^{13}C, and ^{15}N enriched sample, sugar molecules have been detected (Lücke et al., 1999). Furthermore, the samples have been dissolved in phosphate buffers with sightly different pH: 7.2 for Abbate and 7.4 in our case. The ligand used in our studies is 2-methoxy-3-isobutylpyrazine, IBMP, that induces different shifts in the frequencies of our protein-ligand complex with respect to the complex with one of the natural pheromones, the 2-*sec* butyl 4-5 dihydrothiazole.

In the following chapter, we will briefly revise procedures for protein assignments, with particular focus on protein backbone assignment.

4.2.1 Resonance Assignment Procedure

The first step in an NMR study consists in the assignment of each frequency to a specific nucleus in the protein under investigation. The routine method is based on three types of information: chemical shift environments, through-bond interactions (via scalar couplings), and through-space interactions (via dipolar couplings). Different strategies are used depending on the size of the protein, but general guidelines can be traced.

At the beginning, the proton (or carbon) frequencies are categorized, based on their chemical shifts: for the vast majority of proteins, amide protons (H^N) resonate between 10.0 and 6.5 ppm, and alpha protons (H^α) between 6.0 and 3.5 ppm. Kraulis (Kraulis, 1994) further separates these ranges depending on the amino-acid type; nowadays, similar tables are available for carbon and nitrogen shifts.

Through-bonds interactions are used to connect resonances of one atom with those of neighbour atoms, usually up to three bonds. Another useful property of three-bond scalar couplings is their dependence on the dihedral angle formed by the three covalent bonds, as first pointed out by Karplus (Karplus, 1959). Dipolar couplings depend on the spatial distance between the atoms investigated and are thus used to obtain information on the three-dimensional fold of the protein. For small non-labelled proteins they can be used to sequentially assign the spin systems.

4.2.2 The Experiments

In a 1D NMR proton spectrum, the amide protons are the best resolved, and are the reference used as starting point for backbone assignment. Observation of direct and relayed through-bond connectivities between amino protons and backbone nuclei are used to identify the spin systems. The first nucleus to be connected to H^N by HSQC is the directly bonded nitrogen, using the one-bond H-N scalar coupling ($\approx$ -90 Hz). Sequential information is obtained using the 3D HNCO method which correlates amide H and N chemical shifts of one residue with the chemical shift of the preceeding carbonyl C' carbon by using the one-bond N-C' scalar coupling ($\approx$ 15 Hz). The sequential connectivities provided by this experiment are very useful, in addition to connectivities given by HN(CA)CO. The latter experiment provides both intraresidue (between H_i^N, N_i and C'_i) and interresidue connections (between H_i^N, N_i and C'_{i-1}). This is possible because one-bond $J(N_iC_i^\alpha)$ and two-bonds $J(N_iC_{i-1}^\alpha)$ scalar couplings are similar ($^1J_{NC^\alpha} \approx$ 7-11 Hz, $^2J_{NC^\alpha} \approx$ 4-9), so that a mixture of intraresidue (i.e. N_i C_i^α) and sequential coherence transfer processes (i.e. N_i C_{i-1}^α) will occur during the transfer time.

A similar approach is used to assign C^α carbons: in this case the sequential connectivities are given by HN(CO)CA, where the magnetization is transferred to the C^α of the preceeding residue through the carbonyl carbon ($^1J_{C'C^\alpha} \approx$ 55 Hz), while the sequential and intraresidue connectivities are obtained by HNCA. Again, the one- and two-bond N-C^α scalar couplings are active during the magnetization transfer from nitrogen to both C_i^α and C_{i-1}^α, resulting in a mixture of two processes. At this stage, all the heavy backbone atoms plus the amide protons have been assigned.

Another couple of experiments that can be used to confirm C^{α} assignments and to add C^{β} ones is the CBCANH and CBCA(CO)NH; in analogy to HNCA/HN(CO)CA and to HNCO/HN(CA)CO, the CBCA(CO)NH gives sequential correlations while CBCANH gives both inter- and intra-residue correlations.

A schematic representation of the most common 3D experiments used for assignment is presented in figure 4.2.1.

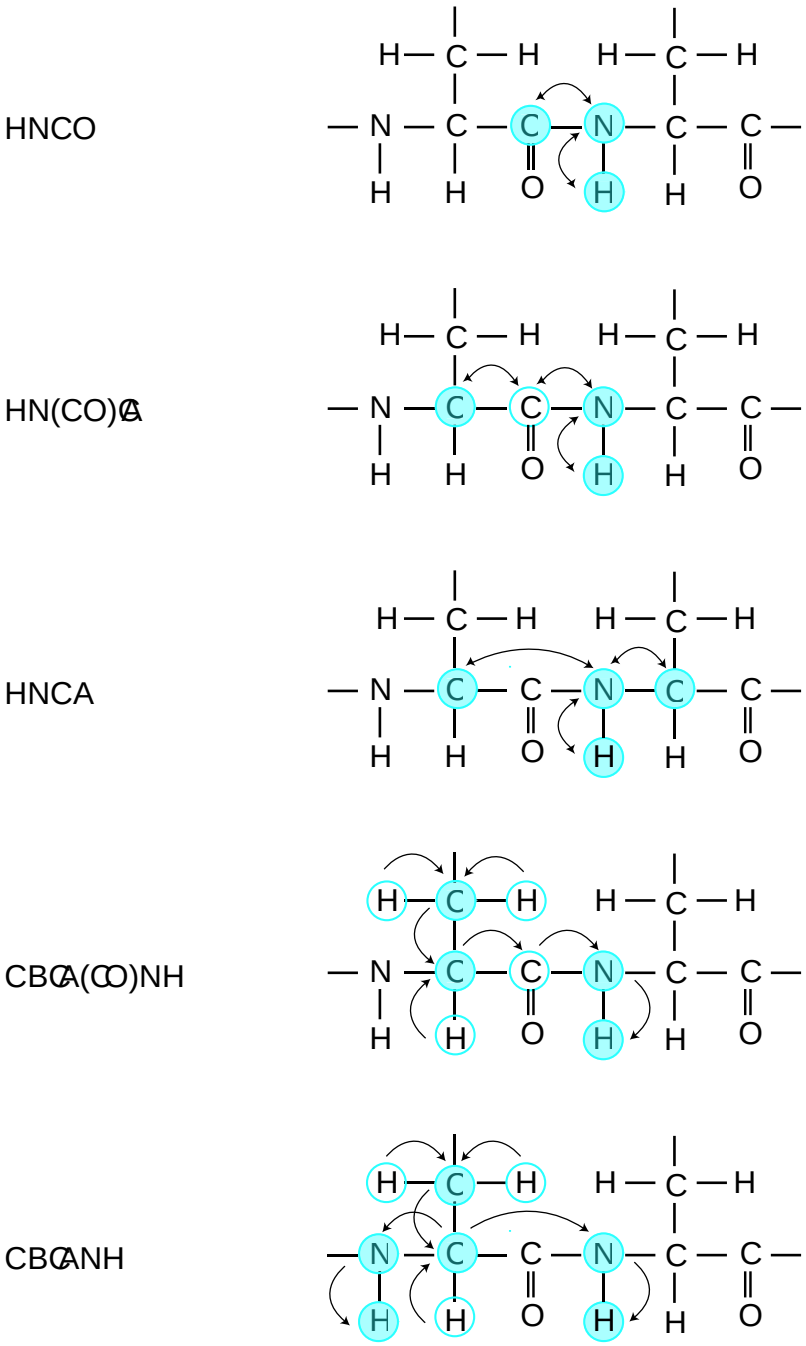

Figure 4.2.1: Schematic view of the triple resonance experiments used in sequential assignment. Only the experiments that have been discussed in the text are shown. Filled circles represent nuclei which frequencies are detected, while open circle indicates nuclei where the magnetization is transferred. The arrows indicate the magnetisation path during the experiment.

4.2.3 MUP I Assignment

For our studies the backbone assignment only is necessary, so the side-chain assignment was not carried out. Both apo- and holo-MUP I samples (Bingham et al., 2004) were dissolved in 10% D_2O/ 90% H_2O, and the pH was adjusted to 7.4 with phosphate saline buffer. The sequential assignments were obtained by 3D HNCO/HNCA and CBCA(CO)NH/CBCANH methods at 300 and 308 K. Backbone assignment was carried out using the Sparky 3 software package (T. D. Goddard and D. G. Kneller, University of California, San Francisco, USA). In figure 4.2.2 (A) and (B), the HSQC with peak assignments are shown for both apo- and holo-MUP I.

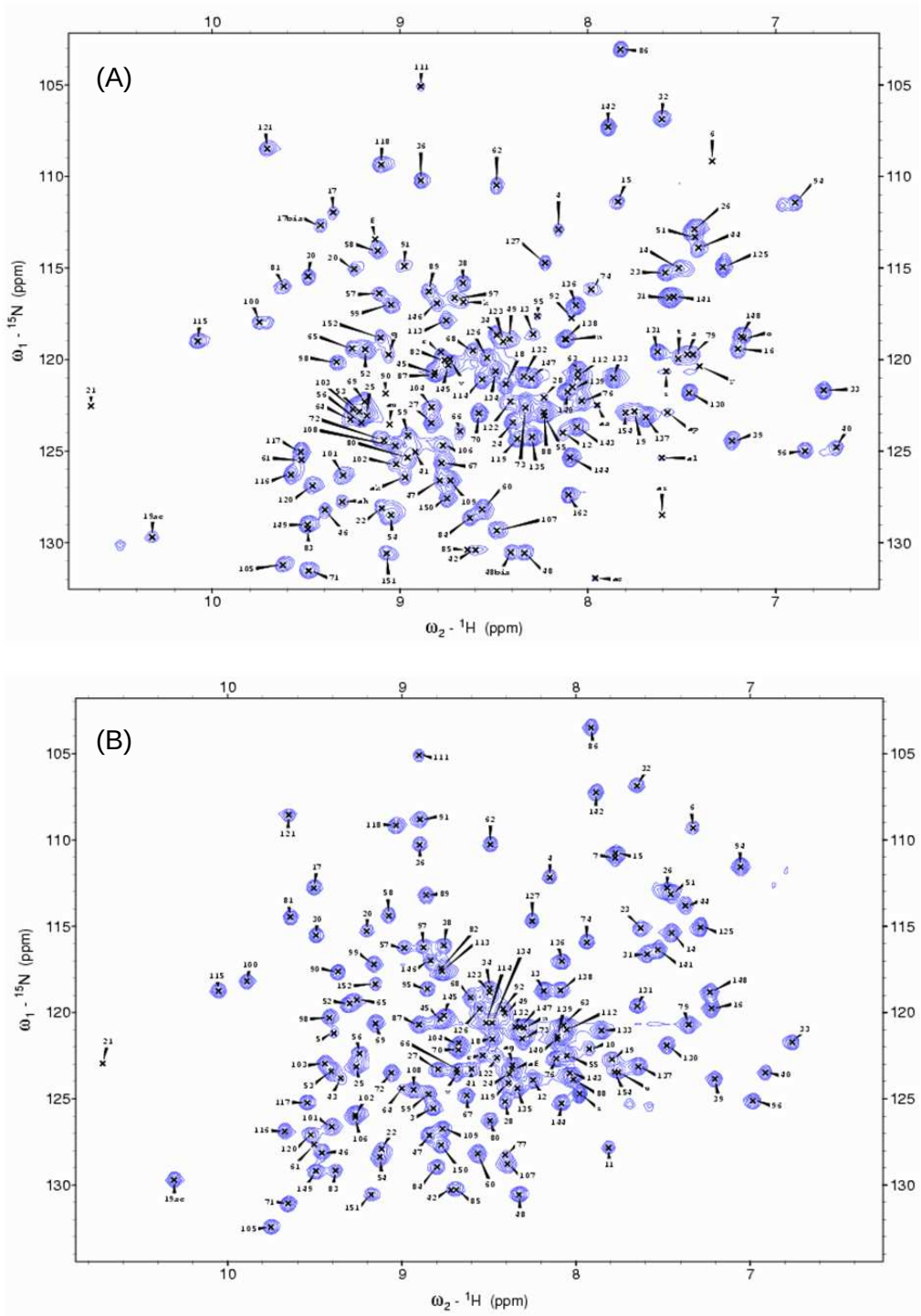

Figure 4.2.2: Partial ^{15}N, ^{1}H correlation spectra (HSQC) with assignment of apo- (A) and holo-MUP I (B), at T = 308 K and B_0 = 14 T (600 MHz).

Chapter 5

Isothermal Titration Calorimetry

Interactions between biological macromolecules are of fundamental importance in an enormous variety of biological processes like protein-ligand, protein-protein, protein-nucleic acid interactions. A deeper understanding of these interactions is only possible if the nature of the forces involved in the stabilization are known, i.e. the thermodynamic parameters associated with the binding process are known. The energy evolved in a binding reaction can be determined to measure the binding equilibrium constant: isothermal titration calorimetry (ITC) is the most quantitative method available to determine the thermodynamic properties. In a single experiment, ITC allows simultaneous determination of all binding parameters: binding constant K_B, enthalpy ΔH^0 and the stoichiometry of the interaction n (Blandamer, 1998; Holdgate, 2001; O'Brian et al., 2001). The Gibbs energy, ΔG^0, can be calculated from K_B using the relation:

$$\Delta G^0 = -RTln(K_B)$$

Once ΔG^0 is computed, the entropy can easily been reckoned. Finally the heat capacity can be derived if a series of experiments is performed while varying the temperature.

In this chapter, I will give a short overview on the potentiality and the limits of this powerful technique.

5.1 Instrument

Due to its high signal-to-noise ratio and the small volume of macromolecule solution required, the OMEGA isothermal titration calorimeter has become the dominant type and brand of calorimeter (Wiseman et al., 1989). In this instrument, small aliquots of one reactant are introduced and mixed with the solution containing the other reactant in a stepwise manner, and the heat developped or absorbed by the reaction is measured and converted into enthalpy at each step. The calorimeter consists of a pair of chemically resistant cells, the reference and the sample cells, see figure 5.1.1. Both are placed into an adiabatic jacket, and connected with independent heaters to thermoelectric devices (thermocouples) which measure the difference in temperature between the two cells and also between the cell and the jacket. During the experiment the two cells are mantained at the same temperature by heating or refrigerating the sample cell: the applied voltage needed to keep the difference in temperature equal to zero is the measured signal. Exothermic reactions will heat the sample cell; the sample cell will no longer need to be heated and the computer will register a negative signal, while for endothermic reaction the opposite behaviour is registered. The integration

of this time-dependent electric signal gives the amount of heat evolved or absorbed by the reaction. To avoid heat losses from the cells to the surroundings, the external jacket is mantained at the same temperature as the cells by an independent heater. To minimize systematic errors, the reference cell is normally filled up with the same buffer used to dissolve the macromolecule in the sample cell. The ligand is injected into the sample cell by a syringe, the needle of which is used to stir the solution.

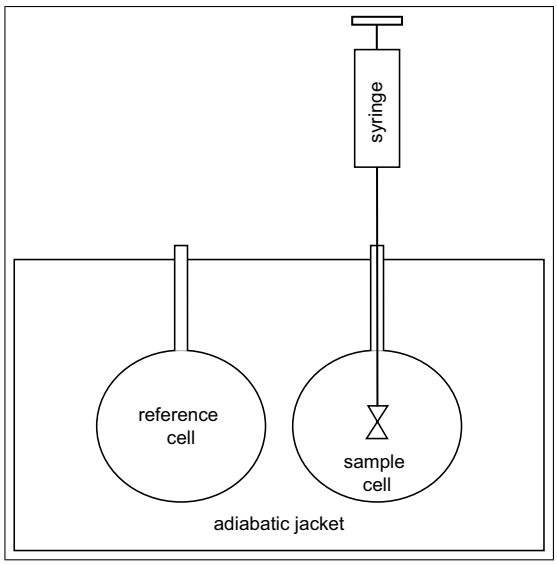

Figure 5.1.1: Schematic diagram of an ITC instrument. Two cells are contained into an adiabatic jacket, a syringe is inserted into the sample cell, both to inject the titrant and to stir the solution.

5.2 The Wiseman Equation

We shall discuss the Wiseman equation in the simple case of a single-site reaction (Wiseman et al., 1989):

$$M + L = ML \tag{5.2.1}$$

where M is the titrand, L the titrant and ML the complex, or in our case, M is a macromolecule, and L a ligand. The binding constant is defined as:

$$K_B = \frac{[ML]}{[M][L]} \tag{5.2.2}$$

The total amount of macromolecule M_T and of ligand L_T are known quantities at each step, while the concentration of free protein, of the free ligand and of the complex are changing after each injection according to the binding constant, therefore they are not known. So it is easier to consider the total titrant and titrand concentrations instead of the time-dependent free ones.

$$M_T = [M] + [ML] = \frac{[ML]}{K_B[L]} + [ML] \tag{5.2.3}$$

$$L_T = [L] + [ML] \tag{5.2.4}$$

After solving eq. 5.2.4 for [L] and substituting it in eq. 5.2.3, we obtain a quadratic expression in [ML]:

$$[ML]^2 - [ML]\left(\frac{1}{K_B} + L_T + M_T\right) + M_T L_T = 0 \tag{5.2.5}$$

The above eq. 5.2.5 has only one real root value:

$$[ML] = \frac{(L_T + M_T + 1/K_B) - \sqrt{(L_T + M_T + 1/K_B)^2 - 4M_T L_T}}{2} \tag{5.2.6}$$

Differentiating and substituting, $X_R = L_T/M_T$, $c = K_B M_T$ and $r = 1/c = 1/K_B M_T$, in eq. 5.2.6 yield:

$$\begin{aligned} \frac{d[ML]}{dL_T} &= \frac{1}{2}\left(1 - \frac{2(X_R + 1 + r) - 4}{2\sqrt{(X_R + 1 + r)^2 - 4X_R}}\right) \\ \frac{d[ML]}{dL_T} &= \frac{1}{2} + \frac{1 - X_R - r}{2\sqrt{(X_R + 1 + r)^2 - 4X_R}} \end{aligned}$$

The change in M_T can be related to the heat changes as:

$$dQ = d[ML]\Delta HV \tag{5.2.7}$$

$$\frac{dQ}{dL_T} = \Delta HV\left(\frac{1}{2} + \frac{1 - X_R - r}{2\sqrt{(X_R + 1 + r)^2 - 4X_R}}\right) \tag{5.2.8}$$

where Q is the heat developped or absorbed, ΔH is the molar heat of binding and V the cell volume. The Wiseman isotherm (Wiseman et al., 1989) relates the stepwise change in heat of the system normalized with respect to moles of ligand added per injection dQ/dL_T to the absolute ratio of ligand to receptor concentration L_T at any point in the course of the titration.

Using the Wiseman equation, it is possible to simulate binding curves and a few of them are shown in figure 5.2.1. As it can be seen from figure 5.2.1, the curve shape is strongly dependent on the c value, a dimensionless number obtained multiplying K_B with M_T. The best results are obtained for an interval of c values between 1000 and

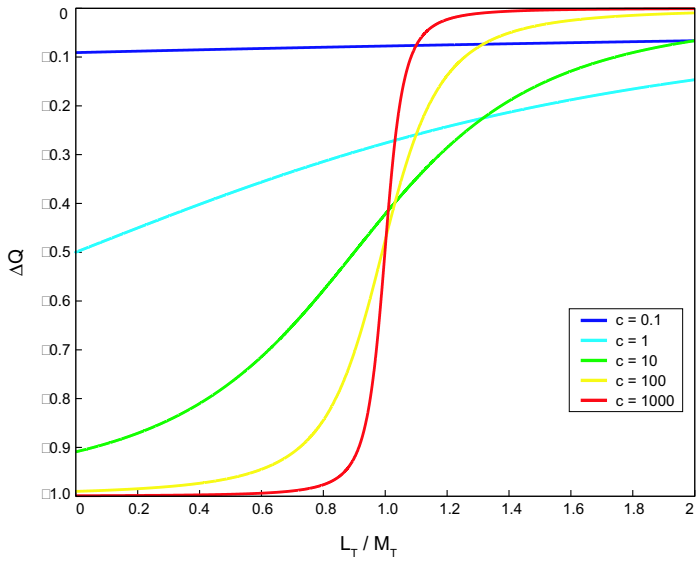

Figure 5.2.1: Simulated Wiseman binding isotherms for various values of c, that is, the product of total protein concentration with the association constant, $c = 1/r = K_B M_T$.

1 (Wiseman et al., 1989). So, in the design of a new experiment, it is vital to find the optimal titrand concentration to fall within the ideal c value range.

Assuming a constant protein concentration, the value of K_B can be used to distinguish three cases: very tight binding, where $c \to \infty$, intermediate-strong binding, with c values falling within the ideal range and weak binding where c is smaller than one. In the first case, the ligand immediately binds to saturation and the curve has a rectangular shape with a slope tending to infinity. Decreasing the protein concentration will result in a smaller c allowing more accurate analysis. Unfortunately, in a few cases, the optimal concentration is too small to yield measurable heat changes. For intermediate binding strenght, the molar heat of binding ΔH can be easily extracted from the total area under the curve and from its shape. In the third case the curve is almost flat, see figure 5.2.1, leading to an inaccurate extrapolation of K_B values.

Again, changing the protein concentration could restore the best conditions, but for some systems higher titrand concentrations might not be accessible due to insolubility or aggregation. To overcome this problem, a displacement experiment might be performed: the solution in the cell initially contains the saturated complex of the receptor with a low affinity ligand instead of only the macromolecule. A high affinity ligand displaces the low affinity one and the usual parameters can be obtained if the difference in binding enthalpy is appropriate (Khalifah et al., 1993; Hu and Eftink, 1994). A recent publication (Turnbull and Daranas, 2003) discusses the extention of ITC measurements to low c values, if extreme care is used in the design and in the execution of the experiments.

5.3 Measurements on Major Urinary Protein

This work has been carried out in professor S. W. Homans' laboratory in Leeds, UK, and has been published in the *Journal of the American Chemical Society*.

ITC experiments were conducted using a MicroCal VP-ITC unit operating at 300 and 308 K. The presence of air bubbles in the ITC solution is a source of error due to the different heat capacity of the gas with respect to the liquid. As a consequence, before running the experiment, all solutions are generally degassed in vacuo. The presence of air bubbles can seriously affect the integration of the heat developped as it can be easily seen in figure 5.3.1. Due to its high volatility, the 2-methoxy-3-isobutylpyrazine ligand was not degassed but solved in a degassed Phosphate Saline Buffer, PBS, and all concentrations were measured by UV adsorption (Major Urinary Protein I ϵ_{280}

$= 10650\ M^{-1}cm^{-1}$; IBMP $\epsilon_{220} = 4980\ M^{-1}cm^{-1}$) shortly before the titration, M_T concentration being around 20 μM.

The usual ITC procedure consists of two protein-ligand titrations and one or two buffer-ligand titrations. Although not usually considered when explaining the ITC theory, a significant contribution to the total heat change comes from the dilution of the ligand in the cell; a buffer-ligand ITC is therefore performed to measure and subtract the contribution of dilution from the heat of binding. In this manner, the ITC results, i.e. protein-ligand minus buffer-ligand, are only representative of the ligand-protein interaction. After the syringe insertion, an equilibration time is needed; during this time, the ligand and the protein diffuse trough the needle tip, providing a local change in concentrations and formation of the complex. To compensate this process, the first injection consists of a small amount of ligand that is routinely discharged. Figure 5.3.1 shows in the top the typical heat changes vs time and in the bottom the heat divided by the ligand concentration vs molar ration between ligand and protein. These latter points were fitted by Origin[1] using the standard one-site model supplied by MicroCal, which is based on the Wiseman isotherm, see eq. 5.2.8. The errors are calculated on repeated experiments. The resulting thermodynamic parameters are shown in table 5.3.

IBMP has an affinity in the micromolar range; it has favourable contributions from the binding enthalpy (ΔH_b) and an unfavorable binding entropy (ΔS_b). The binding

[1] Origin, OriginLab Corporation.

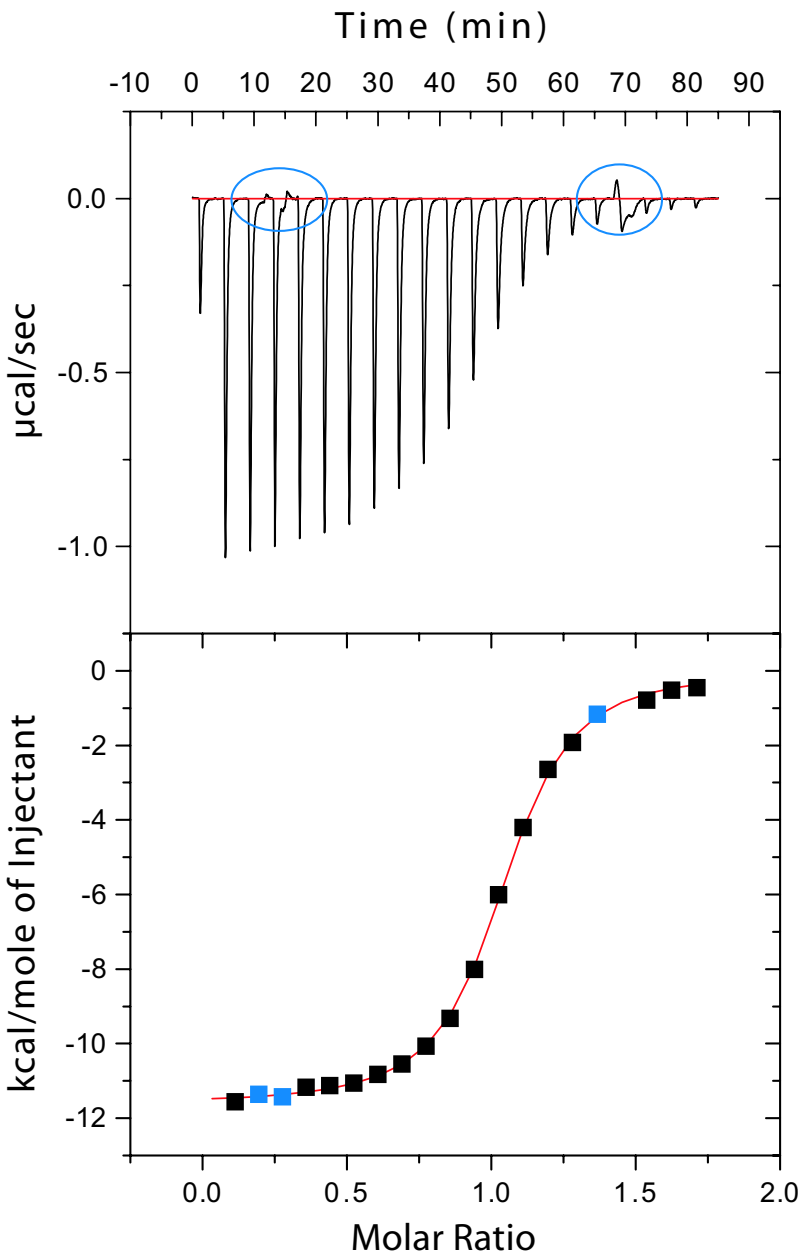

Figure 5.3.1: Top: ITC heat variation after each injection. Note that the first peak corresponds to a small amount of injected ligand. The presence of air bubbles can be detected from the anomalies of the peak shapes, as highlighted by the blue circles. In this case, the amount of air developped is small and leads to negligible errors, as it can be seen from the integrated points, highlighted in blue, in the bottom figure. Bottom: the corrected heat developped per mole of injectand which constitutes the Wiseman isotherm.

Temp. $[K]$	ΔH^0 $[KJ/mol]$	Stoichiom.	$T\Delta S^0$ $[KJ/mol]$	ΔG^0 $[KJ/mol]$	K_B $[\mu M]$
308	-47.89 ± 0.86	1.01 ± 0.02	-9.39 ± 0.87	-38.5 ± 0.11	0.30 ± 0.01
300	-49.79 ± 0.29	0.98 ± 0.02	-12.34 ± 0.20	-37.45 ± 0.21	0.33 ± 0.01

Table 5.3.1: Thermodynamic parameters for the binding of IBMP to Major Urinary Protein I derived from ITC at two temperatures. The errors derive from repeated experiments.

site of Major Urinary Protein I is very hydrophobic, and it can allocate only one ligand which forms an hydrogen bond between one of its ring nitrogens and the hydroxyl group of Tyr 120 in Major Urinary Protein I (Bingham et al., 2004). The creation of a single hydrogen bond and the expulsion of four water molecules from the cavity could account for a value of ΔG between 1.5 and 0.6 KJ/mol (Pace et al., 1996). The discrepancy between the expected and the observed thermodynamic values is related to the scale of the interactions which are considered: the expected values are estimated from local detailed interactions while ITC measures global thermodynamic changes.

Chapter 6

Conformational Exchange: Overview and Applications to Major Urinary Protein I

Large molecules like proteins have many degrees of internal flexibility that are usually fundamental for their functions. NMR has the unique property to detect mobility on different time scales. Motions which occur between pico- and nano-seconds are referred to as fast motions, and include mainly vibrations and side chain rotations. These motions are generally sampled measuring the longitudinal R_1, the transverse R_2 and the NOE relaxation rates. These three rates are then combined to compute the so-called order parameter, S^2, with values ranging between one and zero; a higher value indicates lower mobility. This technique has been applied to apo-MUP I and its complex with 2-methoxy-3-isobutylpyrazine (Bingham et al., 2004). Slower motions, between micro- and milli-seconds, are detected by relaxation dispersion curves of CPMG and $R_{1\rho}$ measurements. The former methods have been used to detect motions in both apo- and holo-MUP I.

6.1 Chemical Exchange

The term *chemical exchange* includes the motional processes involving the making and breaking of chemical bonds and the changes of conformations in a relatively rigid segment of the protein. Chemical exchange processes spam over a very wide range of timescale, from nano seconds to seconds or longer.

Chemical exchange processes are usually visualized in term of chemical reactions where an initial conformation A moves toward a second conformation B:

$$\mathrm{A} \underset{k_-}{\overset{k_+}{\rightleftharpoons}} \mathrm{B}$$

where k_+ and k_- are the conversion rates. Although intermediate steps, or a different stoichiometry of the reactions, cannot be excluded *a priori*, it is generally assumed that there are only two states: A and B. It is also assumed that the two different chemical environments are responsible for a difference in chemical shifts between the nuclei in the two conformations, ω_A and ω_B. Furthermore, the system instantaneously jumps between the two states, so no intermediate states are present. The ensemble of these approximations is called *the two-site exchange model*. If the system is at equilibrium, then $p_A k_+ = p_B k_-$ and p_A and p_B are referred to as the equilibrium populations. In the text that follows p_A and p_B are always meant as equilibrium populations. Since the sum of the population is $p_A + p_B = 1$, the conversion rates can be written as $k_+ = p_B k_{ex}$ and $k_- = p_A k_{ex}$, where the exchange rate $k_{ex} = k_+ + k_-$ provides a measure of the time-scale of the dynamics when compared with the difference in chemical shift between the two sites, see section 6.1.1.

6.1.1 Carr-Purcell-Meiboon-Gill Experiments

In this section, we merely present results of major interest without entering into the details of their derivation. The considered experiment is the following: a non-selective $\pi/2$-pulse is used to create single quantum coherence (SQC) I_x before a train of π-pulses is applied periodically. For the rest of this thesis, the following conventions are used: τ_{cp} stands for the period between two π-pulses. If the intervals τ_{cp} between the π-pulses are chosen correctly, the evolution of the chemical shifts is refocused. In other words, the order of the coherence p is reversed by the π-pulses, and at $t = \frac{1}{2}\tau_{cp}$ an echo is observed (the phase of the magnetization is equivalent to the initial phase just after the excitation pulse). The effect of the exchange process depends on the difference in the chemical shift frequencies of the two sites, $\Delta\omega = \omega_A - \omega_B$, as compared to the exchange rate, k_{ex}. Depending on these two values, it is possible to divide the chemical exchange time scale in three major areas: fast, intermediate and slow exchange.

$$k_{ex} > \Delta\omega \qquad \textit{Fast exchange}$$

$$k_{ex} \approx \Delta\omega \qquad \textit{Intermediate exchange}$$

$$k_{ex} < \Delta\omega \qquad \textit{Slow exchange}$$

A general expression for the transverse relaxation rate constant, $R_2(1/\tau_{cp})$, valid for all exchange time-scales has been derived by Carver and Richards (Carver and Richards, 1972):

$$R_2^{obs}(1/\tau_{cp}) = \frac{1}{2}\left\{R_{2A}^0 + R_{2B}^0 + k_{ex} - \frac{1}{\tau_{cp}}\, cosh^{-1}\left[D_+ cosh(\eta_+) - D_- cos(\eta_-)\right]\right\} \tag{6.1.1}$$

With

$$\begin{aligned} D_{\pm} &= \frac{1}{2}\left[\pm 1 + \frac{\Psi + 2\Delta\omega^2}{(\Psi^2+\zeta^2)^{1/2}}\right] \\ \eta_{\pm} &= \frac{\tau_{cp}}{\sqrt{2}}\left[\pm\Psi + (\Psi^2+\zeta^2)^{1/2}\right]^{1/2} \\ \Psi &= (R^0_{2,A} - R^0_{2,B} - p_A k_{ex} + p_B k_{ex})^2 - \Delta\omega^2 + 4p_A p_B k_{ex}^2 \\ \zeta &= 2\Delta\omega\left(R^0_{2,A} - R^0_{2,B} - p_A k_{ex} + p_B k_{ex}\right) \end{aligned}$$

Where $R^0_{2,i}$ is the auto-relaxation rate (expressed in s^{-1}) at infinitely large pulse repetition frequency, which corresponds to the absence of chemical exchange, and the other terms have been mentioned earlier. Due to technical problems, it is not always possible to pulse fast enough to average out the contributions of the exchange. Under these conditions $R_2(1/\tau_{cp} \to \infty)$ can be taken as an approximate value of $R^0_{2,i}$, which can be estimated more precisely using other techniques. Due to the complexity of eq. 6.1.1 it is very difficult to understand the behaviour of the relaxation dispersion curves in the presence of exchange. Thus, several approximate expressions have been derived as a function of the time-scale regime and of the relative ratio between the populations. These approximations are shortly described below.

Ishima and Torchia have derived an approximate expression which is valid for all time scales provided that $p_A \gg p_B$ (Ishima and Torchia, 1999):[1]

$$R_2^{obs}(1/\tau_{cp}) = R_2(1/\tau_{cp} \to \infty) + p_A p_B \Delta\omega^2 k_{ex} / \left[k_{ex}^2 + \left(p_A^2\Delta\omega^4 + 144/\tau_{cp}^4\right)^{1/2}\right] \quad (6.1.2)$$

[1] In case $p_A \ll p_B$, it is sufficient to exchange the labels of the two and change the sign in $\Delta\omega$.

In the fast-exchange regime and in the approximation of skewed populations, eq. 6.1.1 can be approximated to give (Luz and Meiboom, 1963):

$$R_2^{obs}(1/\tau_{cp}) = R_2(1/\tau_{cp} \to \infty) + R_{ex}\left[1 - \frac{2\,tanh\,(k_{ex}\tau_{cp}/2)}{k_{ex}\tau_{cp}}\right] \quad (6.1.3)$$

$$R_2^{obs}(1/\tau_{cp}) = R_2(1/\tau_{cp} \to \infty) + \frac{p_A p_B \Delta\omega^2}{k_{ex}}\left[1 - \frac{2\,tanh\,(k_{ex}\tau_{cp}/2)}{k_{ex}\tau_{cp}}\right] \quad (6.1.4)$$

where the expression of $R_{ex} = (p_A p_B \Delta\omega^2)/k_{ex}$, in eq. 6.1.4 is valid in the limit of skewed populations only. Tollinger et al. have derived an expression which is valid in the limit of slow exchange (Tollinger et al., 2001):

$$R_2^{obs}(1/\tau_{cp}) = R_{2A} + k_+\left[1 - \frac{sin\ (2\Delta\omega\tau_{cp})}{2\Delta\omega\tau_{cp}}\right] \quad (6.1.5)$$

$$R_2^{obs}(1/\tau_{cp}) = R_{2A} + p_B k_{ex}\left[1 - \frac{sin\ (2\Delta\omega\tau_{cp})}{2\Delta\omega\tau_{cp}}\right]$$

As seen before in eq. 6.1.1, R_{2A} stands for the transverse relaxation rate of site A in the absence of exchange. Using this simple equation, the oscillations which occur in the slow pulsing regime can be better interpolated.

The chemical exchange contribution to relaxation is defined as: $R_{ex} = R_2(1/\tau_{cp} \to 0) - R_2(1/\tau_{cp} \to \infty) = \Delta R_2(0, \infty)$. Using eq. 6.1.1 it is possible to verify that R_{ex} depends quadratically on $\Delta\omega$ for fast exchange, while it is independent in the case of slow exchange. Using this field dependence, Millet et al. defined a parameter, called α, which is function of the ratio $k_{ex}/\Delta\omega$ and thus can be used for defining the exchange time-scale (Millet et al., 2000).

6.1.2 Effects of Temperature on Chemical Exchange

The temperature dependence of the chemical exchange rates arise through the temperature dependence of three parameters: the exchange constants $k_{\pm}$, the populations of the two sites p_A and p_B and the variations in chemical shifts of the two sites which could lead to a difference in $\Delta\omega$. This latter contribution is usually considered to be negligible to a first approximation (Palmer et al., 2001). Thus, the temperature dependence of R_{ex} is given by the Arrhenius equation: $k_+ = A_0\, exp\,\{-E_a/(k_B T)\}$ and by the Boltzmann distribution: $p_A = \{1 + exp\,[-\Delta G/(k_B T)]\}^{-1}$, where A_0 is a pre-exponential factor, E_a the activation energy of the process and ΔG is the difference in the free energy between the two states A and B (Mandel et al., 1996). Increasing the temperature increases k_{ex}: this shifts $k_{ex}/\Delta\omega$ to larger values. As a consequence, R_{ex} increases with the temperature if the exchange process is in the slow limit, and decreases in the opposite case. Thus, the sign of the temperature dependence of R_{ex}, dR_{ex}/dT, indicates whether the exchange is in the fast or in the slow regime.

6.2 Application of Carr-Purcell-Meiboon-Gill Experiments to Major Urinary Protein I

6.2.1 The Experiments: Materials and Methods

The sequences used in this study derive from a modification of the relaxation-compensated CPMG sequences A and B published by Palmer and co-workers (Palmer et al., 2001). The main modification consists in the inclusion of pulses on both $^{13}C'$ and

$^{13}C^{\alpha}$ to minimize the effects of scalar couplings between ^{15}N and the neighbouring carbons. Data were collected with intervals (τ_{cp}) between the two π pulses of 1.0, 1.5, 2.0, 4.0, 6.6, 10.8 and 21.5 ms. Each 2D dataset consisted of 64 and 512 points in the t_1 and t_2 dimensions respectively. For each t_1 increment 32 scans were accumulated for the faster repetition rates while 64 scans were necessary to obtain a good signal to noise ratio for the experiments with τ_{cp} larger than 4 ms. The spectral widths were 1824 and 8389 Hz in the ω_1 and ω_2 dimensions. The experiments have been performed at 308 K. Data processing has been performed using the GNU Package NMRPipe/NMRDraw/NlinLS (Delaglio et al., 1995). The whole series of experiments have been repeated twice both for checking consistency of the rates and for averaging of the errors.

Relaxation rates were obtained by least-squared fitting of the decays to exponential functions (Matlab, 1992, Matlab Reference Guide, Natick, Massachusetts). Errors of the decay rates were estimated by Monte-Carlo analysis using 200 synthetic data points. The rates can be found in tables 6.3.1 and 6.3.2 for apo- and holo-MUP I respectively. The relaxation dispersions plots have been fitted using eq. 6.1.2 and eq. 6.1.3, and the fitted value for apo- can be found in table 6.3.3. The errors in the dynamic parameters have also been estimated by Mont-Carlo analysis, as done previously for the errors in the decay rates. All residues have been fitted, even those where no *a priori* estimate of the presence of chemical exchange could have been obtained, so that they look flat.

6.3 Results and Discussions

In figure 6.3.1 a few relaxation dispersion plots are shown for apo- and holo-MUP I at 308 K. In the apo form, up to 92 residues were retained for the analysis, after the rejection of all residues where overlap in the spectra, or low signal to noise ratio were present. Among the remaining residues, up to 11 show detectable presence of chemical exchange. Only 2 residues are located in loops, i.e. in regions where one expects more mobility, all others, 9, are located in the β-barrel. It is also interesting to notice that four residues, Met 69, Val 70, Ala 71 and Asp 72 are located in the β-D sheet, spatially close to other two exchanging residues, Ser 81 and Val 82, which are located in the β-E sheet. Indeed, Asp 72 gives unambiguous NOEs with both the previous residues and it is probably connected with Ser 81 by two hydrogen bonds (Lücke et al., 1999). This suggests the presence of a concerted motion in this part of the β-barrel, which could be necessary to allow the pheromone to reach the cavity. No presence of chemical exchange has been found in the long terminal α-helix, see figure 6.3.2A. From the data in table 6.3.3, two main exchange processes are present in apo-MUP I: one with k_{ex} of about 700 s^{-1}, and the second with exchange constant of about 1500 s^{-1}.

For holo-MUP I 91 residues have been retained for the analysis, using the same criteria for discarding the residues as for the apo form. Using strictly the same procedure for the fitting, chemical exchange has not been found in any residues.

It results from these data, that MUP I becomes less mobile upon binding, and this is in agreement with the increase in backbone order parameter S^2 measured by Bingham

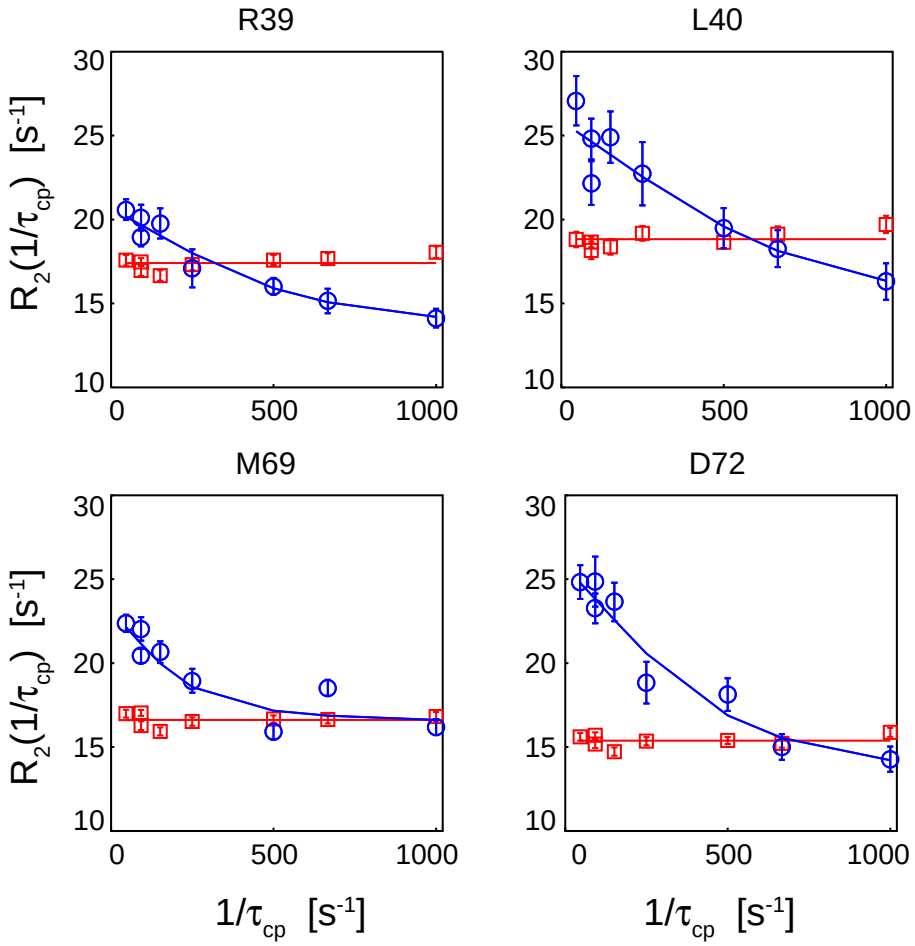

Figure 6.3.1: Relaxation dispersion plots for four residues in both apo- (blue circles) and holo-MUP I (red squard). The curves represent the best fits using eq. 6.1.3 or the average of the values when the relaxation dispersion data are flat.

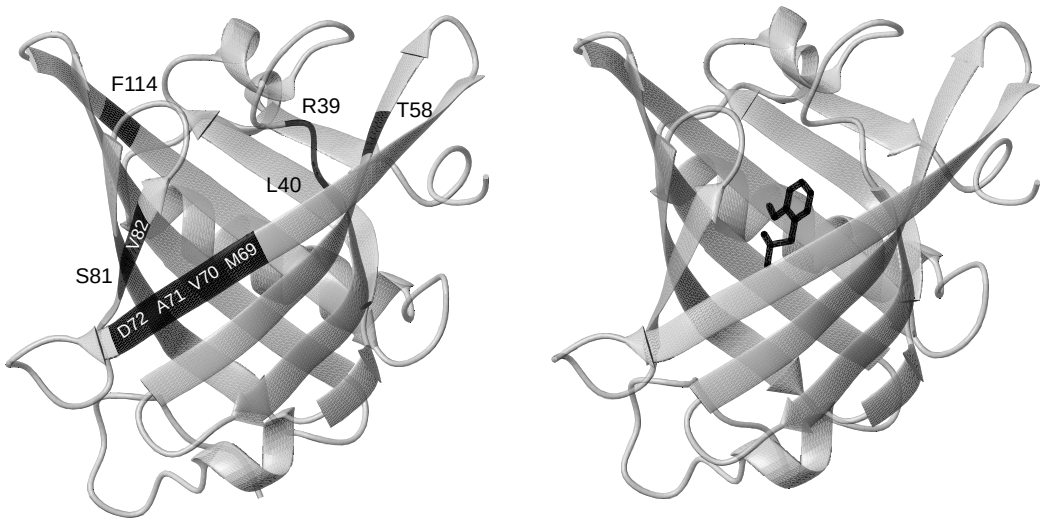

(A) (B)

Figure 6.3.2: Ribbon diagram of apo- (A) and holo-MUP I (B) at 308, where in black are shown the residues where chemical exchange has been found.

et al. (Bingham et al., 2004). Although the two methods measure motions which occur at two different time-scales, a few conclusions can be drawn. Of course, the most important is the agreement in the general behaviour: the loss of dynamics upon complexation. The comparison residue by residue is more difficult, but it is remarkable that only one residue, Thr 58, shows a different behaviour between the two experiments. Chemical exchange has been found in Thr 58 in apo-MUP I only, thus indicating a restriction upon complexation; the opposite behaviour has been found with the Lipari and Szabo methodology (Bingham et al., 2004).

Table 6.3.1: Relaxation rates $R_2(\tau_c)$ for apo-MUP I for different τ_c values with relative errors (308 K, 600 MHz). The first six rates, with τ_c up to 10.8 ms, and the last two data points, with τ_c equal to 10.8 and 21.6 ms, have been recorded with sequence A and B respectively.

Res.	1 $\pm\varepsilon$ [s^{-1}]	1.5 $\pm\varepsilon$ [s^{-1}]	2 $\pm\varepsilon$ [s^{-1}]	4 $\pm\varepsilon$ [s^{-1}]	6.6 $\pm\varepsilon$ [s^{-1}]	10.8 $\pm\varepsilon$ [s^{-1}]	10.8 $\pm\varepsilon$ [s^{-1}]	21.6 $\pm\varepsilon$ [s^{-1}]
K14	15.5 ± 0.7	16.3 ± 0.9	18.1 ± 0.7	19.4 ± 1.3	17.6 ± 0.9	17.6 ± 0.9	17.0 ± 0.6	17.2 ± 0.7
I15	15.8 ± 0.6	17.2 ± 0.7	18.2 ± 0.6	18.3 ± 0.9	18.8 ± 0.7	17.7 ± 0.6	17.1 ± 0.4	17.3 ± 0.5
N16	13.5 ± 0.5	14.0 ± 0.6	15.1 ± 0.5	14.2 ± 0.8	15.1 ± 0.6	15.7 ± 0.5	14.9 ± 0.4	15.6 ± 0.4
G17	14.0 ± 0.9	16.1 ± 1.1	16.5 ± 1.0	19.5 ± 1.7	17.4 ± 1.2	17.3 ± 1.3	16.8 ± 0.8	17.0 ± 0.9
E18	15.5 ± 0.7	15.4 ± 0.7	16.4 ± 0.6	16.7 ± 1.1	17.4 ± 0.8	18.2 ± 0.8	17.4 ± 0.6	18.0 ± 0.7
H20	15.8 ± 1.2	16.3 ± 1.4	17.3 ± 1.2	17.1 ± 1.9	19.0 ± 1.5	17.9 ± 1.3	17.0 ± 1.1	17.7 ± 1.1
I23	14.4 ± 0.5	14.7 ± 0.5	15.5 ± 0.5	15.4 ± 0.8	16.2 ± 0.7	15.2 ± 0.5	15.2 ± 0.4	16.9 ± 0.4
L24	15.1 ± 0.5	15.5 ± 0.4	15.8 ± 0.5	15.3 ± 0.7	16.0 ± 0.5	14.6 ± 0.4	14.2 ± 0.3	14.6 ± 0.3
D27	13.5 ± 0.3	13.7 ± 0.4	15.0 ± 0.4	14.3 ± 0.5	15.0 ± 0.4	13.8 ± 0.3	13.9 ± 0.3	13.9 ± 0.2
E33	13.7 ± 0.3	14.3 ± 0.3	14.6 ± 0.2	15.0 ± 0.4	14.3 ± 0.3	13.4 ± 0.2	13.1 ± 0.2	13.4 ± 0.2
G36	13.2 ± 0.4	12.7 ± 0.5	13.9 ± 0.3	13.8 ± 0.7	13.0 ± 0.5	12.6 ± 0.4	11.4 ± 0.3	11.2 ± 0.3
F38	13.0 ± 0.5	13.6 ± 0.5	14.7 ± 0.4	13.8 ± 0.8	15.0 ± 0.6	14.9 ± 0.5	14.1 ± 0.4	14.2 ± 0.3
R39	14.1 ± 0.6	15.1 ± 0.7	16.0 ± 0.5	17.1 ± 1.1	19.8 ± 0.9	20.1 ± 0.8	18.9 ± 0.5	20.6 ± 0.6
L40	16.3 ± 1.1	18.3 ± 1.1	19.5 ± 1.2	22.7 ± 1.9	24.9 ± 1.5	22.2 ± 1.3	24.8 ± 1.2	27.1 ± 1.5

Continued on next page

Table 6.3.1 – continued from previous page

Res.	1 $\pm\varepsilon$ [s^{-1}]	1.5 $\pm\varepsilon$ [s^{-1}]	2 $\pm\varepsilon$ [s^{-1}]	4 $\pm\varepsilon$ [s^{-1}]	6.6 $\pm\varepsilon$ [s^{-1}]	10.8 $\pm\varepsilon$ [s^{-1}]	10.8 $\pm\varepsilon$ [s^{-1}]	21.6 $\pm\varepsilon$ [s^{-1}]
Q44	16.5 ± 0.9	17.8 ± 1.0	16.9 ± 0.9	17.1 ± 1.4	18.1 ± 1.0	17.8 ± 0.9	17.7 ± 0.8	18.6 ± 0.9
H46	14.8 ± 0.8	16.9 ± 0.8	16.5 ± 0.8	17.9 ± 1.1	17.7 ± 0.8	16.4 ± 0.7	16.1 ± 0.5	16.5 ± 0.5
V47	12.4 ± 0.8	13.0 ± 0.8	16.0 ± 1.0	14.2 ± 1.2	14.9 ± 0.9	14.6 ± 0.8	14.6 ± 0.6	16.0 ± 0.6
E49	13.2 ± 0.7	14.5 ± 0.9	14.8 ± 0.6	16.8 ± 1.5	14.4 ± 1.0	14.4 ± 0.7	14.7 ± 0.6	15.8 ± 0.6
L52	13.7 ± 0.4	14.0 ± 0.5	14.4 ± 0.4	14.9 ± 0.6	14.6 ± 0.5	14.3 ± 0.4	13.9 ± 0.3	14.5 ± 0.4
L54	14.3 ± 0.6	14.8 ± 0.6	15.8 ± 0.6	15.2 ± 0.8	15.6 ± 0.6	14.4 ± 0.4	14.1 ± 0.4	15.1 ± 0.4
H57	16.4 ± 1.2	15.6 ± 1.3	16.3 ± 1.1	15.2 ± 1.7	17.2 ± 1.5	16.6 ± 1.3	15.9 ± 0.9	15.6 ± 0.9
T58	15.9 ± 0.6	16.3 ± 0.8	15.9 ± 0.6	16.7 ± 1.1	18.5 ± 0.8	18.7 ± 0.8	18.1 ± 0.5	19.5 ± 0.7
V59	16.8 ± 1.1	17.6 ± 1.2	16.7 ± 1.0	17.0 ± 1.7	17.9 ± 1.2	17.7 ± 1.1	16.0 ± 0.8	17.4 ± 0.9
R60	15.5 ± 0.5	16.8 ± 0.5	15.8 ± 0.5	15.4 ± 0.8	15.6 ± 0.5	13.9 ± 0.4	12.9 ± 0.4	12.7 ± 0.3
S65	15.9 ± 1.6	14.5 ± 1.9	15.7 ± 1.4	16.4 ± 2.6	14.8 ± 1.8	15.0 ± 1.4	15.2 ± 1.3	15.0 ± 1.2
L67	14.0 ± 0.6	15.6 ± 0.7	14.9 ± 0.6	15.0 ± 0.9	16.0 ± 0.7	15.7 ± 0.6	15.0 ± 0.5	16.3 ± 0.5
M69	16.2 ± 0.5	18.5 ± 0.5	15.9 ± 0.5	18.9 ± 0.7	20.6 ± 0.6	22.0 ± 0.7	20.4 ± 0.4	22.4 ± 0.5
V70	12.5 ± 0.4	12.8 ± 0.4	14.6 ± 0.4	15.8 ± 0.6	18.3 ± 0.5	19.5 ± 0.6	19.0 ± 0.4	21.3 ± 0.5
A71	16.1 ± 0.7	16.6 ± 0.9	16.3 ± 0.8	19.4 ± 1.1	19.8 ± 0.9	21.7 ± 1.1	19.8 ± 0.6	21.5 ± 0.8
K73	12.5 ± 0.3	12.6 ± 0.3	14.0 ± 0.3	13.9 ± 0.5	13.8 ± 0.3	13.9 ± 0.3	13.2 ± 0.2	14.3 ± 0.2
K76	16.3 ± 0.5	16.1 ± 0.7	17.6 ± 0.4	16.6 ± 1.1	15.6 ± 0.8	16.4 ± 0.6	15.6 ± 0.4	15.7 ± 0.4
E79	13.3 ± 0.6	14.9 ± 1.0	15.6 ± 0.5	16.8 ± 1.4	17.8 ± 1.2	17.3 ± 0.9	16.0 ± 0.6	16.8 ± 0.6

Continued on next page

Table 6.3.1 – continued from previous page

Res.	1 $\pm\varepsilon$ [s^{-1}]	1.5 $\pm\varepsilon$ [s^{-1}]	2 $\pm\varepsilon$ [s^{-1}]	4 $\pm\varepsilon$ [s^{-1}]	6.6 $\pm\varepsilon$ [s^{-1}]	10.8 $\pm\varepsilon$ [s^{-1}]	10.8 $\pm\varepsilon$ [s^{-1}]	21.6 $\pm\varepsilon$ [s^{-1}]
S81	15.3 ± 1.3	18.1 ± 1.5	22.2 ± 1.8	26.8 ± 2.5	33.9 ± 3.4	24.6 ± 2.1	33.3 ± 2.0	33.0 ± 2.4
V82	21.8 ± 1.4	23.6 ± 1.5	26.7 ± 2.1	34.8 ± 2.8	44.4 ± 3.4	46.4 ± 8.2	42.7 ± 2.2	43.0 ± 2.9
Y84	14.3 ± 0.7	15.6 ± 0.8	15.4 ± 0.7	16.2 ± 1.2	15.9 ± 0.8	16.2 ± 0.8	14.3 ± 0.5	16.3 ± 0.6
G86	15.2 ± 0.4	16.5 ± 0.7	15.3 ± 0.3	15.1 ± 0.7	16.0 ± 0.6	16.4 ± 0.4	13.2 ± 0.3	15.0 ± 0.3
K94	14.7 ± 0.4	14.3 ± 0.4	15.1 ± 0.4	14.8 ± 0.6	14.9 ± 0.5	14.7 ± 0.4	13.4 ± 0.3	14.1 ± 0.3
D96	16.8 ± 0.6	17.7 ± 0.8	18.1 ± 0.5	17.6 ± 1.2	19.0 ± 0.8	16.9 ± 0.6	16.0 ± 0.5	16.5 ± 0.5
Y97	18.2 ± 1.5	17.8 ± 1.9	19.7 ± 1.4	21.5 ± 2.9	20.6 ± 1.9	18.8 ± 1.9	18.8 ± 1.2	19.3 ± 1.3
D98	13.6 ± 0.5	14.3 ± 0.7	14.9 ± 0.5	16.6 ± 1.0	17.2 ± 0.8	16.4 ± 0.6	16.5 ± 0.5	16.3 ± 0.5
N99	14.1 ± 0.4	14.4 ± 0.6	14.6 ± 0.4	14.9 ± 0.8	15.1 ± 0.6	14.1 ± 0.4	14.3 ± 0.4	14.5 ± 0.4
F100	14.3 ± 1.0	15.2 ± 1.1	16.2 ± 1.0	15.2 ± 1.4	16.0 ± 1.2	16.3 ± 1.0	16.3 ± 0.8	16.8 ± 0.9
L101	18.4 ± 0.8	19.7 ± 0.8	20.3 ± 1.0	22.2 ± 1.4	23.7 ± 1.1	22.6 ± 1.2	21.1 ± 0.7	22.2 ± 0.8
H104	16.5 ± 1.1	18.2 ± 1.2	16.5 ± 1.1	18.6 ± 1.7	18.8 ± 1.3	18.0 ± 1.2	17.4 ± 0.9	18.9 ± 1.0
L105	19.4 ± 1.9	21.5 ± 2.5	21.5 ± 2.7	23.9 ± 2.9	26.7 ± 2.5	23.3 ± 2.5	25.3 ± 1.8	27.1 ± 2.3
N107	17.7 ± 1.2	17.9 ± 1.2	17.5 ± 1.3	16.9 ± 1.5	18.2 ± 1.2	17.3 ± 1.1	16.3 ± 0.8	18.3 ± 0.9
E108	14.7 ± 0.5	14.6 ± 0.5	14.9 ± 0.5	14.8 ± 0.7	15.9 ± 0.6	15.0 ± 0.5	14.7 ± 0.4	15.7 ± 0.4
K109	13.4 ± 0.3	14.1 ± 0.3	14.9 ± 0.3	15.1 ± 0.6	14.2 ± 0.4	12.8 ± 0.3	12.4 ± 0.2	12.7 ± 0.2
G111	14.5 ± 1.2	15.6 ± 1.3	16.2 ± 1.2	15.6 ± 1.8	16.2 ± 1.3	16.5 ± 1.2	15.7 ± 1.0	17.3 ± 1.1
F114	14.0 ± 0.5	14.8 ± 0.6	15.3 ± 0.5	16.6 ± 0.9	17.2 ± 0.7	18.1 ± 0.7	17.2 ± 0.5	18.6 ± 0.6

Continued on next page

Table 6.3.1 – continued from previous page

Res.	1 $\pm\varepsilon$ [s^{-1}]	1.5 $\pm\varepsilon$ [s^{-1}]	2 $\pm\varepsilon$ [s^{-1}]	4 $\pm\varepsilon$ [s^{-1}]	6.6 $\pm\varepsilon$ [s^{-1}]	10.8 $\pm\varepsilon$ [s^{-1}]	10.8 $\pm\varepsilon$ [s^{-1}]	21.6 $\pm\varepsilon$ [s^{-1}]
Q115	13.9 ± 0.6	14.6 ± 0.6	14.8 ± 0.6	14.5 ± 0.8	14.4 ± 0.6	14.1 ± 0.5	13.9 ± 0.4	14.5 ± 0.4
L116	14.4 ± 0.6	16.1 ± 0.6	16.6 ± 0.6	17.1 ± 0.9	18.4 ± 0.7	17.7 ± 0.6	17.4 ± 0.5	19.5 ± 0.5
M117	15.1 ± 0.4	15.9 ± 0.4	17.1 ± 0.4	18.0 ± 0.6	17.8 ± 0.4	16.1 ± 0.4	16.9 ± 0.3	17.3 ± 0.3
G118	14.9 ± 0.6	15.1 ± 0.6	15.9 ± 0.6	15.5 ± 0.9	15.9 ± 0.6	16.7 ± 0.6	15.8 ± 0.4	16.6 ± 0.4
L119	14.3 ± 0.5	13.5 ± 0.5	16.6 ± 0.6	15.1 ± 0.9	15.5 ± 0.5	16.2 ± 0.6	15.1 ± 0.4	16.0 ± 0.4
E123	14.2 ± 1.1	13.9 ± 1.1	14.7 ± 1.1	13.7 ± 1.6	15.4 ± 1.1	14.0 ± 0.9	13.7 ± 0.8	14.6 ± 0.8
D125	11.8 ± 0.2	12.1 ± 0.3	12.8 ± 0.2	13.1 ± 0.4	12.8 ± 0.3	12.5 ± 0.2	12.1 ± 0.2	13.1 ± 0.2
L126	13.7 ± 0.6	14.0 ± 0.7	14.8 ± 0.7	14.2 ± 1.1	14.5 ± 0.6	14.0 ± 0.5	13.5 ± 0.5	14.1 ± 0.5
I130	14.8 ± 0.2	15.2 ± 0.3	16.1 ± 0.2	15.4 ± 0.5	15.2 ± 0.4	14.6 ± 0.3	13.3 ± 0.2	14.0 ± 0.2
K131	14.3 ± 0.3	15.2 ± 0.4	15.7 ± 0.3	15.8 ± 0.5	15.5 ± 0.3	15.3 ± 0.3	14.4 ± 0.2	14.9 ± 0.2
E132	14.0 ± 0.2	14.2 ± 0.2	14.7 ± 0.2	14.1 ± 0.3	14.4 ± 0.3	13.6 ± 0.2	13.0 ± 0.2	13.5 ± 0.2
R133	13.3 ± 0.2	13.8 ± 0.2	14.3 ± 0.2	14.5 ± 0.3	14.2 ± 0.2	13.5 ± 0.1	12.7 ± 0.1	13.2 ± 0.1
F134	13.8 ± 0.2	14.0 ± 0.3	15.1 ± 0.3	14.8 ± 0.4	15.5 ± 0.3	14.7 ± 0.2	14.2 ± 0.2	14.7 ± 0.2
A135	13.0 ± 0.2	12.7 ± 0.3	14.5 ± 0.2	14.2 ± 0.4	14.1 ± 0.2	13.5 ± 0.2	12.9 ± 0.2	13.2 ± 0.2
Q136	12.8 ± 0.2	13.4 ± 0.2	13.9 ± 0.2	14.2 ± 0.3	14.0 ± 0.2	12.9 ± 0.1	12.8 ± 0.1	13.1 ± 0.1
L137	13.9 ± 0.2	13.7 ± 0.2	14.8 ± 0.2	15.1 ± 0.3	14.6 ± 0.2	13.4 ± 0.2	13.1 ± 0.1	13.7 ± 0.1
C138	14.0 ± 0.3	14.8 ± 0.3	15.6 ± 0.3	15.6 ± 0.4	15.4 ± 0.3	14.4 ± 0.3	14.0 ± 0.2	14.4 ± 0.2
E140	13.3 ± 0.2	13.4 ± 0.2	14.1 ± 0.2	14.2 ± 0.3	13.7 ± 0.2	12.8 ± 0.1	12.6 ± 0.1	12.9 ± 0.1

Continued on next page

Table 6.3.1 – continued from previous page

Res.	1 $\pm\varepsilon$ [s^{-1}]	1.5 $\pm\varepsilon$ [s^{-1}]	2 $\pm\varepsilon$ [s^{-1}]	4 $\pm\varepsilon$ [s^{-1}]	6.6 $\pm\varepsilon$ [s^{-1}]	10.8 $\pm\varepsilon$ [s^{-1}]	10.8 $\pm\varepsilon$ [s^{-1}]	21.6 $\pm\varepsilon$ [s^{-1}]
G142	15.3 ± 0.3	15.1 ± 0.3	15.2 ± 0.2	14.7 ± 0.4	14.2 ± 0.3	13.3 ± 0.2	12.7 ± 0.2	13.3 ± 0.2
I143	13.9 ± 0.3	13.9 ± 0.3	14.7 ± 0.3	14.1 ± 0.4	13.9 ± 0.3	13.1 ± 0.2	12.7 ± 0.2	13.0 ± 0.2
L144	13.4 ± 0.2	13.7 ± 0.2	14.4 ± 0.2	14.4 ± 0.3	14.2 ± 0.2	13.2 ± 0.2	12.5 ± 0.1	13.2 ± 0.1
N147	13.2 ± 0.2	14.0 ± 0.3	13.9 ± 0.2	15.2 ± 0.4	13.7 ± 0.3	13.0 ± 0.2	11.9 ± 0.2	12.4 ± 0.2
I148	12.6 ± 0.2	12.9 ± 0.3	13.3 ± 0.2	13.2 ± 0.4	13.1 ± 0.3	12.2 ± 0.2	11.9 ± 0.2	12.1 ± 0.2

Table 6.3.2: Relaxation rates $R_2(\tau_c)$ for holo-MUP I for different τ_c values with relative errors (308 K, 600 MHz). See table 6.3.1 for further details.

Res.	1 $\pm\varepsilon$ [s^{-1}]	1.5 $\pm\varepsilon$ [s^{-1}]	2 $\pm\varepsilon$ [s^{-1}]	4 $\pm\varepsilon$ [s^{-1}]	6.6 $\pm\varepsilon$ [s^{-1}]	10.8 $\pm\varepsilon$ [s^{-1}]	10.8 $\pm\varepsilon$ [s^{-1}]	21.6 $\pm\varepsilon$ [s^{-1}]
A3	16.4 ± 0.5	15.5 ± 0.4	16.4 ± 0.4	15.8 ± 0.5	14.8 ± 0.4	15.9 ± 0.4	16.2 ± 0.3	17.3 ± 0.4
S4	18.7 ± 0.5	18.0 ± 0.4	18.0 ± 0.4	17.5 ± 0.4	17.4 ± 0.4	17.7 ± 0.5	17.8 ± 0.3	18.2 ± 0.4
T6	21.8 ± 1.0	21.1 ± 0.8	20.2 ± 0.7	20.2 ± 0.9	21.2 ± 0.9	21.6 ± 1.1	21.0 ± 0.6	23.5 ± 1.0
V12	17.1 ± 0.3	17.1 ± 0.2	17.2 ± 0.2	17.3 ± 0.2	16.3 ± 0.2	16.4 ± 0.3	16.8 ± 0.2	17.6 ± 0.3
E13	16.1 ± 0.1	15.9 ± 0.1	16.0 ± 0.1	15.7 ± 0.1	15.5 ± 0.1	15.8 ± 0.1	16.2 ± 0.1	15.8 ± 0.1
K14	17.6 ± 0.2	17.4 ± 0.2	17.5 ± 0.2	17.5 ± 0.2	16.8 ± 0.2	17.1 ± 0.2	17.3 ± 0.1	17.2 ± 0.2
N16	17.1 ± 0.2	16.9 ± 0.2	17.1 ± 0.2	16.7 ± 0.2	16.3 ± 0.2	16.9 ± 0.2	17.8 ± 0.1	17.3 ± 0.2
G17	17.4 ± 0.4	17.0 ± 0.4	17.2 ± 0.3	16.6 ± 0.4	16.2 ± 0.4	16.5 ± 0.4	17.6 ± 0.3	17.3 ± 0.4
E18	16.7 ± 0.4	16.1 ± 0.3	16.6 ± 0.3	16.3 ± 0.3	16.1 ± 0.3	16.7 ± 0.4	17.8 ± 0.3	18.0 ± 0.3
W19	23.4 ± 1.0	22.7 ± 1.0	22.4 ± 0.9	22.3 ± 1.0	20.6 ± 0.9	22.0 ± 1.1	23.1 ± 0.7	23.0 ± 1.0
H20	19.9 ± 0.8	19.9 ± 0.7	19.5 ± 0.6	19.6 ± 0.7	19.0 ± 0.6	18.6 ± 0.8	19.6 ± 0.5	19.6 ± 0.7
I23	18.3 ± 0.4	18.1 ± 0.4	18.1 ± 0.4	17.7 ± 0.4	16.8 ± 0.4	17.5 ± 0.4	18.1 ± 0.3	18.4 ± 0.4
A25	17.5 ± 0.3	16.7 ± 0.3	16.3 ± 0.2	16.6 ± 0.3	16.0 ± 0.2	16.5 ± 0.3	16.9 ± 0.2	17.5 ± 0.3
D27	19.6 ± 0.4	18.2 ± 0.3	17.5 ± 0.3	17.9 ± 0.3	16.5 ± 0.3	17.4 ± 0.4	16.8 ± 0.2	17.3 ± 0.3
K28	14.2 ± 0.5	14.0 ± 0.4	15.3 ± 0.4	16.1 ± 0.5	15.6 ± 0.4	16.6 ± 0.5	16.2 ± 0.4	16.1 ± 0.4

Continued on next page

Table 6.3.2 – continued from previous page

Res.	1 $\pm\varepsilon$ [s^{-1}]	1.5 $\pm\varepsilon$ [s^{-1}]	2 $\pm\varepsilon$ [s^{-1}]	4 $\pm\varepsilon$ [s^{-1}]	6.6 $\pm\varepsilon$ [s^{-1}]	10.8 $\pm\varepsilon$ [s^{-1}]	10.8 $\pm\varepsilon$ [s^{-1}]	21.6 $\pm\varepsilon$ [s^{-1}]
E30	16.9 ± 0.3	16.7 ± 0.2	16.4 ± 0.2	16.2 ± 0.3	15.7 ± 0.2	16.4 ± 0.3	16.6 ± 0.2	16.5 ± 0.2
K31	17.1 ± 0.4	17.2 ± 0.3	17.9 ± 0.3	17.5 ± 0.3	17.1 ± 0.3	17.5 ± 0.4	18.1 ± 0.3	18.0 ± 0.4
E33	17.2 ± 0.3	16.7 ± 0.3	16.5 ± 0.2	16.5 ± 0.3	15.9 ± 0.3	16.1 ± 0.3	16.9 ± 0.2	17.0 ± 0.3
D34	17.8 ± 0.5	17.3 ± 0.5	17.0 ± 0.4	17.3 ± 0.4	17.1 ± 0.5	17.3 ± 0.5	17.2 ± 0.3	17.2 ± 0.5
G36	18.6 ± 0.4	15.9 ± 0.3	16.0 ± 0.3	15.6 ± 0.3	14.1 ± 0.3	15.0 ± 0.4	15.1 ± 0.2	15.0 ± 0.3
F38	16.5 ± 0.5	16.4 ± 0.5	16.5 ± 0.4	16.4 ± 0.4	16.0 ± 0.4	16.8 ± 0.4	17.1 ± 0.3	17.7 ± 0.5
R39	18.0 ± 0.3	17.7 ± 0.3	17.6 ± 0.3	17.3 ± 0.3	16.7 ± 0.3	17.0 ± 0.3	17.5 ± 0.2	17.6 ± 0.3
L40	19.7 ± 0.5	19.1 ± 0.5	18.6 ± 0.4	19.2 ± 0.4	18.4 ± 0.5	18.2 ± 0.5	18.7 ± 0.3	18.8 ± 0.5
F41	23.5 ± 1.0	22.9 ± 0.9	22.2 ± 0.8	22.1 ± 0.8	21.2 ± 0.8	21.8 ± 1.0	20.9 ± 0.6	21.7 ± 0.9
Q44	20.5 ± 0.5	20.4 ± 0.4	20.5 ± 0.4	20.1 ± 0.4	19.8 ± 0.4	20.6 ± 0.5	21.7 ± 0.3	21.4 ± 0.5
I45	17.8 ± 0.3	17.1 ± 0.3	17.3 ± 0.3	16.6 ± 0.3	16.2 ± 0.3	16.8 ± 0.4	17.9 ± 0.2	17.8 ± 0.3
H46	21.1 ± 0.4	18.8 ± 0.3	20.2 ± 0.3	18.0 ± 0.3	17.5 ± 0.3	16.9 ± 0.3	17.1 ± 0.2	17.3 ± 0.3
V47	17.9 ± 0.4	17.4 ± 0.3	18.0 ± 0.3	17.1 ± 0.3	15.9 ± 0.3	16.5 ± 0.3	16.9 ± 0.2	18.2 ± 0.3
V53	17.3 ± 0.3	16.6 ± 0.3	16.7 ± 0.3	16.7 ± 0.3	15.8 ± 0.2	16.1 ± 0.3	17.4 ± 0.2	17.0 ± 0.3
L54	16.2 ± 0.4	17.3 ± 0.3	16.8 ± 0.3	16.8 ± 0.3	16.6 ± 0.3	17.2 ± 0.4	17.7 ± 0.3	18.5 ± 0.4
K55	16.5 ± 0.3	15.6 ± 0.3	15.8 ± 0.2	14.9 ± 0.3	14.4 ± 0.3	15.2 ± 0.3	18.1 ± 0.2	17.8 ± 0.3
F56	19.8 ± 0.4	18.7 ± 0.4	17.9 ± 0.3	17.5 ± 0.4	16.6 ± 0.3	17.3 ± 0.4	17.4 ± 0.3	17.8 ± 0.4
H57	19.1 ± 0.6	18.8 ± 0.6	20.0 ± 0.6	19.0 ± 0.6	18.7 ± 0.5	19.1 ± 0.6	19.6 ± 0.4	19.7 ± 0.6

Continued on next page

Table 6.3.2 – continued from previous page

Res.	1 $\pm\varepsilon$ [s^{-1}]	1.5 $\pm\varepsilon$ [s^{-1}]	2 $\pm\varepsilon$ [s^{-1}]	4 $\pm\varepsilon$ [s^{-1}]	6.6 $\pm\varepsilon$ [s^{-1}]	10.8 $\pm\varepsilon$ [s^{-1}]	10.8 $\pm\varepsilon$ [s^{-1}]	21.6 $\pm\varepsilon$ [s^{-1}]
T58	17.9 ± 0.4	17.3 ± 0.4	17.0 ± 0.3	16.9 ± 0.4	16.7 ± 0.4	17.5 ± 0.4	17.4 ± 0.3	17.6 ± 0.3
E62	23.6 ± 0.5	22.3 ± 0.5	22.0 ± 0.5	22.1 ± 0.5	20.4 ± 0.4	21.2 ± 0.5	21.6 ± 0.3	21.8 ± 0.5
E66	19.9 ± 0.4	19.9 ± 0.4	19.8 ± 0.4	20.1 ± 0.4	19.2 ± 0.4	19.6 ± 0.5	20.1 ± 0.3	19.8 ± 0.4
L67	17.5 ± 0.3	16.8 ± 0.3	16.7 ± 0.3	16.5 ± 0.3	16.0 ± 0.3	16.3 ± 0.3	16.9 ± 0.2	17.8 ± 0.3
S68	16.8 ± 0.4	16.2 ± 0.3	16.4 ± 0.3	16.1 ± 0.4	15.5 ± 0.3	16.4 ± 0.3	17.2 ± 0.3	17.4 ± 0.3
M69	16.8 ± 0.3	16.6 ± 0.2	16.7 ± 0.2	16.5 ± 0.3	15.9 ± 0.2	16.3 ± 0.3	17.0 ± 0.2	17.0 ± 0.2
D72	15.9 ± 0.3	15.2 ± 0.3	15.4 ± 0.2	15.3 ± 0.3	14.7 ± 0.2	15.2 ± 0.2	15.7 ± 0.2	15.6 ± 0.2
K73	14.8 ± 0.3	14.6 ± 0.2	14.8 ± 0.2	14.3 ± 0.2	14.0 ± 0.2	14.6 ± 0.2	15.5 ± 0.2	15.5 ± 0.2
T74	17.0 ± 0.3	16.9 ± 0.3	16.7 ± 0.3	16.6 ± 0.3	16.2 ± 0.3	16.5 ± 0.3	16.3 ± 0.2	16.2 ± 0.2
K76	15.3 ± 0.2	14.8 ± 0.2	15.1 ± 0.2	15.7 ± 0.2	15.4 ± 0.2	16.0 ± 0.2	16.3 ± 0.1	15.7 ± 0.2
E79	16.1 ± 0.3	15.8 ± 0.2	15.6 ± 0.2	15.9 ± 0.2	15.3 ± 0.2	15.7 ± 0.2	15.9 ± 0.2	16.0 ± 0.2
Y80	19.8 ± 0.6	19.6 ± 0.6	19.6 ± 0.5	18.9 ± 0.5	18.1 ± 0.6	18.9 ± 0.6	18.5 ± 0.4	19.8 ± 0.6
S81	15.9 ± 0.4	15.9 ± 0.3	16.0 ± 0.3	15.7 ± 0.4	15.4 ± 0.4	15.9 ± 0.4	16.7 ± 0.3	16.4 ± 0.4
Y84	18.1 ± 0.5	17.9 ± 0.4	18.8 ± 0.4	17.5 ± 0.4	16.9 ± 0.4	17.3 ± 0.4	16.7 ± 0.3	16.3 ± 0.4
F87	16.8 ± 0.3	16.2 ± 0.3	16.3 ± 0.2	16.2 ± 0.3	15.7 ± 0.3	15.9 ± 0.3	16.0 ± 0.2	16.3 ± 0.3
N88	15.9 ± 0.2	15.5 ± 0.2	15.4 ± 0.1	15.4 ± 0.2	14.5 ± 0.2	15.2 ± 0.2	16.5 ± 0.1	16.5 ± 0.2
T89	16.7 ± 0.4	15.9 ± 0.3	16.0 ± 0.3	15.7 ± 0.3	15.3 ± 0.3	15.9 ± 0.4	16.7 ± 0.3	16.4 ± 0.3
F90	16.3 ± 0.3	16.4 ± 0.3	16.5 ± 0.3	16.2 ± 0.3	15.8 ± 0.3	16.2 ± 0.3	16.7 ± 0.2	16.5 ± 0.3

Continued on next page

Table 6.3.2 – continued from previous page

Res.	1 $\pm\varepsilon$ [s^{-1}]	1.5 $\pm\varepsilon$ [s^{-1}]	2 $\pm\varepsilon$ [s^{-1}]	4 $\pm\varepsilon$ [s^{-1}]	6.6 $\pm\varepsilon$ [s^{-1}]	10.8 $\pm\varepsilon$ [s^{-1}]	10.8 $\pm\varepsilon$ [s^{-1}]	21.6 $\pm\varepsilon$ [s^{-1}]
T91	19.4 ± 0.6	18.5 ± 0.5	19.9 ± 0.4	18.5 ± 0.5	17.8 ± 0.5	18.0 ± 0.5	17.7 ± 0.3	18.5 ± 0.5
K94	17.6 ± 0.2	16.5 ± 0.2	16.8 ± 0.2	16.1 ± 0.2	15.8 ± 0.2	16.5 ± 0.2	16.6 ± 0.1	16.8 ± 0.2
T95	17.9 ± 0.5	17.5 ± 0.4	18.0 ± 0.3	17.5 ± 0.4	17.2 ± 0.4	17.4 ± 0.4	17.7 ± 0.3	17.8 ± 0.4
D96	20.3 ± 0.5	19.3 ± 0.4	19.0 ± 0.4	18.6 ± 0.4	18.0 ± 0.4	18.3 ± 0.5	18.5 ± 0.3	17.9 ± 0.4
Y97	19.0 ± 0.6	18.5 ± 0.5	19.0 ± 0.5	17.9 ± 0.5	17.3 ± 0.5	18.1 ± 0.6	20.1 ± 0.4	20.2 ± 0.6
D98	18.1 ± 0.3	17.6 ± 0.3	17.5 ± 0.3	16.8 ± 0.3	16.8 ± 0.3	16.8 ± 0.3	17.0 ± 0.2	17.3 ± 0.3
N99	17.1 ± 0.4	17.0 ± 0.3	16.8 ± 0.3	17.1 ± 0.3	15.9 ± 0.3	16.4 ± 0.3	16.7 ± 0.2	16.7 ± 0.3
F100	18.3 ± 0.4	18.3 ± 0.4	18.2 ± 0.4	18.0 ± 0.4	17.7 ± 0.4	18.6 ± 0.5	18.0 ± 0.3	17.9 ± 0.4
L101	21.8 ± 0.5	21.1 ± 0.5	20.7 ± 0.4	20.3 ± 0.5	19.8 ± 0.4	19.6 ± 0.5	19.1 ± 0.3	18.7 ± 0.4
A103	18.3 ± 0.4	17.7 ± 0.4	17.4 ± 0.4	17.3 ± 0.4	16.8 ± 0.3	17.1 ± 0.4	17.2 ± 0.3	17.4 ± 0.4
N107	21.9 ± 0.6	19.9 ± 0.5	21.8 ± 0.5	19.0 ± 0.5	18.0 ± 0.5	18.5 ± 0.6	18.8 ± 0.4	18.1 ± 0.5
E108	16.0 ± 0.4	15.4 ± 0.3	15.4 ± 0.3	15.3 ± 0.3	14.6 ± 0.3	15.1 ± 0.3	16.0 ± 0.2	16.1 ± 0.3
F114	15.4 ± 0.4	15.0 ± 0.3	15.0 ± 0.3	14.7 ± 0.4	14.2 ± 0.3	15.1 ± 0.3	16.9 ± 0.3	16.5 ± 0.4
Q115	16.5 ± 0.4	16.6 ± 0.4	16.5 ± 0.4	16.7 ± 0.4	15.8 ± 0.4	16.0 ± 0.4	16.3 ± 0.3	16.4 ± 0.4
L116	18.6 ± 0.5	19.1 ± 0.5	19.0 ± 0.4	17.4 ± 0.5	16.7 ± 0.4	17.0 ± 0.4	17.5 ± 0.3	18.6 ± 0.5
M117	18.3 ± 0.4	17.3 ± 0.3	17.5 ± 0.3	16.8 ± 0.4	16.4 ± 0.3	16.8 ± 0.4	17.1 ± 0.2	17.1 ± 0.3
G118	20.1 ± 0.4	18.5 ± 0.3	18.7 ± 0.3	17.8 ± 0.4	16.9 ± 0.3	17.5 ± 0.4	17.9 ± 0.3	18.3 ± 0.3
L119	16.6 ± 0.5	16.0 ± 0.4	16.7 ± 0.3	16.9 ± 0.4	15.6 ± 0.4	16.8 ± 0.4	18.9 ± 0.3	18.2 ± 0.4

Continued on next page

Table 6.3.2 – continued from previous page

Res.	1 $\pm\varepsilon$ [s^{-1}]	1.5 $\pm\varepsilon$ [s^{-1}]	2 $\pm\varepsilon$ [s^{-1}]	4 $\pm\varepsilon$ [s^{-1}]	6.6 $\pm\varepsilon$ [s^{-1}]	10.8 $\pm\varepsilon$ [s^{-1}]	10.8 $\pm\varepsilon$ [s^{-1}]	21.6 $\pm\varepsilon$ [s^{-1}]
Y120	19.8 ± 0.8	20.5 ± 0.7	20.8 ± 0.7	19.6 ± 0.7	18.7 ± 0.6	19.2 ± 0.8	19.4 ± 0.5	21.7 ± 0.7
G121	20.1 ± 0.9	18.3 ± 0.8	19.2 ± 0.7	18.4 ± 0.8	18.2 ± 0.8	19.4 ± 1.1	20.3 ± 0.7	20.3 ± 1.0
E123	14.1 ± 0.7	14.1 ± 0.6	14.6 ± 0.5	13.7 ± 0.6	13.2 ± 0.5	14.1 ± 0.6	16.1 ± 0.4	16.8 ± 0.6
D125	14.9 ± 0.2	14.8 ± 0.1	14.9 ± 0.1	14.7 ± 0.2	14.1 ± 0.1	14.6 ± 0.2	15.4 ± 0.1	15.5 ± 0.1
L126	14.4 ± 0.3	14.5 ± 0.3	14.6 ± 0.3	14.4 ± 0.3	13.5 ± 0.3	14.3 ± 0.3	15.7 ± 0.2	16.0 ± 0.3
S127	18.3 ± 0.4	18.0 ± 0.4	18.3 ± 0.3	17.6 ± 0.4	17.6 ± 0.4	17.7 ± 0.4	17.9 ± 0.3	17.9 ± 0.4
I130	17.9 ± 0.2	17.2 ± 0.2	17.2 ± 0.2	17.2 ± 0.2	16.4 ± 0.2	16.6 ± 0.2	16.9 ± 0.2	16.3 ± 0.2
K131	18.7 ± 0.3	18.4 ± 0.3	18.7 ± 0.3	17.7 ± 0.3	17.7 ± 0.3	18.4 ± 0.4	18.2 ± 0.2	18.0 ± 0.3
E132	17.3 ± 0.2	16.6 ± 0.2	16.6 ± 0.1	16.0 ± 0.2	15.4 ± 0.1	15.8 ± 0.2	16.4 ± 0.1	16.5 ± 0.2
R133	17.3 ± 0.2	16.8 ± 0.2	16.6 ± 0.1	16.9 ± 0.2	16.1 ± 0.2	16.4 ± 0.2	16.6 ± 0.1	16.2 ± 0.2
F134	16.6 ± 0.3	16.5 ± 0.3	16.6 ± 0.2	16.3 ± 0.3	15.3 ± 0.3	16.2 ± 0.4	18.2 ± 0.2	18.2 ± 0.3
A135	16.1 ± 0.2	15.6 ± 0.2	16.1 ± 0.2	15.8 ± 0.2	15.1 ± 0.2	16.0 ± 0.2	16.7 ± 0.2	16.3 ± 0.2
Q136	16.7 ± 0.2	16.3 ± 0.2	16.5 ± 0.2	16.0 ± 0.2	15.9 ± 0.2	16.0 ± 0.2	16.3 ± 0.1	16.1 ± 0.2
L137	17.6 ± 0.2	16.8 ± 0.2	16.3 ± 0.2	16.7 ± 0.2	16.1 ± 0.2	16.6 ± 0.2	16.8 ± 0.1	17.2 ± 0.2
C138	17.0 ± 0.3	16.8 ± 0.2	16.7 ± 0.2	16.3 ± 0.3	15.8 ± 0.2	16.5 ± 0.3	17.2 ± 0.2	17.3 ± 0.2
L144	17.7 ± 0.2	16.8 ± 0.2	16.7 ± 0.2	16.5 ± 0.2	16.6 ± 0.2	16.7 ± 0.2	16.5 ± 0.2	16.8 ± 0.2
R145	16.9 ± 0.2	16.6 ± 0.2	16.6 ± 0.2	16.1 ± 0.2	15.9 ± 0.2	16.2 ± 0.3	17.3 ± 0.2	17.3 ± 0.2
E146	19.1 ± 0.5	18.4 ± 0.4	19.2 ± 0.3	18.0 ± 0.4	17.4 ± 0.4	18.1 ± 0.5	19.5 ± 0.3	19.7 ± 0.4

Continued on next page

Table 6.3.2 – continued from previous page

Res.	1 $\pm\varepsilon$ [s^{-1}]	1.5 $\pm\varepsilon$ [s^{-1}]	2 $\pm\varepsilon$ [s^{-1}]	4 $\pm\varepsilon$ [s^{-1}]	6.6 $\pm\varepsilon$ [s^{-1}]	10.8 $\pm\varepsilon$ [s^{-1}]	10.8 $\pm\varepsilon$ [s^{-1}]	21.6 $\pm\varepsilon$ [s^{-1}]
I148	15.3 ± 0.2	15.1 ± 0.2	15.0 ± 0.2	14.8 ± 0.2	14.1 ± 0.2	14.4 ± 0.2	15.4 ± 0.2	15.5 ± 0.2
I149	19.1 ± 0.5	18.6 ± 0.5	18.8 ± 0.4	17.7 ± 0.4	16.8 ± 0.4	17.2 ± 0.4	17.4 ± 0.3	18.8 ± 0.4
D150	17.2 ± 0.3	16.8 ± 0.3	18.7 ± 0.3	17.3 ± 0.3	15.7 ± 0.3	16.4 ± 0.3	17.1 ± 0.2	17.8 ± 0.3
S152	26.9 ± 0.8	25.8 ± 0.8	25.8 ± 0.7	26.2 ± 0.8	25.0 ± 0.7	25.9 ± 1.0	25.7 ± 0.6	25.4 ± 0.9
A154	21.1 ± 0.6	20.8 ± 0.6	20.5 ± 0.6	21.2 ± 0.6	19.5 ± 0.6	20.5 ± 0.7	21.2 ± 0.4	21.5 ± 0.7

Table 6.3.3: Relaxation dispersion parameters as determined by fitting the relaxation rates $R(\tau_c)$ of apo-MUP I (308 K, 600 MHz) by eq. 6.1.3.

Res	$R_{ex} \pm \varepsilon$	$k_{ex} \pm \varepsilon$ $[s^{-1}]$	$R_2^0 \pm \varepsilon$ $[s^{-1}]$
R39	10.8 ± 0.9	1384 ± 16	13.2 ± 1.1
L40	17.3 ± 4.4	1780 ± 12	13.9 ± 3.3
T58	4.3 ± 1.7	522 ± 11	15.8 ± 0.5
M69	9.7 ± 0.9	628 ± 5	16 4 ± 0.4
V70	9.7 ± 0.5	777 ± 2	12.2 ± 0.6
A71	6.2 ± 0.8	902 ± 9	15.6 ± 0.6
D72	18.7 ± 1.7	1233 ± 17	12.8 ± 1.4
S81	23.1 ± 4.1	1997 ± 10	9.6 ± 4.5
V82	28.8 ± 2.9	1159 ± 20	18.6 ± 2.4
T89	36.3 ± 4.0	1438 ± 40	14.1 ± 3.9
F114	5.1 ± 1.3	1432 ± 14	10.0 ± 3.8

Chapter 7

Effects of Protein-Pheromone Complexation on Correlated Chemical Shift Modulations

In this chapter, we present a novel experiment which has been mainly developped by Julien Wist on Ubiquitin and has been published in *Applied Magnetic Resonance*. The application to MUP I has been published in the *Journal of Biomolecular NMR*.

7.1 Introduction

Slow internal motions include all movements in a protein that are slower than the correlation time τ_c, i.e., all dynamics with a time scale in the range of μs to ms. For spherical proteins, the correlation time is between 3 and 30 ns, roughly proportional to half of the molecular weight expressed in kDa. Usually, in this range fall motions like rotations about dihedral angles, loosening or making of hydrogen bonds, large scale flapping of loops, large scale side chain conformational rearrangements and slow backbone motions.

It is known that the making or the breaking of hydrogen bonds has an effect on the CSA and Dipolar tensors of the atoms involved in the hydrogen bond (see eqs. 81 and 82 in Frueh (Frueh, 2002)), reflected in the changes of isotropic chemical shifts of both amide proton and nitrogen nuclei. In a less spectacular way other mechanisms, like rotations that are responsible for slow motions, affect the isotropic chemical shifts.

The experiment described in this chapter, is designed to detect slow motions of the backbone carbonyl C' and amide N nuclei, using the difference between the relaxation rates of Zero- and Double-Quantum Coherences (ZQC and DQC respectively). Only mechanisms that affect both nuclei involved in the coherence could result in a difference in the relaxation rates between zero- and double-quantum coherences, as explained in section 3.3.

7.2 The Experiments

7.2.1 The Pulse Sequence

To determine the auto-relaxation rates of ZQC(C'_+N_-) and DQC(C'_+N_+), we used the pulse sequences of figure 7.2.1 (Wist et al., 2005). The preparation period allows one to transfer the magnetization from the amide proton (H^N_z) into a two-spin order term $2C'_zN_z$ at point (a). A z-filter is then applied to suppress phase distortions due to changes in the RF field amplitudes and spurious coherence (Sørensen et al., 1984). Two simultaneous $\pi/2$ pulses create $2C'_xN_y$ at (b), i.e., a combination of zero- and double-quantum coherences. During the relaxation interval τ_m, i.e. between (b) and (c), two π pulses are applied to refocus both the chemical shifts and the J-couplings

that affect the C' and N nuclei. During this period several relaxation mechanisms are active, such as the desired cross-correlated $R_{C'N}^{CSM/CSM}$, and others that cannot be refocused, such as $R_{C'N}^{CSA/CSA}$ and the dipolar contributions that involve two external atoms, like $R_{C'X,NX}^{DD/DD}$ where X stands for C^{α}, H^{N} or H^{α}, etc. After the relaxation period, another z-filter is applied to suppress unwanted coherences. The subsequent period is used to label the magnetization by the ^{15}N chemical shift in a semi-constant time fashion (Logan et al., 1993) and then transferred back to the amide protons using the sensitivity enhancement technique (Palmer et al., 1991; Kay et al., 1992). Solvent suppression is achieved using a selective flip-back pulse (Grzesiek and Bax, 1992) combined with gradient selection.

7.2.2 Material and Methods

Both apo- and holo-MUP I samples were dissolved in 10% D_2O/ 90% H_2O, and the pH was adjusted to 7.4 with phosphate saline buffer. For the DQC and ZQC methods, each 2D dataset consisted of 64 and 512 points in the t_1 and t_2 dimensions respectively. The spectral widths were 1824 and 8389 Hz in the ω_1 and ω_2 dimensions. For each t_1 increment 64 scans were accumulated with a relaxation delay of 1.2 s. The relaxation intervals T were 1, 4, 8, 16, 24, and 32 ms. The experimental time required for each 2D experiment was 2.5 h. Data processing has been performed using the GNU Package NMRPipe/NMRDraw/NlinLS (Delaglio et al., 1995). Relaxation rates were obtained by least-squared fitting of the decays to exponential functions (Matlab, 1992, Matlab Reference Guide, Natick, Massachusetts). Errors of the decay rates were estimated by Monte-Carlo analysis using 500 synthetic data points. Errors in the rates were

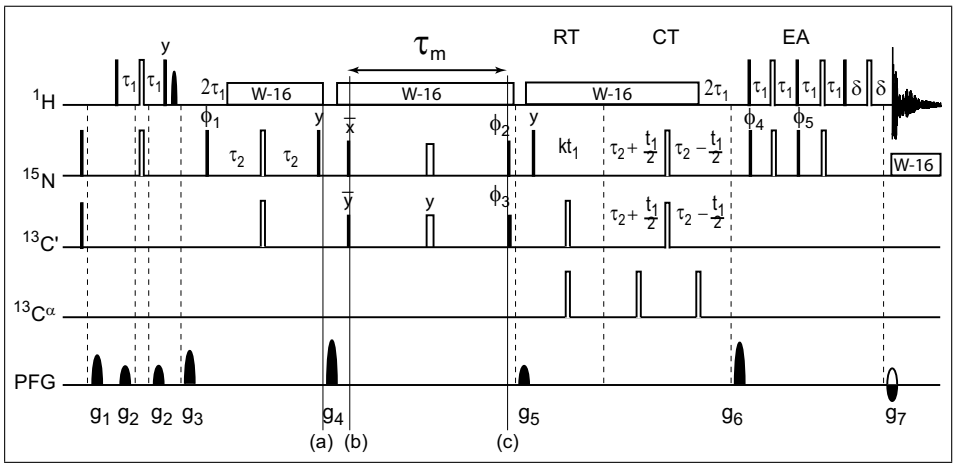

Figure 7.2.1: Pulse sequence designed to measure the auto-relaxation rates of DQC(C'_+N_+) and ZQC (C'_+N_-). Black and white rectangles represent $\pi/2$ and π pulses respectively. All pulses are applied along the x axes, unless specified otherwise. The ^{1}H, ^{15}N, ^{13}C carriers are centred at 4.7, 118 and 175 ppm, respectively. 90° and 180° pulses are applied to ^{13}C with field strengths of $\Delta/\sqrt{15}$ and $\Delta/\sqrt{3}$, Δ being defined as the difference in Hz between the centres of the C' and C^α regions (Δ = 17.6 kHz at 600 MHz). Pulses applied to C^α are phase modulated. During the mixing time τ_m, the evolution of the multiple-quantum coherence is refocused by two simultaneous π-pulses. The delays are set to τ_1 = 2.7 ms ($\approx$ 1/4J(NH)), τ_2 = 12.0 ms ($\approx$ 1/4J(C'N)), and δ = 1.3 ms. The ^{15}N magnetization evolves during a semi-constant time period comprised of two intervals RT (real time) and CT (constant time). Quadrature detection is achieved in ω_1 by the enhanced-sensitivity pulsed field gradient method. WALTZ-16 sequences are used to perform proton and nitrogen decoupling with RF field strengths of 3.5 kHz and 1.2 kHz respectively. The phase cycle (16 steps) is $\phi_1 = 8(x,-x)$, $\phi_2 = 4(y),4(-x),4(-y),4(x)$, $\phi_3 = 4(x),4(y),4(-x),4(-y)$, $\phi_4 = 4(x,x,-x,-x)$, $\phi_5 = 4(y,y,-y,-y)$. For the selection of DQC or ZQC, $\phi_{rec} = 4(x,-x,-x,x)$ or $\phi_{rec} = 2(x,-x,-x,x,-x,x,x,-x)$ respectively. The duration of all sine-shaped gradients is 1 ms and their peak amplitudes are g_{1x} = 31 G/cm, g_{2y} = 20 G/cm, g_{3z} = 19.5 G/cm, g_{4x} = 45 G/cm, g_{5z} = 30 G/cm,g_{6z} = 39.5 G/cm, $g_{7z} = -4$ G/cm.

then obtained by error propagation. The rates can be found in tables 7.5.1 and 7.5.2.

7.3 Theory

For each pair of neighbouring residues (i-1, i), one can determine the 'raw' difference of the experimental decay rates of Double Quantum Coherence (C'_+N_+) and Zero Quantum Coherence (C'_+N_-):

$$R_i^{exp} = \frac{1}{2}[R_i(DQC) - R_i(ZQC)] \tag{7.3.1}$$

Relaxation theory shows that three cross-correlated fluctuations contribute to this rate (Frueh et al., 2001; Dittmer and Bodenhausen, 2004), as sketched in figure 7.3.1:

$$R_i^{theor} = R_i^{CSM/CSM} + R_i^{CSA/CSA} + R_i^{DD/DD} \tag{7.3.2}$$

The first two terms are proportional to B_0^2, while the third one is essentially field independent. The *chemical shift anisotropy/chemical shift anisotropy* (CSA/CSA) and *dipole-dipole/dipole-dipole* (DD/DD) cross-correlation terms (the latter comprising sums over all pairs of neighbouring nuclei) are roughly proportional to τ_c (which is on the order of 10 ns), while the *chemical shift modulation/chemical shift modulation* (CSM/CSM) terms depend only on slow internal motions with a time-scale τ_{int} (typically in a range between μs and ms). These rates arise from slow modulations of the isotropic chemical shifts of C' and N that are due to structural fluctuations, notably to variations of the dihedral angles ϕ and ψ in the protein backbone, as shown

by *ab initio* calculations (Arnold and Oldfield, 2000). Only when τ_{int} is much larger than τ_c do the resulting modulations of the isotropic shifts affect the relaxation of the coherences ZQC(C'_+N_-) and DQC(C'_+N_+) (Frueh et al., 2001).

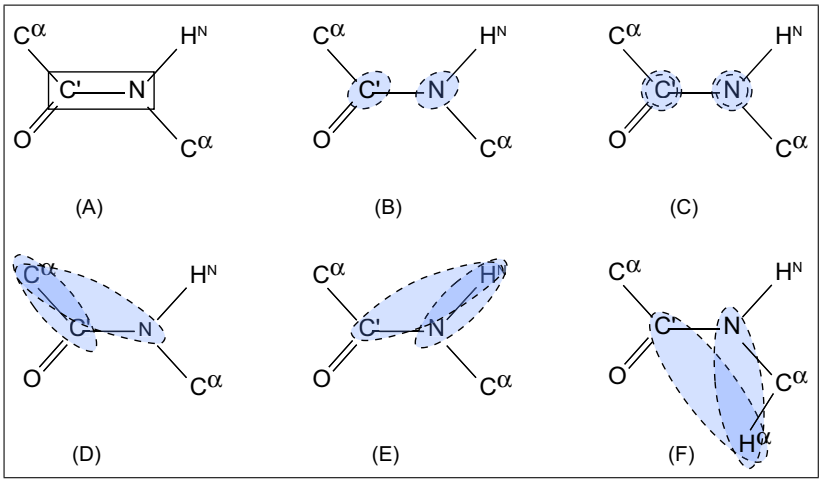

Figure 7.3.1: Schematic representation of: (A) Two-spin double DQC (C'$_{\pm}$N$_{\pm}$) and zero quantum coherence ZQC (C'$_{\pm}$N$_{\mp}$) in neighbouring amino acids in proteins. (B) CSA/CSA cross-correlation due to concerted modulations of the anisotropic parts of the chemical shift tensors (represented by ellipses), (C) CSM/CSM cross-correlation due to concerted fluctuations of the isotropic parts of the chemical shifts (dotted circles), (D-F) Dipole/dipole interference involving an external spin: (D) C_i^{α}, (E) H_i^N and (F) H^{α}. Such mechanisms contribute to auto-relaxation of the two-spin DQC and ZQC, induce differential line broadening, and cannot be averaged out using non-selective π-pulses.

7.3.1 Dipolar Contributions

The dipolar contributions to the decay rates of the DQC(C'_+N_+) and ZQC(C'_+N_-) coherences are due to a combination of auto- and cross-correlated effects, see section 3.3. The auto-correlation dipolar contribution can be computed for each residue as

follows:

$$R^{auto} = \frac{1}{2}\frac{K^2}{r_{C'N}^6}\left(\frac{1}{2}J_0^{DQ} - \frac{1}{12}J_0^{ZQ}\right) \tag{7.3.3}$$

where

$$\begin{aligned} K &= \frac{\sqrt{6}\mu_0\hbar\gamma_N\gamma_{C'}}{4\pi} \\ J_0^{DQ} &= \frac{2}{5}S_{DQ}^2\frac{\tau_c}{1+((\omega_N+\omega_C)\tau_c)^2} \\ J_0^{ZQ} &= \frac{2}{5}S_{ZQ}^2\frac{\tau_c}{1+((\omega_N-\omega_C)\tau_c)^2} \end{aligned}$$

The average auto-correlated C'-N/C'-N dipole-dipole rates can be estimated to be $R^{DD/DD} = 0.027\ s^{-1}$ in holo-MUP I (τ_c = 8.9 ns at 308 K) and $R^{DD/DD} = 0.033\ s^{-1}$ in apo-MUP I (τ_c = 7.1 ns at 308 K), under the worst-case assumption that the backbone is rigid (all local order parameters $S^2 = 1$). These auto-correlated DD/DD contributions can thus be safely neglected. On the other hand, several cross-correlated dipolar mechanisms that involve external nuclei may contribute to $R^{DD/DD}$, i.e., C'-X/N-X or C'-X/N-Y, where X and Y can stand for a proton (H^N, H^α etc.) or a carbon-13 nucleus (e.g., C^α), as sketched in figure 7.3.1. The cross-correlated contributions can be estimated using the following formulas:

$$R^{cross} = \frac{1}{2}d_{C'X}d_{NY}\frac{1}{3}J^{DD/DD}(0)\frac{1}{2}\left(3cos^2(\theta_{C'X,NY}) - 1\right) \tag{7.3.4}$$

where

$$\begin{aligned} d_{C'X} &= \sqrt{6}\frac{\mu_0}{4\pi}\hbar\frac{\gamma_{C'}\gamma_X}{r^3_{C'X}} \\ d_{NY} &= \sqrt{6}\frac{\mu_0}{4\pi}\hbar\frac{\gamma_N\gamma_Y}{r^3_{NY}} \\ J^{DD/DD}(0) &= \frac{2\tau_c}{5} \end{aligned} \tag{7.3.5}$$

Using bond distances and angles extracted from the X-ray structures of the apo and holo forms,[1] we estimated several cross-correlated contributions $R^{DD/DD}$ at 308 K. Due to their high gyromagnetic ratio, all protons H^ι_j that are closer than 5 Å[2] to N(i) and to C'(i-1) have to be included in the calculations. As example a few rates $R^{C'H^N/NH^N}$ are given in table 7.3.1 as a function of the distance $r_{C'H^N}$ and r_{NH^N}.

j	k	$r_{C'_{43}H^N_j}$ [Å]	$r_{N_{44}H^N_k}$ [Å]	$R^{DD/DD}_{43j,44k}$ [s^{-1}]	j	k	$r_{C'_{135}H^N_j}$ [Å]	$r_{N_{136}H^N_k}$ [Å]	$R^{DD/DD}_{135j,136k}$ [s^{-1}]
44	44	2.03	1.01	-2.50	135	136	3.17	1.01	-0.96
43	44	2.73	1.01	-1.71	136	136	2.04	1.01	-2.49
43	43	2.73	2.54	-0.08	137	136	3.04	1.01	0.59
19	44	2.91	1.01	-0.63	138	136	2.97	1.01	0.44

Table 7.3.1: $R^{DD/DD}_{(i-1)j,ik}$ for residues Gln 44 and Gln 136 with distances $r_{C'_{(i-1)}H^N_j}$ and $r_{N_iH^N_k}$. Note that Gln 44 is buried inside the β-barrel while Gln 136 is part of the long α helix.

For most residues, the main contributions to these $R^{DD/DD}$ rates are due to the amide proton ($X = H^N$), such that the estimated rates do not critically depend on the precise knowledge of the structure (Bytchenkoff et al., 2005).

[1] PDB files: 1QY1 and 1QY0 for holo and apo respectively. Note in the the cavity of the apo form in not truly empty: it contains glycerol which as been used as cryo-protectant and bound to MUP I. A truly empty crystal structure of MUP I as been obtained only for the F120Y mutant.

[2] The value of 5 Å has be chosen considering the accepted limits for nuclear overhauser effect.

7.3.2 Chemical Shift Anisotropy

The CSA/CSA contributions in eq. 7.3.2 are also affected by complexation, since both the correlation time τ_c and the CSA tensors of many C' and N nuclei are significantly modified upon complexation. The HSQC spectrum in figure 7.3.2 shows that the isotropic shifts of many N and H^N nuclei are affected. Similar changes are also observed for the isotropic C' shifts: the quantitative differences in chemical shifts of these three nuclei are shown in figure 7.3.3.

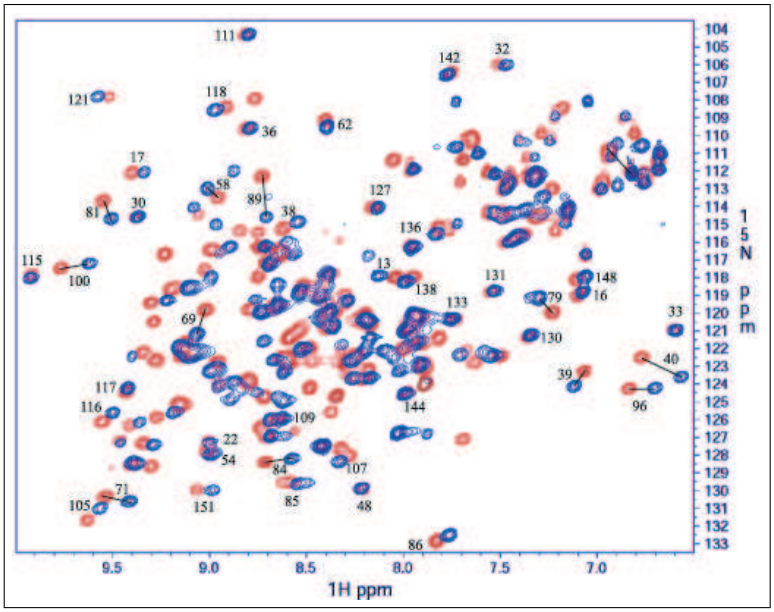

Figure 7.3.2: Partial ^{15}N, ^{1}H correlation spectra (HSQC) with some assignments of apo-MUP I (blue) and holo-MUP I (red), i.e., with the pheromone 2-methoxy-3-isobutylpyrazine (IBMP) as ligand, both dissolved in 10% D_2O / 90% H_2,O pH adjusted to 7.4 with phosphate saline buffer, and measured at T = 308 K and B_0 = 14 T (600 MHz).

A recent study of fourteen complementary cross- and auto-correlation rates in Ubiquitin (Loth et al., 2005) indicates that some of the principal components of CSA tensors of C', N and H^N, see figure 7.3.4, are nearly invariant from one amino-acid

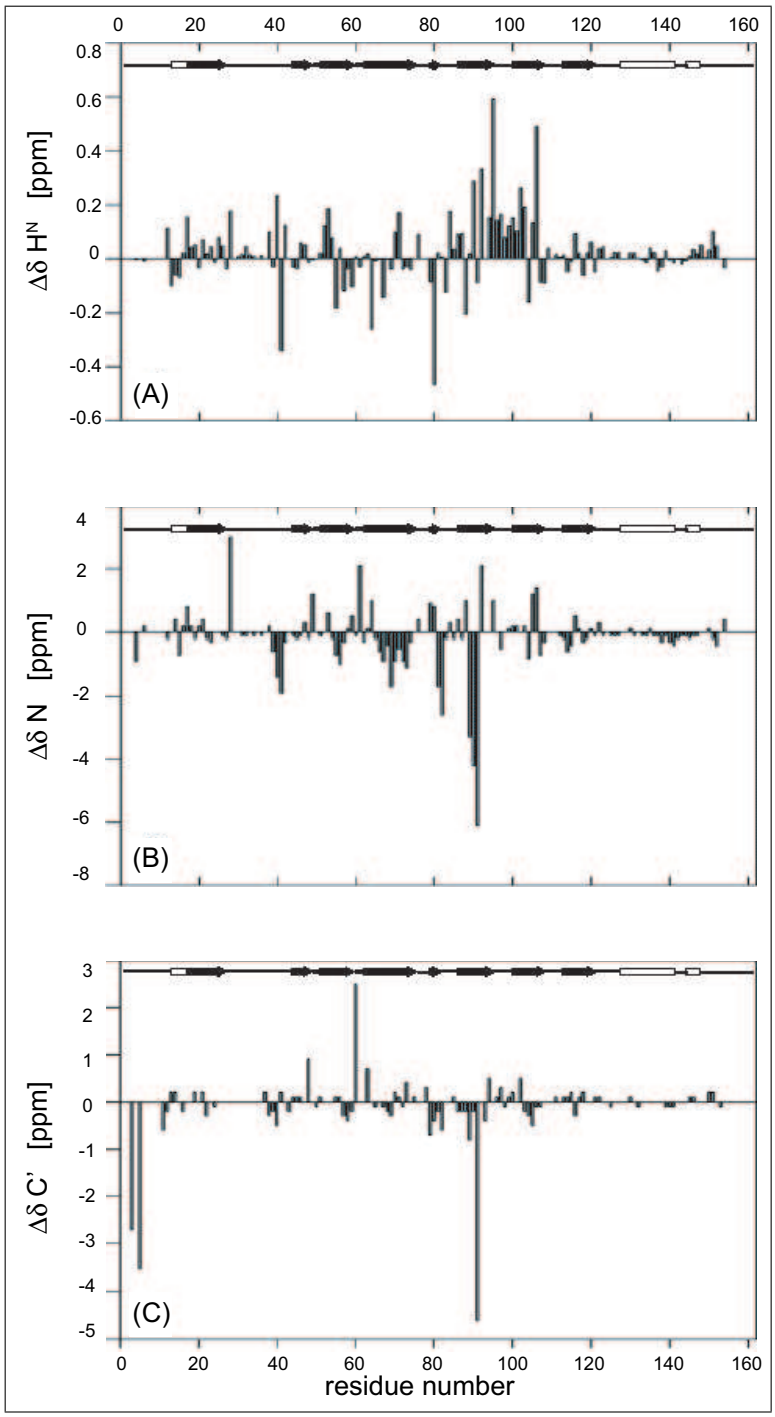

Figure 7.3.3: Differences in chemical shifts upon complexation for the backbone nuclei H^N (A), N (B) and C' (C).

to another, while other components are proportional to the isotropic shifts. The site-specific CSA tensors have been determined in Ubiquitin using different motional models: (a) isotropic wobbling-in-a-cone, (b) three-dimensional Gaussian Axial Fluctuations (3D-GAF) with a common correlation time around all three orthogonal axes, (c) a model which allows the amide protons to move out of the peptide plane with an internal correlation $\tau_{int} = 40$ ps, (d) the same model with $\tau_{int} = 400$ ps, and (e) the same as (d), but where the nitrogen CSA tensors are assumed to follow the motions of the amide protons. These five models lead to five slightly different estimates of the site-specific CSA tensors of the C' and N nuclei.

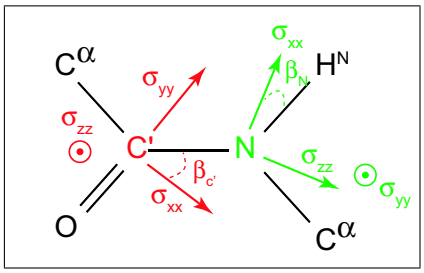

Figure 7.3.4: Local structure of a peptide plane in a protein. Ideally, all atoms lie in the same plane. The principal components and the orientation of the CSA tensors of the carbonyl (C'), nitrogen (N) are represented in red and green respectively. The principal components of the CSA tensors are defined so that $\sigma_{zz} < \sigma_{yy} < \sigma_{xx}$ (i.e., σ_{zz} most and σ_{xx} least shielded) and $(\sigma_{zz} + \sigma_{yy} + \sigma_{xx})/3 = \sigma_{iso}$. One of the components lies perpendicular to the peptide plane, so that the orientation of each CSA tensor can be defined by one angle β.

In accordance with Loth et al., (Loth et al., 2005) we prefer the 3D-GAF model ('model b') to extract the CSA tensors of Ubiquitin. For the CSA tensors of C' nuclei, the σ_{yy} components are roughly proportional to the isotropic shifts ($\sigma_{yy} \approx 3\,\sigma_{iso} - 334.9$ ppm), while the other two components are almost invariant ($\sigma_{xx} \approx 251.2$ ppm; $\sigma_{zz} \approx 83.6$ ppm). On the other hand, for the CSA tensors of N nuclei, both

σ_{xx} and σ_{yy} components are roughly proportional to the isotropic shifts ($\sigma_{xx} \approx \sigma_{iso} +$ 105.5 ppm; $\sigma_{yy} \approx 2\,\sigma_{iso} - 163.2$ ppm), while the third component is almost invariant ($\sigma_{zz} \approx 57.7$ ppm). These empirical rules could in principle be verified for MUP I, but the consistency of our observations in Ubiquitin leads us to assume that the same relations can be used for apo- and holo-MUP I. The $\mathrm{R}_i^{CSA/CSA}$ rates can thus be estimated for apo- and holo-MUP I from the knowledge of the isotropic shifts and the correlation times, as represented by blue bars in the histogram of figure 7.3.5 and tables 7.5.3 and 7.5.4. Note that the knowledge of the structure is immaterial.

7.3.3 Chemical Shift Modulation

We can now subtract the estimated rates $\mathrm{R}_i^{CSA/CSA}$ and $\mathrm{R}_i^{DD/DD}$ from the 'raw' experimental relaxation rates of eq. 7.3.1 to obtain the CSM/CSM contributions shown in figure 7.4.2B:

$$R_i^{CSM/CSM} = R_i^{exp} - R_i^{CSA/CSA} - R_i^{DD/DD} \tag{7.3.6}$$

Note that the CSM/CSM cross-correlation rate on the left-hand side is a hybrid quantity, since the first term on the right-hand side represents 'raw' experimental rates, while the last two rates are estimated from (imperfect) knowledge of isotropic shifts, CSA tensors, and rotational correlation times. We should bear in mind that uncertainties about the structure have little effect. Ideally, the CSM/CSM cross-correlation rates thus obtained should not be affected by any CSA and DD contributions, and be due only to slow fluctuations of the isotropic chemical shifts, see eqs. 88 and 89 in

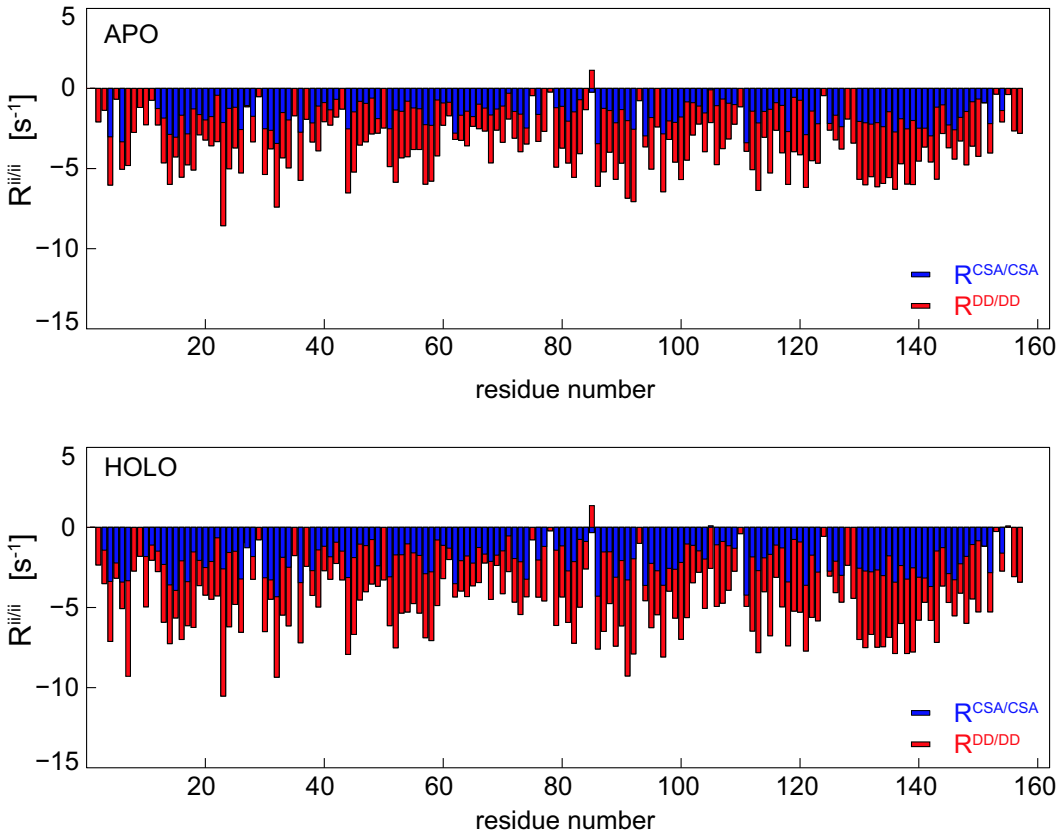

Figure 7.3.5: Histogram showing estimated $R_i^{DD/DD}$ rates (red) in apo and holo-MUP I, based on internuclear distances and dihedral angles derived from the X-ray structures and on the experimentally determined correlation times of the two proteins (τ_c = 7.1 ns for apo-MUP I, and τ_c = 8.9 ns for holo-MUP I.) Estimated $R_i^{CSA/CSA}$ rates (blue) are based on CSA tensors of C' and N nuclei extracted from measurements on Ubiquitin that were interpreted with the help of the 3-dimensional Gaussian Axial Fluctuation (3D-GAF) model (b) of local motions of the peptide planes.

the work of Frueh (Frueh, 2002). If the internal motions can be modelled (as usually assumed) in terms of instantaneous jumps between two different conformations A and B with populations p_A and p_B, and if these jumps are fast enough so that one cannot distinguish two distinct resonances for the two conformations (traditionally called the 'fast exchange limit' of chemical exchange processes, although the exchange between conformations is of course much slower than the Larmor frequency), the rate can be described by (Frueh, 2002):

$$R_i^{CSM/CSM} = 2p_A p_B \tau_{ex} \Delta\omega_{AB}^{C'} \Delta\omega_{AB}^{N} \tag{7.3.7}$$

where $\tau_{ex} = 1/(\mathrm{k}_{AB} + \mathrm{k}_{BA})$ is inversely proportional to the sum of the forward and backward exchange rates between the conformations A and B in the apo form, and $\Delta\omega_{AB}^{C'} = \omega_A^{C'} - \omega_B^{C'}$ and $\Delta\omega_{AB}^{N} = \omega_A^{N} - \omega_B^{N}$ are the changes in isotropic chemical shifts experienced by the C' and N nuclei when jumping between conformations A and B. Likewise, there may be two different conformations A' and B' in the holo form, with $\tau_{ex} = 1/(\mathrm{k}_{A'B'} + \mathrm{k}_{B'A'})$, leading to a holo rate $\mathrm{R}_i^{CSM/CSM}$ defined in analogy to eq. 7.3.7. The rates $\Delta R_i^{CSM/CSM}$(apo) and $\Delta R_i^{CSM/CSM}$(holo) may be either positive or negative depending on whether the changes in the isotropic shifts of the C' and N nuclei are correlated or anti-correlated, i.e., whether local motions cause the chemical shifts to move in the same or in opposite directions upon a jump between conformations A and B, or between A' and B'. Eq. 7.3.7 is analogous to the behaviour of exchange contributions to the line-widths of single-quantum spectra. In fact, the CSM/CSM rate is analogous to an $\mathrm{R}_{ex}/\mathrm{R}_{ex}$ cross-correlation rate. We shall

focus attention on *changes* in cross-correlation rates upon complex formation:

$$\Delta R_i^{CSM/CSM} = \Delta R_i^{CSM/CSM}(holo) - \Delta R_i^{CSM/CSM}(apo) \tag{7.3.8}$$

which amounts to:

$$\Delta R_i^{CSM/CSM} = 2p_{A'}p_{B'}\tau'_{ex}\Delta\omega^{C'}_{A'B'}\Delta\omega^{N}_{A'B'}(holo) - 2p_Ap_B\tau_{ex}\Delta\omega^{C'}_{AB}\Delta\omega^{N}_{AB}(apo) \tag{7.3.9}$$

Clearly, to the extent that eq. 7.3.7 is applicable, $\Delta R_i^{CSM/CSM}$ changes can arise either from changes in dynamic parameters (populations p_A, p_B and residence time τ_{ex}) or from changes in "static" parameters and $\Delta\omega^{C'}_{AB}$ and $\Delta\omega^{N}_{AB}$ that arise either from structural differences between the conformations A and B or A' and B' in the apo or holo forms, or from chemical shift changes induced by ligand binding. The latter needs not necessarily to involve changes in structure between the apo and holo forms.

7.3.4 Temperature Dependence

If it is assumed that the static parameters $\Delta\omega^{C'}_{AB}$ and $\Delta\omega^{N}_{AB}$ are independent of temperature, (Palmer et al., 2001) while the dynamic parmeters p_A, p_B and τ_{ex} obviously depend on the temperature, the temperature dependence of the $\Delta R_i^{CSM/CSM}$ rates allows one to separate dynamic and static factors. The temperature dependence of the $\mathrm{R}_i^{CSM/CSM}$ rates can be determined from the measurement of experimental rates $\mathrm{R}_i^{exp}(\mathrm{T})$ as a function of temperature, followed by the subtraction of $\mathrm{R}_i^{CSA/CSA}(\mathrm{T})$ and $\mathrm{R}_i^{DD/DD}(\mathrm{T})$ at each temperature. Ideally, one should measure the temperature

dependence of the isotropic shifts of both C' and N nuclei in order to determine the CSA parameters as a function of T, and one should determine the (slight) variations of structure as a function of temperature. We are interested in changes of only C' and N shifts, because the H^N shifts have no effect on the C' and N tensors according to Loth et al. (Loth et al., 2005). The largest changes in N shifts were found for residues Lys 73 in apo-MUP I: 0.7 ppm. For this residue, the tensor values have been computed at 300 and 308 K according to the relative isotropic shifts, and then used in the calculation of $R_i^{CSA/CSA}(T)$. The differences between values computed taking into account the changes of isotropic chemical shifts and the τ_c temperature dependence, $R_{308}^{CSA/CSA} - R_{300}^{CSA/CSA} = 0.33\, s^{-1}$, and those reckoned considering only the latter, $\Delta R^{CSA/CSA} = 0.24\, s^{-1}$, are consistent within experimental errors.

As checked above, it is sufficient to scale the $R_i^{CSA/CSA}(T)$ and $R_i^{DD/DD}(T)$ rates estimated at T_0 = 308 K according to the ratio of correlation times $\tau_c(T)/\tau_c(T_0)$. The temperature dependence of the correlation time can be derived from the Stokes-Einstein equation:

$$\tau_c = \frac{4\pi\eta_w r_H^3}{3k_B T} \tag{7.3.10}$$

where η_w is the viscosity of the solvent and r_H is the effective hydrodynamic radius. According to Atkins, (Atkins, 1994) the viscosity of water η_w as a function of the temperature t [°C], can be expressed by $\eta_w(t) = exp(B/A)$ divided by $\eta_w(20)$ with A=1.37023(t-20)+8.36·$10^{-4}(t-20)^2$ and B=109+t. The hydrodynamic radius r_H includes the size of the protein and an hydration sphere with a radius of r_w = 1.6 - 3.2 Å around it. Increase in temperature usually results in a slight loosening of

hydrogen bonds which means both an increase in the protein radius and a decrease in the hydration sphere; these two effects are assumed to compensate each other, so that r_H is roughly independent of temperature. Over the range of interest, the correlation times can be considered to be a linear function of T, i.e., ${\tau_c}^{holo}$ (T)= -0.1 T + 45.2 ns and ${\tau_c}^{apo}$(T) = -0.1 T + 36.1 ns.

7.4 Results and Discussion

Figure 7.4.1 shows some typical experimental decays of double- (red squares) and zero-quantum coherences (blue circles) recorded at 308 K. Figure 7.4.2A shows the 'raw' experimental relaxation rates R_i for all accessible residues in apo-MUP I (blue circles) and holo-MUP I (red squares). The $R_i^{DD/DD}$ and $R_i^{CSA/CSA}$ rates, estimated at 308 K as discussed above, are shown schematically as histograms in figure 7.3.5. Of a total of 117 observable residues in the apo form, 16 had to be discarded because of overlapping signals, and 12 because of poor signal-to-noise, so that 89 residues could be retained. The 'raw' experimental rates in the apo form range between -12.9 and +2.8 s^{-1}. Applying the same criteria for the holo form, 23 of the 133 observable residues had to be excluded because of overlapping signals, and 2 because of poor signal-to-noise, so that 108 rates could be analysed. The 'raw' experimental rates of the holo form lie in a range between -16.9 and +4.5 s^{-1}. Figure 7.4.2B shows 'corrected' relaxation rates $R_i^{CSM/CSM}$ at 308 K after subtraction of the $R_i^{DD/DD}$ and $R_i^{CSA/CSA}$ contributions according to eq. 7.3.6 for apo-MUP I (blue circles) and holo-MUP I (red squares).

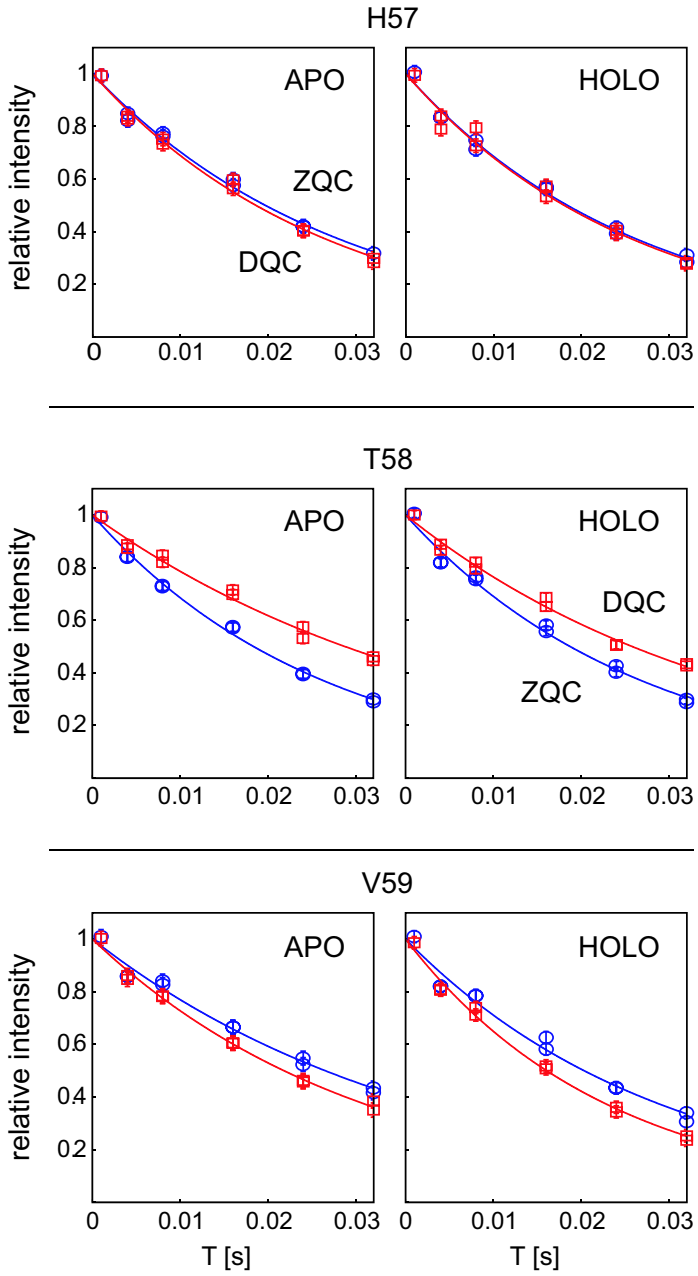

Figure 7.4.1: Three typical experimental decays of DQC(C'_+N_+) (red squares) and ZQC(C'_+N_-) (blue circles) for His 57, Thr 58 and Val 59, in apo-MUP I (left) and holo-MUP I (right), i.e., with the pheromone IBMP as ligand.

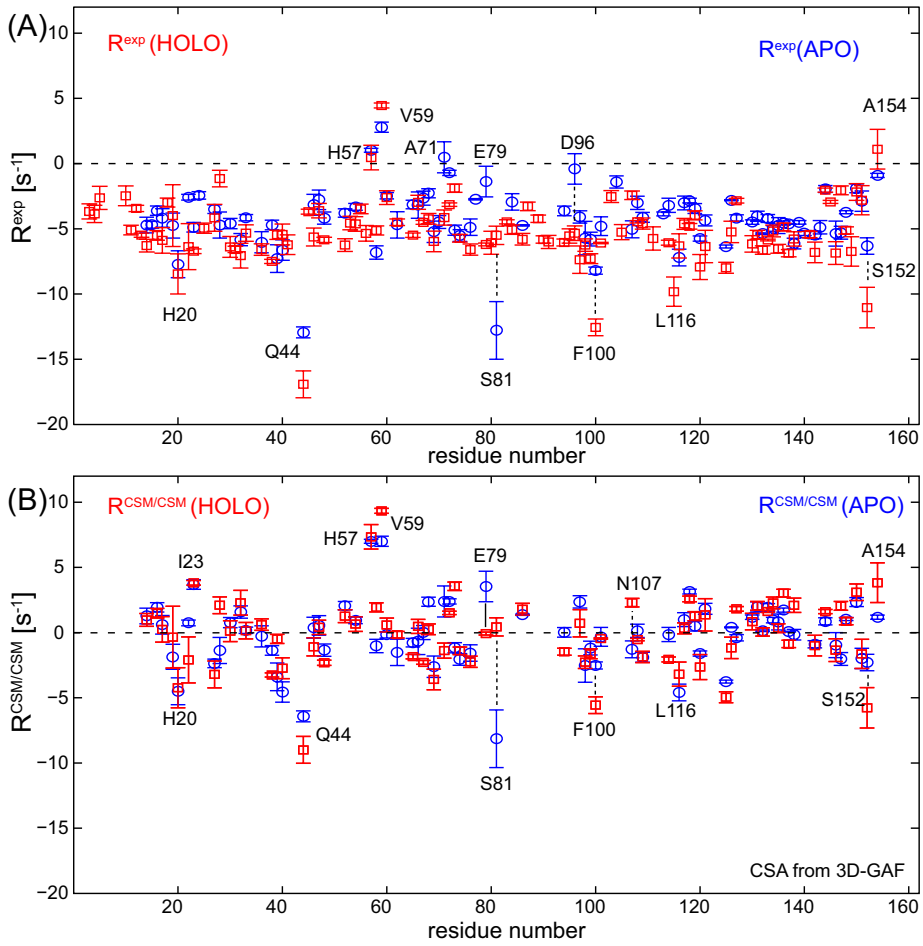

Figure 7.4.2: (A): 'Raw' experimental rates R_i^{exp} as defined in eq. 7.3.1 for apo-MUP I (blue circles) and holo-MUP I (red squares) measured at T = 308 K and 600 MHz; (B) Contributions $R_i^{CSM/CSM}$ due to correlated isotropic chemical shift modulations obtained by subtracting estimated $R_i^{DD/DD}$ and $R_i^{CSA/CSA}$ rates from experimental relaxation rates according to eq. 7.3.6. The $R_i^{CSM/CSM}$ rates are only shown for apo-MUP I (blue circles) and for holo-MUP I (red square) for amino-acids that can be resolved in *both* HSQC spectra.

As discussed above, it is not possible to derive dynamic information directly from the difference $\Delta R_i^{CSM/CSM}$ between the apo and holo forms, since these comprise an admixture of dynamic parameters (populations p_A, p_B and residence time τ_{ex}) and "static" parameters $\Delta\omega_{AB}^{C'}$ and $\Delta\omega_{AB}^{N}$. However, if it is assumed that the static parameters are independent of temperature, (Palmer et al., 2001) the derivative $dR_i^{CSM/CSM}(T)/dT$ with respect to temperature provides information about changes in dynamics between the apo and holo forms.

Figure 7.4A shows the temperature dependence of the experimental rates $R_i^{exp}(T)$ of Lys 14 in apo- and holo-MUP I. In this example, the subtraction of the estimated dipolar and CSA contributions according to eq. 7.3.6 leads to the conclusion that the corrected rates $R_i^{CSM/CSM}(T)$ in figure 7.4B vanish for both apo- and holo-MUP I over the full temperature range that could be investigated. This means that for this residue there are no significant dynamic effects on the time-scale of interest. Other residues have rates whose absolute value decreases with increasing temperature, in analogy to the R_{ex} contribution to transverse ^{15}N relaxation in the fast exchange regime. In His 57 (figure 7.4C), the temperature dependence of both apo- and holo-MUP I forms are very pronounced, but complexation has no visible effect. In Thr 58 (figure 7.4D), the temperature dependence is less pronounced and the slopes are conserved, but the intercepts are clearly affected by complexation. In Phe 100 (figure 7.4E), both slopes and intercepts are modified upon complexation with the pheromone. Finally, Gln 44 (figure 7.4F) shows a linear temperature dependence in apo-MUP I and a highly non-linear behaviour in the holo form, indicating that some dynamic process is dramatically affected by complexation at 295.6 K. In principle, if the logarithms

of the rates were plotted as a function of 1/T, the slopes would correspond to activation energies, but the quality of the data does not allow one to draw quantitative conclusions at this stage.

It is instructive to examine the rates $R_i^{CSM/CSM}$ for apo- and holo-MUP I (figure 7.4.2B): the His 57 residue lies within the 'C-D' loop, see section 4.1.1, while Val 59 is adjacent to it. This loop has been proposed to be the site of interaction with a cell-surface receptor in the structurally related retinol-binding protein. (Sivaprasadarao and Findlay, 1994) Interestingly, $dR_i^{CSM/CSM}/dT$ remains enhanced for these residues in *both* forms of the protein (figure 7.4.4A), suggesting that the enhanced rates can be attributed to slow time-scale dynamics.

Moreover, the dynamics of Val 59 markedly differ between the apo and holo forms (figure 7.4.4B), which is consistent with an earlier observation based on conventional ^{15}N relaxation measurements (Bingham et al., 2004) that residues in this region of the protein 'melt' upon binding with the IBMP ligand. Thus the dynamics of this region of the protein are perturbed over a wide range of time scales upon ligand binding.

A second loop in the region of Phe 100 exhibits substantially enhanced relaxation only in the holo form of the protein (figure 7.4.2), i.e., and it shows an enhanced derivative $dR_i^{CSM/CSM}/dT$ upon complexation (figure 7.4.4B). This region of the protein is known from ^{15}N relaxation measurements (Bingham et al., 2004) to 'freeze' on ligand binding. In contrast, other dynamic differences between apo and holo forms implied by the data in figure 7.4.4, for example in regions in the vicinity of Arg 39, Gln 44, Gly 121 and Leu 126 are not observed in ^{15}N relaxation measurements, suggesting that slow time-scale dynamic processes are dominant in these cases. The enhancement of

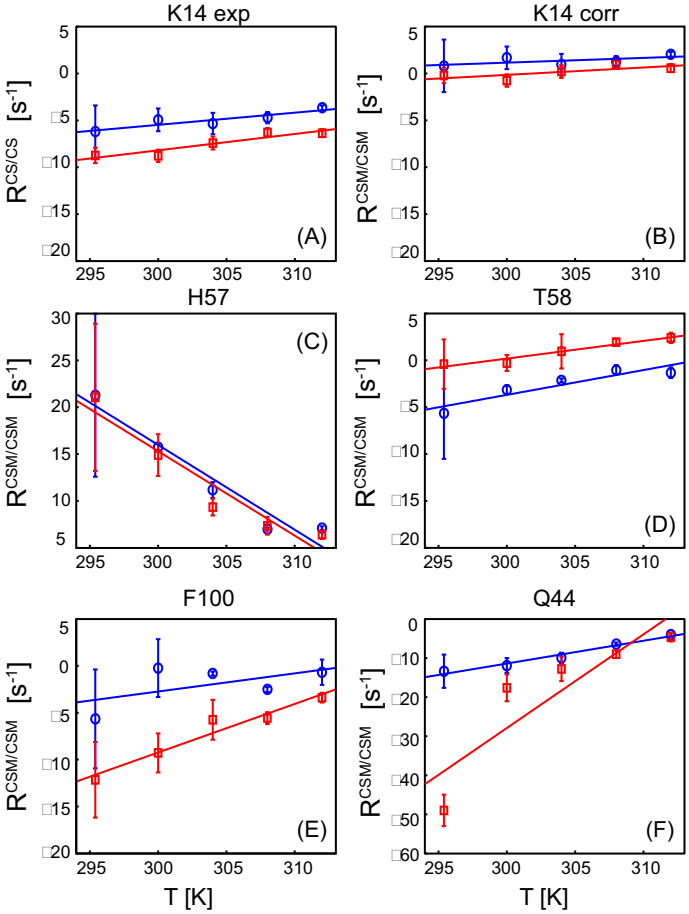

Figure 7.4.3: (A) Experimental rates $R_i^{exp}(T)$ for Lys 14 in apo- (blue circles) and holo-MUP I (red squares) measured at 600 MHz and T = 294.5, 300, 304, 308 and 312 K. (B) Corrected rates $R_i^{CSM/CSM}(T)$ for Lys 14 obtained after subtracting estimated DD/DD and CSA/CSA rates with a temperature dependence given by eq. 7.3.10. In this example, $R_i^{CSM/CSM} \approx 0$ at all temperatures, indicating the absence of any internal dynamics which is typical for many residues. (C)-(F) corrected rates $R_i^{CSM/CSM}(T)$ for His 57, Thr 58, Phe 100, and Gln 44, obtained by subtracting estimated temperature-dependent DD/DD and CSA/CSA rates. For His 57 and Thr 58, the slopes are not affected by complexation, while Gln 44 and, to a lesser extent, Phe 100 feature internal dynamics, that are strongly affected by the presence of the pheromone. Note that all rates $R_i^{CSM/CSM}(T)$ tend to vanish at high temperatures (fast exchange); the signs are negative if the chemical shift modulations $\Delta\omega_{C'}$ and $\Delta\omega_N$ are anti-correlated.

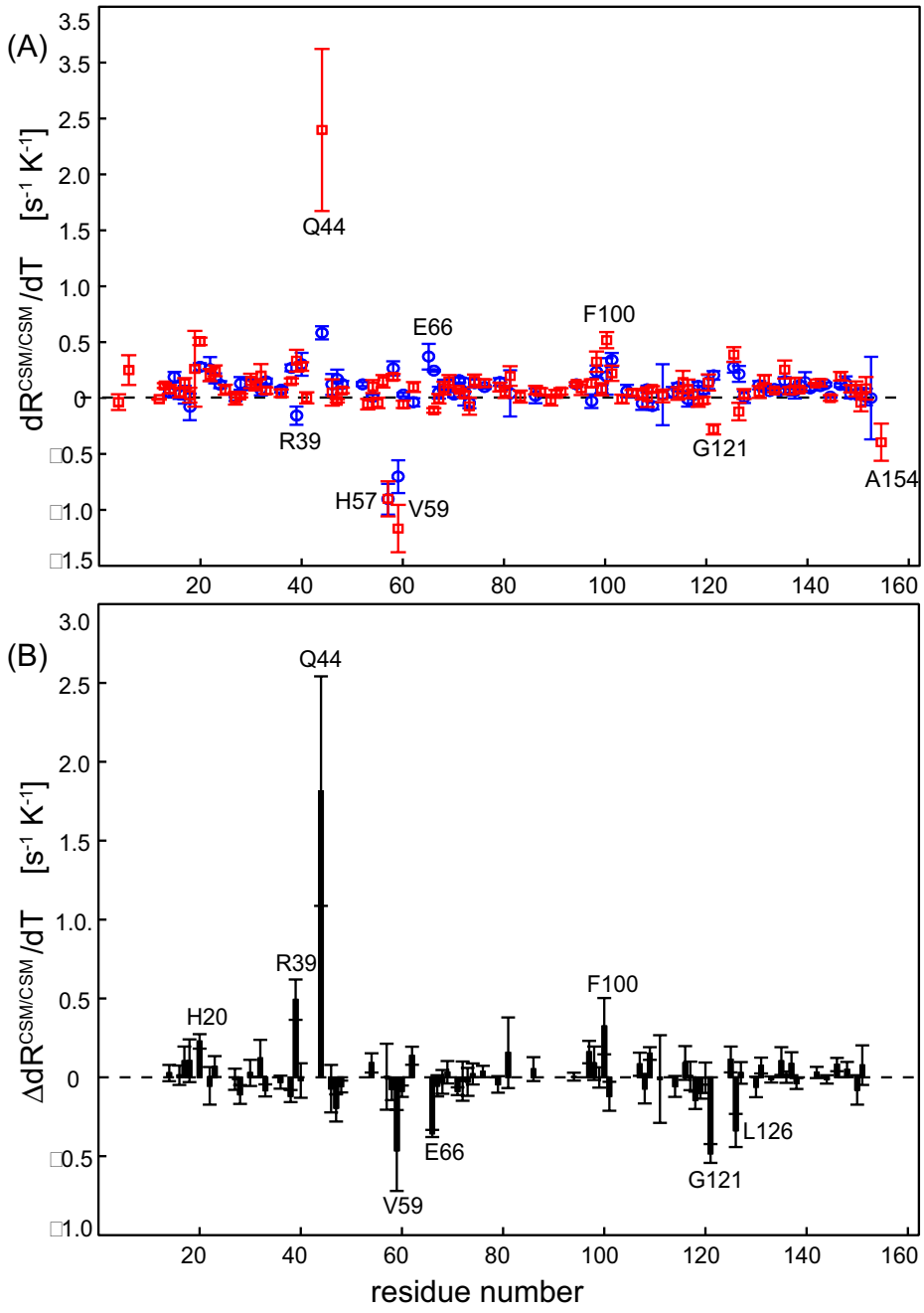

Figure 7.4.4: (A) Derivatives $dR_i^{CSM/CSM}/dT$ for all amino-acids where the signals could be followed as a function of temperature for both apo-MUP I (blue circles) and holo-MUP I (red squares). (B) Differences in the derivatives between the holo and apo forms.

the derivative $dR_i^{CSM/CSM}/dT$ for Gln 44 is surprising in view of the fact that this residue is buried within a β-sheet region of the protein (figure 7.4.5).

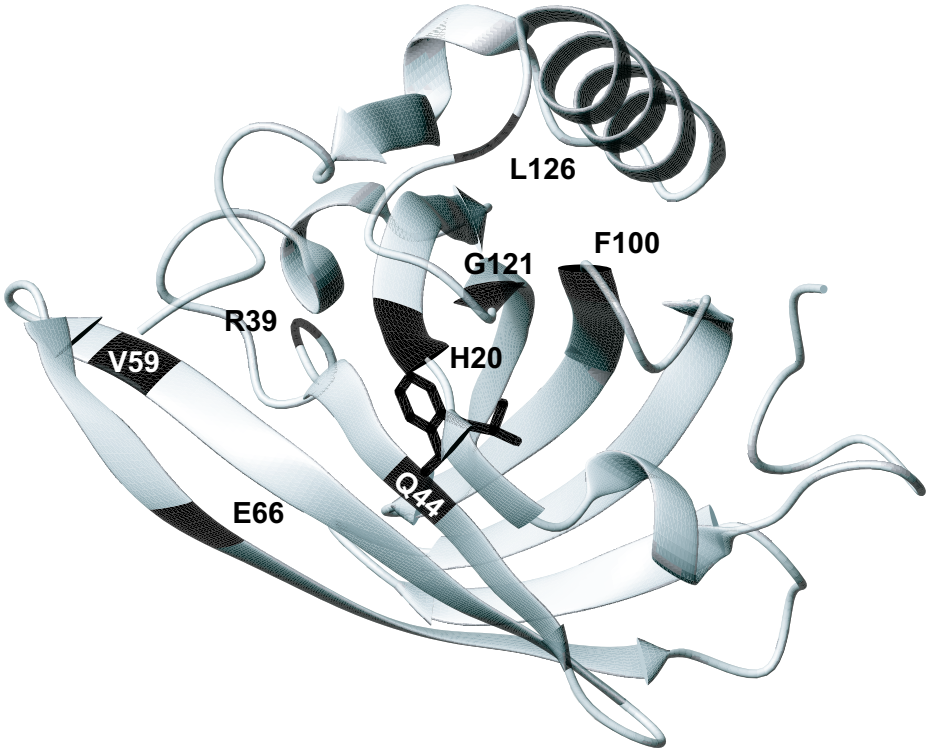

Figure 7.4.5: Ribbon representation of the X-ray structure of holo-MUP I, where the aromatic ring of the pheromone 2-methoxy-3-isobutylpyrazine (IBMP) appears in the centre. Residues whose derivatives $dR_i^{CSM/CSM}/dT$ are enhanced upon ligand binding are emphasized in black. The figure was obtained with the program MOLMOL, (Koradi et al., 1996).

7.5 Conclusions

Upon binding to 2-methoxy-3-isobutylpyrazine (IBMP), Major Urinary Protein I (MUP I) undergoes significant changes in slow internal dynamics. Our observations, based on relaxation rates of C'N double- and zero-quantum coherences, provide evi-

dence of significant changes in correlated internal dynamics in the protein upon ligand binding, on time scales that have not been explored so far. As with conventional backbone ^{15}N relaxation measurements on MUP I (Bingham et al., 2004), there are no obvious correlations between changes in rates $R_i^{CSM/CSM}$ and the location of the residues with respect to the binding site. However, these slow time-scale dynamic changes will clearly contribute to the entropy of ligand binding, and quantitation of the magnitude of these contributions is currently under investigation.

Table 7.5.1: Experimentally observed ('raw') decay rates R_i^{exp} (apo) as defined in eq. 7.3.1 with their errors ε measured at five temperatures 295.4, 300, 304, 308, 312 K, and 600 MHz.

Res.	295.4K $R_i^{exp} \pm \varepsilon$ [s^{-1}]	300K $R_i^{exp} \pm \varepsilon$ [s^{-1}]	304K $R_i^{exp} \pm \varepsilon$ [s^{-1}]	308K $R_i^{exp} \pm \varepsilon$ [s^{-1}]	312K $R_i^{exp} \pm \varepsilon$ [s^{-1}]
K14	-6.21 ± 2.80	-4.94 ± 1.21	-5.33 ± 1.14	-4.71 ± 0.60	-3.66 ± 0.26
I15	-8.45 ± 3.14	-6.06 ± 0.97	-6.36 ± 0.52	-4.69 ± 0.26	-4.16 ± 0.81
N16	-5.81 ± 2.80	-4.13 ± 0.07	-3.97 ± 0.87	-3.61 ± 0.36	-3.87 ± 0.40
G17	-5.54 ± 4.58	-3.83 ± 1.53	-5.92 ± 1.51	-4.17 ± 0.71	-3.47 ± 1.77
E18	-3.45 ± 2.06	-2.17 ± 0.44	-1.01 ± 0.49	—	-3.56 ± 0.39
W19	—	—	—	-4.75 ± 0.96	-3.10 ± 0.38
H20	—	-10.13 ± 0.83	-8.45 ± 0.71	-7.72 ± 1.03	-6.11 ± 0.42
I22	-8.03 ± 7.06	-5.40 ± 1.70	-2.73 ± 0.46	-2.58 ± 0.22	-3.25 ± 0.91
I23	-9.44 ± 2.67	-7.10 ± 0.74	-5.89 ± 0.64	-4.88 ± 0.37	-4.64 ± 0.72
L24	-4.62 ± 2.50	-4.54 ± 1.09	-3.70 ± 0.71	-2.44 ± 0.29	-1.80 ± 0.31
D27	-3.13 ± 2.11	-3.96 ± 0.92	-3.09 ± 0.50	-3.50 ± 0.33	-2.82 ± 0.31
K28	-7.36 ± 1.80	-6.76 ± 0.34	-4.59 ± 0.25	-4.71 ± 1.00	-4.80 ± 0.78
E30	-8.31 ± 1.76	-6.51 ± 0.33	-5.88 ± 0.61	-4.60 ± 0.39	-5.26 ± 1.08
I32	-8.87 ± 2.58	-6.39 ± 0.87	-6.99 ± 0.22	-5.83 ± 0.47	-5.55 ± 0.42
E33	-7.35 ± 1.69	-5.94 ± 0.28	-5.19 ± 0.45	-4.15 ± 0.24	-4.00 ± 0.26
G36	-8.03 ± 2.24	-6.73 ± 0.82	-6.14 ± 0.44	-6.03 ± 0.81	-5.31 ± 0.42
F38	-8.65 ± 2.64	-7.92 ± 1.55	-6.58 ± 1.28	-4.71 ± 0.37	-3.76 ± 0.11
R39	—	-5.31 ± 0.69	-6.14 ± 0.34	-7.29 ± 1.06	-6.38 ± 0.36
L40	-12.89 ± 7.97	-8.82 ± 1.15	-8.40 ± 0.73	-6.63 ± 0.78	-7.29 ± 0.79
Q44	-21.02 ± 4.26	-19.09 ± 1.89	-16.77 ± 1.31	-12.94 ± 0.42	-10.25 ± 0.56

Continued on next page

Table 7.5.1 – continued from previous page

Res.	295.4K $R_i^{exp} \pm \varepsilon$ [s^{-1}]	300K $R_i^{exp} \pm \varepsilon$ [s^{-1}]	304K $R_i^{exp} \pm \varepsilon$ [s^{-1}]	308K $R_i^{exp} \pm \varepsilon$ [s^{-1}]	312K $R_i^{exp} \pm \varepsilon$ [s^{-1}]
H46	-6.05 ± 4.10	-2.92 ± 0.79	-5.03 ± 0.70	-3.16 ± 0.80	-2.51 ± 0.96
V47	—	—	-3.03 ± 1.36	-2.78 ± 0.75	-1.36 ± 0.60
L48	-5.65 ± 2.86	-5.08 ± 1.17	-4.15 ± 1.31	-4.18 ± 0.47	-2.73 ± 0.38
L52	—	-5.38 ± 0.29	-4.86 ± 0.34	-3.79 ± 0.32	-3.10 ± 0.23
L54	-4.41 ± 2.98	-4.40 ± 0.64	-3.96 ± 0.84	-3.32 ± 0.26	-3.54 ± 0.10
H57	14.26 ± 8.70	9.15 ± 0.33	4.89 ± 0.84	1.02 ± 0.15	1.40 ± 0.19
T58	-12.46 ± 4.85	-9.53 ± 0.45	-8.23 ± 0.22	-6.82 ± 0.51	-6.84 ± 0.58
V59	—	7.49 ± 0.56	2.95 ± 0.33	2.79 ± 0.39	-1.13 ± 0.58
R60	-3.61 ± 1.44	-3.10 ± 0.69	-3.08 ± 0.15	-2.47 ± 0.24	-2.67 ± 0.17
E62	-4.01 ± 5.56	-3.98 ± 0.96	-4.11 ± 0.32	-4.70 ± 1.01	-3.56 ± 0.17
S65	—	-7.53 ± 4.58	-4.14 ± 1.31	-3.14 ± 0.33	-2.54 ± 0.63
E66	—	-5.40 ± 0.63	-4.35 ± 0.26	-3.18 ± 1.01	—
L67	-3.38 ± 2.48	-4.56 ± 1.06	-3.36 ± 0.47	-2.65 ± 0.54	-2.59 ± 0.52
S68	-5.13 ± 1.84	-3.81 ± 0.71	-2.29 ± 0.58	-2.28 ± 0.35	-2.25 ± 0.37
M69	-6.73 ± 3.74	-7.15 ± 0.78	-6.49 ± 0.50	-5.23 ± 0.82	-4.51 ± 0.27
V70	-5.25 ± 1.96	-5.44 ± 0.94	-5.17 ± 0.15	-4.48 ± 0.49	-4.18 ± 0.70
A71	-1.70 ± 3.57	-0.41 ± 0.12	-0.12 ± 1.52	0.48 ± 1.19	1.69 ± 0.50
D72	—	-0.51 ± 2.15	-2.15 ± 0.80	-0.71 ± 0.20	0.27 ± 0.67
K73	-4.95 ± 1.74	-4.37 ± 0.86	-5.62 ± 0.20	-5.11 ± 0.39	-4.43 ± 0.38
T74	-7.44 ± 2.44	-6.23 ± 0.27	-6.34 ± 0.70	-5.52 ± 0.45	-4.11 ± 1.01
K76	-7.00 ± 1.42	-6.09 ± 0.54	-5.48 ± 0.20	-4.88 ± 0.63	-4.71 ± 0.48
A77	-4.78 ± 0.56	-3.83 ± 0.14	-3.30 ± 0.02	-2.74 ± 0.05	-2.46 ± 0.17
E79	-4.14 ± 2.60	-2.62 ± 0.80	-2.84 ± 0.43	-1.38 ± 1.17	-0.46 ± 0.57
S81	-13.03 ± 7.16	-13.46 ± 2.91	-9.78 ± 3.08	-12.79 ± 2.21	—

Continued on next page

Table 7.5.1 – continued from previous page

Res.	295.4K $R_i^{exp} \pm \varepsilon$ [s^{-1}]	300K $R_i^{exp} \pm \varepsilon$ [s^{-1}]	304K $R_i^{exp} \pm \varepsilon$ [s^{-1}]	308K $R_i^{exp} \pm \varepsilon$ [s^{-1}]	312K $R_i^{exp} \pm \varepsilon$ [s^{-1}]
Y84	-3.65 ± 3.38	-2.88 ± 1.21	-4.14 ± 0.90	-2.94 ± 0.63	-1.79 ± 0.49
G86	-7.11 ± 1.92	-5.10 ± 0.59	-4.57 ± 0.57	-4.74 ± 0.05	-5.29 ± 0.12
K94	-5.51 ± 2.65	-4.54 ± 0.69	-3.75 ± 0.27	-3.63 ± 0.37	-2.47 ± 0.33
D96	-1.83 ± 3.86	-1.50 ± 1.70	-0.76 ± 0.64	-0.41 ± 1.17	-1.52 ± 0.56
Y97	—	-3.99 ± 0.59	-4.75 ± 0.83	-4.09 ± 0.47	-3.51 ± 0.84
D98	-9.30 ± 3.81	-8.00 ± 0.23	-8.26 ± 0.30	-5.71 ± 1.28	-4.70 ± 1.42
N99	-8.13 ± 2.42	-7.84 ± 1.28	-6.88 ± 0.74	-5.79 ± 0.53	-6.24 ± 0.89
F100	-12.34 ± 5.28	-6.52 ± 3.08	-6.80 ± 0.23	-8.21 ± 0.27	-6.11 ± 1.35
L101	-10.31 ± 4.71	-9.53 ± 0.96	-6.40 ± 1.73	-4.80 ± 0.72	-4.41 ± 0.82
H104	-2.65 ± 3.52	-1.94 ± 0.98	-2.94 ± 0.63	-1.41 ± 0.47	-0.53 ± 0.48
N107	-4.05 ± 3.91	-3.73 ± 0.81	-4.30 ± 0.11	-5.04 ± 0.65	-3.38 ± 0.70
E108	-5.20 ± 2.23	-3.96 ± 0.24	-3.51 ± 0.65	-3.01 ± 0.51	-3.19 ± 0.37
K109	—	—	-3.73 ± 0.48	-4.12 ± 0.38	-4.08 ± 0.35
G111	-6.05 ± 2.38	-7.62 ± 1.68	-5.21 ± 0.90	—	—
T113	-5.18 ± 1.57	-3.66 ± 1.09	-3.93 ± 0.74	-3.86 ± 0.15	-2.28 ± 0.52
F114	-5.00 ± 2.40	-3.50 ± 0.88	-3.05 ± 0.56	-3.20 ± 0.54	-2.30 ± 0.79
L116	-7.46 ± 3.89	-8.15 ± 0.27	-9.06 ± 0.32	-7.20 ± 0.64	-7.36 ± 0.43
M117	-3.33 ± 2.63	-5.43 ± 0.80	-3.95 ± 0.99	-3.02 ± 0.53	-2.81 ± 0.43
G118	-4.93 ± 2.98	-4.86 ± 0.28	-3.04 ± 0.44	-2.84 ± 0.18	-2.02 ± 0.57
L119	-5.47 ± 2.68	-4.55 ± 0.90	-4.87 ± 0.60	-3.45 ± 0.38	-3.48 ± 0.47
Y120	-7.82 ± 3.65	-6.73 ± 0.60	-4.60 ± 0.55	-5.75 ± 0.20	-4.25 ± 1.06
G121	-7.45 ± 5.15	-5.62 ± 3.02	-4.60 ± 1.39	-4.36 ± 0.42	-2.23 ± 0.69
D125	-10.80 ± 1.43	-8.43 ± 0.23	-6.75 ± 0.27	-6.36 ± 0.11	-5.49 ± 0.20
L126	-7.29 ± 2.52	-4.14 ± 1.66	-4.76 ± 0.52	-2.81 ± 0.04	-2.69 ± 0.42

Continued on next page

Table 7.5.1 – continued from previous page

Res.	295.4K $R_i^{exp} \pm \varepsilon$ [s^{-1}]	300K $R_i^{exp} \pm \varepsilon$ [s^{-1}]	304K $R_i^{exp} \pm \varepsilon$ [s^{-1}]	308K $R_i^{exp} \pm \varepsilon$ [s^{-1}]	312K $R_i^{exp} \pm \varepsilon$ [s^{-1}]
S127	-3.83 ± 1.36	-4.02 ± 0.56	-3.03 ± 0.44	-4.17 ± 0.24	-2.54 ± 0.41
I130	-7.56 ± 1.52	-5.96 ± 0.38	-4.96 ± 0.24	-4.49 ± 0.17	-4.42 ± 0.11
K131	-6.26 ± 1.84	-5.00 ± 0.43	-3.92 ± 0.41	-4.04 ± 0.39	-3.26 ± 0.47
E132	—	—	-5.96 ± 0.69	-5.37 ± 0.06	-4.94 ± 0.41
R133	-6.45 ± 1.20	-5.30 ± 0.89	-4.78 ± 0.09	-4.21 ± 0.30	-3.63 ± 0.28
F134	-6.49 ± 1.60	-6.45 ± 0.40	-5.31 ± 0.80	-4.98 ± 0.21	-4.27 ± 0.33
A135	-7.61 ± 1.39	-6.68 ± 0.74	-4.80 ± 0.33	-4.75 ± 0.61	-3.94 ± 0.21
Q136	-6.53 ± 1.24	-6.00 ± 0.35	-4.94 ± 0.13	-4.56 ± 0.16	-4.20 ± 0.08
L137	-5.82 ± 1.29	-7.06 ± 0.93	-5.85 ± 0.49	-4.63 ± 0.03	-4.47 ± 0.25
C138	-9.00 ± 1.79	-7.13 ± 0.68	-7.03 ± 0.28	-6.13 ± 0.41	-5.53 ± 0.21
E139	—	-6.63 ± 0.54	-6.86 ± 0.66	-4.51 ± 0.14	-4.50 ± 0.06
E140	-7.01 ± 1.36	-6.78 ± 0.98	-5.69 ± 0.41	-5.33 ± 0.19	-4.75 ± 0.16
G142	-7.76 ± 1.28	—	-5.94 ± 0.42	-5.48 ± 0.28	-5.04 ± 0.01
I143	-7.63 ± 1.42	-6.24 ± 0.23	-5.86 ± 0.16	-4.88 ± 0.51	-4.27 ± 0.37
L144	-2.68 ± 1.29	-2.58 ± 0.86	-2.34 ± 0.19	-1.95 ± 0.27	-1.96 ± 0.09
E146	-7.74 ± 1.89	-6.55 ± 1.94	-5.80 ± 0.92	-5.37 ± 0.96	-4.80 ± 1.47
N147	—	—	-6.40 ± 0.59	-5.30 ± 0.49	-4.99 ± 0.21
I148	-4.62 ± 1.57	-5.17 ± 0.88	-3.85 ± 0.10	-3.73 ± 0.12	-3.33 ± 0.21
D150	-3.33 ± 2.25	-3.49 ± 0.27	-1.61 ± 0.69	-1.90 ± 0.34	-2.19 ± 0.63
L151	—	-3.63 ± 0.48	-2.31 ± 0.18	-2.88 ± 0.78	-3.16 ± 0.98
S152	—	—	-3.96 ± 1.69	-6.32 ± 0.63	-3.58 ± 0.93
N153	-6.67 ± 7.15	-5.85 ± 1.44	-3.31 ± 0.86	—	—
A154	—	—	—	-0.91 ± 0.16	5.25 ± 0.93

Table 7.5.2: Experimentally observed ('raw') decay rates R_i^{exp} (holo) as defined in eq. 7.3.1 with their errors ε measured at five temperatures 295.4, 300, 304, 308, 312 K, and 600 MHz.

Res.	295.4K $R_i^{exp} \pm \varepsilon$ [s^{-1}]	300K $R_i^{exp} \pm \varepsilon$ [s^{-1}]	304K $R_i^{exp} \pm \varepsilon$ [s^{-1}]	308K $R_i^{exp} \pm \varepsilon$ [s^{-1}]	312K $R_i^{exp} \pm \varepsilon$ [s^{-1}]
S4	-4.87 ± 0.47	-5.96 ± 0.16	-3.80 ± 0.33	-3.86 ± 0.66	-4.72 ± 1.33
S5	-4.79 ± 0.79	-6.19 ± 2.56	-6.00 ± 2.13	-2.63 ± 0.89	—
T6	-12.17 ± 3.84	-11.93 ± 1.04	-7.57 ± 3.33	—	-7.53 ± 1.48
F10	-4.02 ± 0.01	-4.49 ± 0.52	-3.79 ± 0.87	-2.47 ± 0.76	-3.56 ± 1.19
N11	-5.68 ± 0.78	-6.04 ± 0.73	-4.65 ± 1.20	-5.10 ± 0.37	-3.78 ± 2.13
V12	-3.72 ± 0.40	-3.73 ± 0.75	-3.51 ± 0.46	-3.44 ± 0.24	-3.31 ± 0.48
E13	-8.34 ± 0.34	-7.02 ± 0.17	-6.15 ± 0.85	-5.49 ± 0.16	-5.21 ± 0.81
K14	-8.73 ± 0.83	-8.78 ± 0.66	-7.41 ± 0.69	-6.29 ± 0.49	-6.36 ± 0.42
N16	-7.41 ± 1.16	-5.62 ± 0.55	-5.14 ± 0.43	-5.51 ± 0.37	-4.58 ± 0.80
G17	-8.89 ± 0.77	-7.48 ± 0.54	-7.38 ± 0.97	-5.89 ± 0.98	—
E18	-4.74 ± 0.70	-2.33 ± 0.63	-3.59 ± 1.38	-2.99 ± 0.34	-2.23 ± 0.97
W19	—	-8.73 ± 1.68	-1.75 ± 3.63	-3.99 ± 2.37	-3.89 ± 1.19
H20	-15.07 ± 5.87	-13.41 ± 0.51	-10.47 ± 3.36	-8.46 ± 1.54	-5.92 ± 0.31
I22	-8.99 ± 3.15	-6.97 ± 2.21	-6.38 ± 1.57	-6.37 ± 1.76	-3.90 ± 0.78
I23	-12.14 ± 2.66	-10.25 ± 0.42	-9.73 ± 0.90	-6.72 ± 0.18	-6.01 ± 0.71
A25	-6.13 ± 1.47	-6.64 ± 0.45	-5.96 ± 0.60	-4.95 ± 0.39	-4.10 ± 1.38
D27	—	-3.87 ± 0.58	-4.78 ± 1.28	-4.16 ± 1.03	-3.94 ± 0.63
K28	-1.92 ± 0.12	-1.57 ± 0.24	-1.10 ± 0.42	-1.15 ± 0.64	—
E30	-9.29 ± 1.33	-7.59 ± 0.79	-6.26 ± 0.59	-6.39 ± 0.80	—
K31	-8.46 ± 0.72	-7.34 ± 0.49	-6.01 ± 0.51	-6.58 ± 0.24	-5.40 ± 0.44

Continued on next page

Table 7.5.2 – continued from previous page

Res.	295.4K $R_i^{exp} \pm \varepsilon$ [s^{-1}]	300K $R_i^{exp} \pm \varepsilon$ [s^{-1}]	304K $R_i^{exp} \pm \varepsilon$ [s^{-1}]	308K $R_i^{exp} \pm \varepsilon$ [s^{-1}]	312K $R_i^{exp} \pm \varepsilon$ [s^{-1}]
I32	-10.65 ± 1.19	-9.68 ± 1.32	-6.68 ± 0.69	-7.06 ± 0.95	—
E33	-7.64 ± 0.48	-7.10 ± 0.54	-6.57 ± 1.13	-5.33 ± 0.63	-5.66 ± 0.66
G36	-8.94 ± 0.14	-8.46 ± 1.21	-8.00 ± 1.06	-6.59 ± 0.44	-7.03 ± 1.11
F38	-10.49 ± 3.48	-9.76 ± 1.83	-8.92 ± 0.38	-7.50 ± 0.16	-7.34 ± 0.34
R39	-11.96 ± 1.05	-7.32 ± 1.13	-6.45 ± 0.54	-5.46 ± 0.35	-4.76 ± 0.24
L40	-10.23 ± 2.20	-7.79 ± 2.24	-7.29 ± 0.61	-5.44 ± 0.80	-4.89 ± 0.19
F41	—	-7.10 ± 2.55	-7.16 ± 1.34	-6.22 ± 0.75	-6.84 ± 0.87
Q44	-58.27 ± 4.03	-26.36 ± 3.44	-21.09 ± 3.14	-16.92 ± 1.03	-12.20 ± 1.12
I45	—	—	—	-3.69 ± 0.19	-3.65 ± 0.77
H46	-8.43 ± 0.07	-6.89 ± 1.00	-4.37 ± 0.43	-5.63 ± 0.69	-6.88 ± 1.09
V47	-3.67 ± 1.55	-3.67 ± 0.15	-3.35 ± 0.81	-3.61 ± 0.55	-3.11 ± 0.50
L48	-7.49 ± 0.40	-7.15 ± 0.21	-6.00 ± 0.20	-5.85 ± 0.20	-5.78 ± 0.60
L52	—	—	—	-6.25 ± 0.49	-5.20 ± 0.84
V53	-5.75 ± 0.76	-4.47 ± 0.68	-5.31 ± 0.45	-4.56 ± 0.52	-5.42 ± 0.36
L54	-6.74 ± 0.65	-7.50 ± 1.69	-5.45 ± 0.41	-4.63 ± 0.56	-4.58 ± 1.13
K55	-3.82 ± 0.35	-4.35 ± 0.26	-4.83 ± 0.33	-3.48 ± 0.37	-3.82 ± 0.76
F56	-9.07 ± 1.50	-6.36 ± 0.95	-6.32 ± 1.13	-5.35 ± 0.60	-5.08 ± 1.54
H57	12.98 ± 7.87	7.29 ± 2.23	2.12 ± 0.90	0.46 ± 0.94	-0.17 ± 0.43
T58	-8.70 ± 2.64	-8.09 ± 0.85	-6.46 ± 1.83	-5.13 ± 0.35	-4.35 ± 0.55
V59	—	—	10.34 ± 3.45	4.45 ± 0.19	1.47 ± 1.58
R60	-2.04 ± 0.98	-2.79 ± 0.09	-2.98 ± 0.74	-2.61 ± 0.53	-2.40 ± 0.48
D61	-5.64 ± 1.45	-8.32 ± 1.15	—	—	—
E62	-7.37 ± 2.51	-5.87 ± 2.00	-6.18 ± 1.62	-4.50 ± 0.25	-4.86 ± 1.13
S65	—	—	—	-5.49 ± 0.17	-5.09 ± 1.03

Continued on next page

Table 7.5.2 – continued from previous page

Res.	295.4K $R_i^{exp} \pm \varepsilon$ [s^{-1}]	300K $R_i^{exp} \pm \varepsilon$ [s^{-1}]	304K $R_i^{exp} \pm \varepsilon$ [s^{-1}]	308K $R_i^{exp} \pm \varepsilon$ [s^{-1}]	312K $R_i^{exp} \pm \varepsilon$ [s^{-1}]
E66	—	-2.17 ± 0.19	-2.66 ± 0.35	-2.97 ± 0.54	-2.97 ± 0.81
L67	-4.26 ± 1.41	-5.13 ± 0.26	-3.82 ± 1.26	-4.51 ± 0.15	-4.08 ± 1.47
S68	-7.26 ± 0.44	-5.36 ± 0.31	-6.02 ± 0.49	-4.24 ± 0.41	-4.82 ± 0.88
M69	-8.60 ± 1.04	-6.51 ± 0.44	-5.57 ± 0.48	-5.97 ± 0.79	-5.18 ± 0.90
V70	-6.39 ± 0.76	-5.96 ± 0.48	—	—	—
A71	-5.57 ± 1.18	-4.86 ± 0.37	-4.51 ± 0.60	-4.14 ± 0.58	—
D72	-4.64 ± 0.31	-3.83 ± 0.33	-3.11 ± 0.95	-3.15 ± 0.13	-3.07 ± 0.42
K73	—	—	-1.34 ± 1.20	-1.89 ± 0.32	-1.41 ± 0.47
T74	-9.50 ± 0.12	-6.94 ± 0.41	-7.14 ± 0.32	-5.73 ± 0.29	-5.81 ± 0.67
K76	-9.32 ± 0.21	-8.30 ± 0.24	-6.79 ± 0.57	-6.59 ± 0.43	-6.25 ± 0.98
A77	-3.35 ± 0.96	-3.32 ± 1.34	-1.83 ± 0.85	—	—
E79	-7.90 ± 0.70	-7.77 ± 0.22	-5.97 ± 0.42	-6.20 ± 0.11	-4.97 ± 0.22
Y80	-7.76 ± 1.28	-6.14 ± 1.10	-5.39 ± 1.04	-6.07 ± 0.88	-5.58 ± 0.78
S81	-10.05 ± 0.56	-8.06 ± 0.58	-5.35 ± 0.45	-5.50 ± 0.70	-5.71 ± 2.27
V82	-5.47 ± 0.18	-4.87 ± 0.73	—	—	—
T83	-5.59 ± 0.50	-6.59 ± 1.33	-5.34 ± 0.65	-4.47 ± 0.16	-4.99 ± 2.44
Y84	-7.11 ± 0.75	-6.33 ± 0.36	-6.89 ± 1.48	-5.07 ± 0.36	-4.36 ± 1.67
G86	-8.85 ± 0.11	-7.30 ± 0.40	-6.72 ± 0.38	-5.80 ± 0.45	-6.09 ± 0.79
F87	-5.44 ± 0.67	-3.73 ± 1.34	-3.61 ± 0.95	-3.28 ± 0.33	-2.80 ± 0.55
T89	-5.09 ± 0.61	-3.55 ± 0.18	-4.35 ± 1.18	-4.23 ± 0.28	-3.13 ± 0.80
F90	-7.74 ± 1.19	-6.26 ± 0.60	-5.84 ± 0.72	-5.82 ± 0.28	-5.54 ± 0.30
T91	-8.46 ± 2.65	-6.96 ± 0.90	-6.04 ± 0.73	-6.01 ± 0.50	-5.20 ± 0.38
K94	-8.54 ± 0.40	-7.37 ± 0.74	-6.48 ± 0.49	-6.05 ± 0.27	-5.37 ± 0.86
T95	-7.79 ± 0.68	-5.36 ± 0.30	-5.18 ± 0.89	-5.55 ± 0.55	-4.26 ± 0.48

Continued on next page

Table 7.5.2 – continued from previous page

Res.	295.4K $R_i^{exp} \pm \varepsilon$ [s^{-1}]	300K $R_i^{exp} \pm \varepsilon$ [s^{-1}]	304K $R_i^{exp} \pm \varepsilon$ [s^{-1}]	308K $R_i^{exp} \pm \varepsilon$ [s^{-1}]	312K $R_i^{exp} \pm \varepsilon$ [s^{-1}]
D96	-6.75 ± 1.94	-8.75 ± 0.58	-6.57 ± 1.09	-5.34 ± 0.56	-5.30 ± 1.02
Y97	-10.65 ± 1.76	-8.99 ± 1.48	-9.11 ± 2.73	-7.37 ± 1.05	-6.55 ± 0.43
D98	-11.30 ± 1.34	-7.94 ± 0.98	-7.40 ± 0.73	-6.25 ± 0.48	—
N99	-9.90 ± 0.36	-9.77 ± 0.43	-7.96 ± 1.33	-7.29 ± 0.38	-7.97 ± 0.36
F100	-20.36 ± 4.04	-17.01 ± 2.08	-13.09 ± 2.13	-12.56 ± 0.64	-10.06 ± 0.52
L101	-11.30 ± 0.61	-8.96 ± 0.99	-8.91 ± 1.50	-6.09 ± 0.05	-6.67 ± .20
A103	-3.67 ± 1.86	-2.48 ± 1.48	-2.78 ± 1.15	-2.53 ± 0.46	-3.10 ± 1.63
H104	-5.69 ± 1.54	-3.72 ± 0.38	—	—	—
L105	-6.37 ± 1.17	-5.99 ± 1.00	-6.26 ± 1.33	-5.26 ± 0.58	-5.04 ± 2.96
N107	-4.37 ± 1.27	-3.14 ± 0.48	-4.02 ± 1.15	-2.43 ± 0.33	-2.75 ± 1.69
E108	—	—	-4.08 ± 0.22	-4.46 ± 0.09	-3.64 ± 0.39
K109	-6.54 ± 0.28	-5.69 ± 0.89	-4.96 ± 0.86	-4.60 ± 0.43	-4.69 ± 0.32
G111	-8.04 ± 0.58	-7.05 ± 0.27	-6.29 ± 0.84	-5.74 ± 0.89	-6.99 ± 1.27
T113	-6.89 ± 1.04	-6.55 ± 1.09	—	—	—
F114	—	—	-6.04 ± 0.55	-6.07 ± 0.19	-5.33 ± 1.65
Q115	-12.85 ± 1.84	-10.22 ± 3.17	-9.62 ± 2.22	-9.82 ± 1.12	—
L116	-9.72 ± 0.87	-7.28 ± 1.84	-7.83 ± 1.27	-6.31 ± 0.93	-7.74 ± 1.31
M117	-6.08 ± 1.53	-5.78 ± 1.03	-5.70 ± 0.54	-4.63 ± 0.42	—
G118	-4.83 ± 1.58	-5.61 ± 1.61	-4.58 ± 0.68	-4.81 ± 0.22	-3.92 ± 0.53
L119	-4.62 ± 0.75	-5.11 ± 1.48	-4.17 ± 0.64	-3.97 ± 0.35	-4.17 ± 0.40
Y120	-12.02 ± 5.43	-9.10 ± 0.32	-9.54 ± 0.55	-7.93 ± 0.96	-8.35 ± 2.08
G121	-4.47 ± 3.42	-6.22 ± 2.02	-6.07 ± 2.05	-6.36 ± 1.24	-8.04 ± 0.86
D125	-14.36 ± 1.42	-10.86 ± 1.09	-8.97 ± 1.01	-7.99 ± 0.42	-7.03 ± 0.86
L126	—	-4.13 ± 0.84	-5.71 ± 1.91	-5.24 ± 0.82	-5.22 ± 1.28

Continued on next page

Table 7.5.2 – continued from previous page

Res.	295.4K $R_i^{exp} \pm \varepsilon$ [s^{-1}]	300K $R_i^{exp} \pm \varepsilon$ [s^{-1}]	304K $R_i^{exp} \pm \varepsilon$ [s^{-1}]	308K $R_i^{exp} \pm \varepsilon$ [s^{-1}]	312K $R_i^{exp} \pm \varepsilon$ [s^{-1}]
S127	-4.09 ± 0.19	-4.79 ± 0.46	-3.39 ± 1.00	-2.85 ± 0.18	-3.02 ± 0.96
I130	-8.25 ± 0.19	-8.43 ± 0.32	-8.15 ± 0.59	-6.16 ± 0.63	-6.33 ± 0.68
K131	-9.46 ± 1.78	-6.99 ± 0.33	-6.73 ± 1.03	-5.46 ± 0.34	-4.79 ± 0.36
E132	—	—	—	-6.63 ± 0.32	-6.23 ± 0.83
R133	-8.28 ± 0.29	-7.15 ± 0.23	-6.37 ± 0.44	-5.86 ± 0.07	-5.49 ± 0.39
F134	—	—	—	-5.17 ± 0.45	-5.25 ± 0.57
A135	-12.02 ± 1.41	-8.95 ± 0.72	-6.82 ± 0.33	-6.53 ± 0.34	-6.19 ± 0.64
Q136	-7.65 ± 0.66	-5.93 ± 0.80	-5.91 ± 1.01	-4.86 ± 0.30	-4.71 ± 0.52
L137	-10.27 ± 0.90	-8.05 ± 0.72	-7.89 ± 0.32	-6.87 ± 0.28	-6.28 ± 0.39
C138	-8.23 ± 1.01	-7.59 ± 1.36	-6.88 ± 0.46	-5.78 ± 0.55	-5.41 ± 0.55
H141	-7.93 ± 1.28	-7.00 ± 0.41	-6.33 ± 0.74	-5.44 ± 0.24	-4.74 ± 0.38
G142	-10.24 ± 0.15	-8.54 ± 0.28	-8.05 ± 0.62	-6.81 ± 0.79	-6.74 ± 1.12
L144	-3.14 ± 0.82	-2.95 ± 0.34	-2.88 ± 0.65	-2.04 ± 0.16	-2.60 ± 0.45
R145	—	—	—	-2.94 ± 0.12	-3.01 ± 0.86
E146	-9.59 ± 0.66	-8.53 ± 0.66	-6.78 ± 0.55	-6.86 ± 0.87	-4.91 ± 1.63
N147	—	—	—	-2.05 ± 0.34	-2.44 ± 0.53
I148	-7.68 ± 0.70	-5.97 ± 0.95	-5.60 ± 0.74	-5.12 ± 0.27	-4.81 ± 0.70
I149	-7.78 ± 0.37	-9.06 ± 1.93	-7.83 ± 1.20	-6.74 ± 1.13	-5.96 ± 0.67
D150	-3.84 ± 0.55	-4.18 ± 1.50	-4.30 ± 1.60	-2.18 ± 0.64	-4.25 ± 0.33
L151	-4.82 ± 5.32	-6.17 ± 1.96	-3.29 ± 0.27	-2.81 ± 1.12	-4.36 ± 0.89
S152	—	—	—	-11.04 ± 1.55	-11.91 ± 0.30
A154	—	6.21 ± 1.53	3.03 ± 2.07	1.10 ± 1.52	2.04 ± 1.88

Table 7.5.3: Estimated values of $R_i^{DD/DD}$ and $R_i^{CSA/CSA}$ in apo-MUP I. The CSA tensors were obtained from measurements on Ubiquitin using five distinct models: (a) Isotropic local wobbling-in-a-cone; (b) 3D-GAF model with a common correlation time for all internal motions around three orthogonal axes; (c) model in which the amide proton H^N is allowed to move out of the peptide plane separately while the remaining peptide plane moves around an axis parallel to the average NH^N bond with an internal correlation time of 40 ps; (d) same as (c) but with an internal correlation time of 400 ps; (e) same as (d) but with a nitrogen-15 CSA tensor that follows the motion of the NH^N bond.

	$R_i^{DD/DD}$	$R_i^{CSA/CSA}$		$R_i^{CSA/CSA}$		
Model:		(a)	(b)	(c)	(d)	(e)
Residue	$[s^{-1}]$	$[s^{-1}]$	$[s^{-1}]$	$[s^{-1}]$	$[s^{-1}]$	$[s^{-1}]$
E2	-2.08	—	—	—	—	—
A3	-1.36	—	—	—	—	—
S4	-3.02	-2.08	-3.02	-2.42	-2.44	-2.98
S5	-0.67	—	—	—	—	—
T6	-1.72	-2.38	-3.33	-2.76	-2.72	-3.26
G7	-4.81	—	—	—	—	—
R8	-2.74	—	—	—	—	—
N9	-1.19	—	—	—	—	—
F10	-2.26	—	—	—	—	—
N11	-0.74	—	—	—	—	—
V12	-1.02	-0.28	-1.25	-0.62	-0.85	-1.32
E13	-2.78	-0.84	-1.85	-1.24	-1.39	-1.88
K14	-3.12	-1.86	-2.87	-2.23	-2.30	-2.86

Continued on next page

Table 7.5.3 – continued from previous page

	$R_i^{DD/DD}$	$R_i^{CSA/CSA}$		$R_i^{CSA/CSA}$		
Model:		(a)	(b)	(c)	(d)	(e)
Residue	[s^{-1}]	[s^{-1}]	[s^{-1}]	[s^{-1}]	[s^{-1}]	[s^{-1}]
I15	-1.22	-2.04	-3.05	-2.45	-2.46	-3.00
N16	-3.87	-0.70	-1.68	-1.07	-1.23	-1.70
G17	-1.93	-1.84	-2.83	-2.24	-2.27	-2.80
E18	-3.82	-0.36	-1.28	-0.69	-0.87	-1.31
W19	-1.26	-0.68	-1.63	-1.00	-1.19	-1.69
H20	-1.25	-1.03	-1.97	-1.41	-1.50	-1.95
T21	-1.81	-0.74	-1.76	-1.10	-1.30	-1.83
I22	-2.89	0.58	-0.43	0.21	-0.11	-0.55
I23	-6.44	-1.17	-2.13	-1.55	-1.63	-2.11
L24	-3.76	-0.26	-1.25	-0.62	-0.84	-1.32
A25	-2.53	-0.17	-1.18	-0.55	-0.77	-1.24
S26	-2.70	-1.57	-2.57	-1.98	-2.03	-2.54
D27	-0.07	-0.07	-1.07	-0.44	-0.68	-1.13
K28	-1.59	-0.79	-1.74	-1.11	-1.29	-1.79
R29	-0.51	—	—	—	—	—
E30	-2.85	-1.52	-2.51	-1.90	-1.98	-2.51
K31	-1.15	-1.63	-2.62	-1.98	-2.07	-2.62
I32	-3.97	-2.47	-3.43	-2.88	-2.81	-3.34
E33	-2.81	-0.51	-1.51	-0.88	-1.08	-1.56
D34	-2.98	-1.02	-1.97	-1.37	-1.50	-1.99
N35	-1.70	—	—	—	—	—
G36	-3.00	-1.77	-2.74	-2.18	-2.19	-2.68
N37	-1.92	—	—	—	—	—
F38	-1.19	-1.16	-2.15	-1.56	-1.66	-2.15

Continued on next page

Table 7.5.3 – continued from previous page

	$R_i^{DD/DD}$	$R_i^{CSA/CSA}$		$R_i^{CSA/CSA}$		
Model:		(a)	(b)	(c)	(d)	(e)
Residue	[s^{-1}]	[s^{-1}]	[s^{-1}]	[s^{-1}]	[s^{-1}]	[s^{-1}]
R39	-2.79	-0.11	-1.11	-0.47	-0.71	-1.18
L40	-1.19	0.07	-0.88	-0.27	-0.51	-0.95
F41	-0.95	-0.33	-1.34	-0.67	-0.92	-1.42
L42	-1.10	0.33	-0.68	0.01	-0.33	-0.82
E43	-1.28	—	—	—	—	—
Q44	-3.98	-1.55	-2.53	-1.94	-2.00	-2.50
I45	-3.74	-0.51	-1.47	-0.87	-1.04	-1.50
H46	-2.72	0.21	-0.81	-0.14	-0.45	-0.93
V47	-2.39	0.06	-0.94	-0.28	-0.56	-1.03
L48	-2.22	0.39	-0.61	0.07	-0.26	-0.75
E49	-0.90	-0.91	-1.89	-1.27	-1.42	-1.91
K50	-2.47	—	—	—	—	—
S51	-2.36	-1.55	-2.52	-1.94	-1.99	-2.48
L52	-4.51	-0.40	-1.34	-0.77	-0.93	-1.36
V53	-2.90	-0.41	-1.43	-0.78	-1.00	-1.49
L54	-3.46	0.21	-0.80	-0.13	-0.43	-0.92
K55	-2.59	-0.23	-1.22	-0.59	-0.81	-1.28
F56	-2.54	-0.30	-1.27	-0.64	-0.86	-1.33
H57	-3.71	-1.32	-2.27	-1.67	-1.76	-2.26
T58	-3.48	-1.35	-2.31	-1.73	-1.80	-2.28
V59	-3.48	0.27	-0.72	-0.11	-0.37	-0.79
R60	-1.39	0.09	-0.91	-0.24	-0.53	-1.02
D61	-0.83	0.12	-0.87	-0.23	-0.50	-0.95
E62	-0.39	-1.87	-2.79	-2.25	-2.24	-2.73

Continued on next page

Table 7.5.3 – continued from previous page

	$R_i^{DD/DD}$	$R_i^{CSA/CSA}$		$R_i^{CSA/CSA}$		
Model:		(a)	(b)	(c)	(d)	(e)
Residue	[s^{-1}]	[s^{-1}]	[s^{-1}]	[s^{-1}]	[s^{-1}]	[s^{-1}]
E63	-1.57	-0.69	-1.67	-1.05	-1.22	-1.71
C64	-2.15	-0.45	-1.43	-0.79	-1.00	-1.49
S65	-0.61	-0.80	-1.76	-1.15	-1.30	-1.78
E66	-1.52	-0.02	-0.98	-0.37	-0.61	-1.05
L67	-1.42	-0.23	-1.23	-0.57	-0.82	-1.32
S68	-2.98	-0.69	-1.66	-1.05	-1.21	-1.69
M69	-1.31	-0.34	-1.29	-0.68	-0.88	-1.34
V70	-2.27	-0.10	-1.10	-0.48	-0.71	-1.16
A71	-1.60	0.72	-0.30	0.38	0.01	-0.45
D72	-1.66	-0.44	-1.44	-0.78	-1.01	-1.52
K73	-2.34	-0.60	-1.61	-0.96	-1.17	-1.67
T74	-0.98	-1.47	-2.48	-1.85	-1.95	-2.48
E75	-0.45	—	—	—	—	—
K76	-1.69	-0.59	-1.62	-0.97	-1.17	-1.68
A77	-2.67	—	—	—	—	—
G78	-0.22	—	—	—	—	—
E79	-3.71	-0.22	-1.20	-0.62	-0.80	-1.23
Y80	-2.61	-0.14	-1.12	-0.47	-0.72	-1.20
S81	-2.61	-1.07	-2.04	-1.46	-1.56	-2.04
V82	-4.09	-0.48	-1.47	-0.86	-1.04	-1.50
T83	-3.36	0.31	-0.71	-0.03	-0.35	-0.83
Y84	-1.32	—	—	—	—	—
D85	1.61	0.75	-0.24	0.42	0.07	-0.37
G86	-2.66	-2.54	-3.45	-2.96	-2.83	-3.32

Continued on next page

Table 7.5.3 – continued from previous page

	$R_i^{DD/DD}$	$R_i^{CSA/CSA}$		$R_i^{CSA/CSA}$		
Model:		(a)	(b)	(c)	(d)	(e)
Residue	[s^{-1}]	[s^{-1}]	[s^{-1}]	[s^{-1}]	[s^{-1}]	[s^{-1}]
F87	-3.95	-0.29	-1.25	-0.66	-0.84	-1.28
N88	-2.60	-0.41	-1.39	-0.76	-0.96	-1.45
T89	-3.52	-1.19	-2.15	-1.56	-1.66	-2.15
F90	-3.34	-0.29	-1.32	-0.69	-0.91	-1.38
T91	-4.83	-1.10	-2.02	-1.46	-1.54	-1.99
I92	-4.51	-1.57	-2.55	-1.91	-2.01	-2.56
P93	-0.76	—	—	—	—	—
K94	-0.69	-1.96	-2.96	-2.37	-2.38	-2.92
T95	-3.21	-0.87	-1.82	-1.24	-1.36	-1.83
D96	-2.40	—	—	—	—	—
Y97	-3.60	-1.91	-2.84	-2.21	-2.28	-2.84
D98	-1.15	-1.06	-2.03	-1.39	-1.54	-2.06
N99	-2.48	-1.13	-2.12	-1.51	-1.63	-2.13
F100	-3.90	-0.81	-1.79	-1.19	-1.33	-1.80
L101	-3.63	0.11	-0.84	-0.21	-0.48	-0.93
M102	-2.01	0.10	-0.89	-0.25	-0.52	-0.98
A103	-1.11	-0.13	-1.11	-0.49	-0.71	-1.16
H104	-2.41	-0.56	-1.53	-0.90	-1.10	-1.59
L105	-2.04	0.91	-0.09	0.57	0.20	-0.23
I106	-3.67	-0.10	-1.08	-0.45	-0.69	-1.16
N107	-3.08	0.35	-0.67	0.01	-0.32	-0.79
E108	-2.21	0.05	-0.93	-0.30	-0.56	-1.01
K109	-1.21	-0.01	-1.01	-0.35	-0.63	-1.11
D110	-1.14	—	—	—	—	—

Continued on next page

Table 7.5.3 – continued from previous page

	$R_i^{DD/DD}$	$R_i^{CSA/CSA}$		$R_i^{CSA/CSA}$		
Model:		(a)	(b)	(c)	(d)	(e)
Residue	[s^{-1}]	[s^{-1}]	[s^{-1}]	[s^{-1}]	[s^{-1}]	[s^{-1}]
G111	-0.54	-2.44	-3.39	-2.86	-2.77	-3.27
E112	-3.64	-0.45	-1.43	-0.81	-1.00	-1.47
T113	-4.22	-1.17	-2.15	-1.53	-1.66	-2.17
F114	-1.61	-0.47	-1.44	-0.83	-1.02	-1.49
Q115	-3.96	-0.38	-1.31	-0.74	-0.90	-1.32
L116	-1.71	0.09	-0.90	-0.25	-0.52	-0.99
M117	-2.95	-0.05	-1.06	-0.41	-0.67	-1.15
G118	-3.29	-1.71	-2.69	-2.14	-2.14	-2.62
L119	-3.39	0.39	-0.55	0.04	-0.22	-0.62
Y120	-3.40	0.24	-0.74	-0.10	-0.39	-0.84
G121	-3.29	-1.91	-2.88	-2.34	-2.32	-2.81
R122	-3.09	-0.42	-1.42	-0.78	-0.99	-1.47
E123	-2.46	-1.23	-2.20	-1.57	-1.70	-2.23
P124	-0.45	—	—	—	—	—
D125	-0.41	-1.23	-2.19	-1.61	-1.69	-2.17
L126	-1.54	-0.70	-1.67	-1.06	-1.23	-1.70
S127	-1.38	-1.43	-2.39	-1.80	-1.87	-2.37
S128	-1.90	—	—	—	—	—
D129	-3.41	—	—	—	—	—
I130	-3.60	-1.04	-2.06	-1.39	-1.57	-2.12
K131	-3.86	-1.13	-2.14	-1.49	-1.65	-2.18
E132	-3.28	-1.21	-2.23	-1.56	-1.72	-2.28
R133	-4.00	-1.12	-2.13	-1.47	-1.64	-2.19
F134	-3.54	-1.37	-2.39	-1.71	-1.87	-2.44

Continued on next page

Table 7.5.3 – continued from previous page

	$R_i^{DD/DD}$	$R_i^{CSA/CSA}$		$R_i^{CSA/CSA}$		
Model:		(a)	(b)	(c)	(d)	(e)
Residue	[s^{-1}]	[s^{-1}]	[s^{-1}]	[s^{-1}]	[s^{-1}]	[s^{-1}]
A135	-4.10	-0.45	-1.45	-0.79	-1.02	-1.53
Q136	-3.57	-1.70	-2.72	-2.07	-2.16	-2.73
L137	-2.80	-0.86	-1.89	-1.21	-1.42	-1.97
C138	-3.44	-1.50	-2.53	-1.86	-1.99	-2.56
E139	-4.00	-1.00	-2.00	-1.35	-1.52	-2.06
E140	-2.05	-1.47	-2.49	-1.79	-1.95	-2.55
H141	-1.17	-1.49	-2.48	-1.86	-1.95	-2.49
G142	-1.62	-2.02	-2.96	-2.43	-2.39	-2.87
I143	-4.50	-0.17	-1.17	-0.54	-0.77	-1.24
L144	-1.78	-0.07	-1.03	-0.40	-0.65	-1.11
R145	-1.42	-1.26	-2.28	-1.61	-1.77	-2.33
E146	-1.82	-1.57	-2.59	-1.94	-2.05	-2.60
N147	-1.46	-0.84	-1.81	-1.18	-1.35	-1.86
I148	-3.32	-0.51	-1.44	-0.87	-1.02	-1.46
I149	-2.77	0.19	-0.83	-0.15	-0.47	-0.96
D150	-3.57	0.34	-0.67	-0.01	-0.32	-0.77
L151	—	0.12	-0.89	-0.18	-0.51	-1.03
S152	-1.83	-1.20	-2.19	-1.56	-1.69	-2.22
N153	-0.36	—	—	—	—	—
A154	-0.71	-0.39	-1.38	-0.74	-0.96	-1.44
N155	-0.38	—	—	—	—	—
R156	-2.65	—	—	—	—	—
C157	-2.81	—	—	—	—	—

Table 7.5.4: Estimated values of $R_i^{DD/DD}$ and $R_i^{CSA/CSA}$ in holo-MUP I. The CSA tensors were obtained from measurements on Ubiquitin using five distinct models as in table 7.5.3.

	$R_i^{DD/DD}$	$R_i^{CSA/CSA}$		$R_i^{CSA/CSA}$		
Model:		(a)	(b)	(c)	(d)	(e)
Residue	$[s^{-1}]$	$[s^{-1}]$	$[s^{-1}]$	$[s^{-1}]$	$[s^{-1}]$	$[s^{-1}]$
E2	-2.35	—	—	—	—	—
A3	-2.07	-0.15	-1.43	-0.60	-0.93	-1.55
S4	-3.73	-2.24	-3.39	-2.69	-2.70	-3.33
S5	-0.95	-0.96	-2.23	-1.42	-1.65	-2.29
T6	-1.64	-2.25	-3.43	-2.76	-2.74	-3.34
G7	-5.95	-2.15	-3.34	-2.65	-2.66	-3.27
R8	-2.72	—	—	—	—	—
N9	-1.80	—	—	—	—	—
F10	-3.12	-0.58	-1.83	-1.04	-1.29	-1.90
N11	-0.94	0.13	-1.11	-0.28	-0.64	-1.25
V12	-1.27	-0.27	-1.49	-0.70	-0.99	-1.57
E13	-3.60	-1.07	-2.32	-1.55	-1.74	-2.35
K14	-3.66	-2.35	-3.60	-2.80	-2.89	-3.60
I15	-1.70	-2.69	-3.95	-3.20	-3.20	-3.89
N16	-4.90	-0.88	-2.10	-1.34	-1.54	-2.13
G17	-2.73	-2.15	-3.40	-2.66	-2.71	-3.36
E18	-4.71	-0.38	-1.54	-0.80	-1.04	-1.59
W19	-1.56	-0.87	-2.07	-1.27	-1.51	-2.14
H20	-1.71	-1.35	-2.52	-1.81	-1.92	-2.50
T21	-2.34	-0.85	-2.14	-1.31	-1.57	-2.23

Continued on next page

Table 7.5.4 – continued from previous page

	$R_i^{DD/DD}$	$R_i^{CSA/CSA}$		$R_i^{CSA/CSA}$		
Model:		(a)	(b)	(c)	(d)	(e)
Residue	[s^{-1}]	[s^{-1}]	[s^{-1}]	[s^{-1}]	[s^{-1}]	[s^{-1}]
I22	-3.62	0.59	-0.66	0.15	-0.24	-0.79
I23	-7.93	-1.39	-2.60	-1.88	-1.99	-2.58
L24	-4.62	-0.34	-1.58	-0.79	-1.07	-1.66
A25	-3.31	-0.26	-1.50	-0.71	-0.99	-1.57
S26	-3.31	-1.99	-3.24	-2.50	-2.56	-3.19
D27	0.32	0.01	-1.28	-0.49	-0.79	-1.36
K28	-1.41	-0.65	-1.83	-1.02	-1.30	-1.93
R29	-0.77	—	—	—	—	—
E30	-3.34	-1.91	-3.15	-2.38	-2.49	-3.15
K31	-1.20	-2.05	-3.29	-2.50	-2.61	-3.30
I32	-5.01	-3.14	-4.34	-3.65	-3.56	-4.22
E33	-3.60	-0.61	-1.88	-1.08	-1.33	-1.94
D34	-3.65	-1.31	-2.50	-1.74	-1.90	-2.52
N35	-1.75	—	—	—	—	—
G36	-3.74	-2.25	-3.46	-2.76	-2.76	-3.38
N37	-2.43	—	—	—	—	—
F38	-1.54	-1.46	-2.71	-1.95	-2.08	-2.71
R39	-3.55	-0.17	-1.42	-0.62	-0.92	-1.51
L40	-1.52	0.03	-1.18	-0.42	-0.71	-1.26
F41	-1.40	-0.59	-1.84	-1.03	-1.30	-1.93
L42	-1.32	0.33	-0.94	-0.07	-0.49	-1.11
E43	-1.78	-0.25	-1.49	-0.69	-0.98	-1.58
Q44	-4.79	-1.91	-3.14	-2.40	-2.47	-3.10
I45	-4.79	-0.70	-1.89	-1.14	-1.35	-1.93

Continued on next page

Table 7.5.4 – continued from previous page

	$R_i^{DD/DD}$	$R_i^{CSA/CSA}$		$R_i^{CSA/CSA}$		
Model:		(a)	(b)	(c)	(d)	(e)
Residue	[s^{-1}]	[s^{-1}]	[s^{-1}]	[s^{-1}]	[s^{-1}]	[s^{-1}]
H46	-3.48	0.23	-1.05	-0.21	-0.59	-1.20
V47	-2.87	0.10	-1.15	-0.32	-0.68	-1.27
L48	-2.77	0.49	-0.77	0.09	-0.34	-0.94
E49	-1.27	-1.18	-2.40	-1.62	-1.81	-2.45
K50	-3.27	—	—	—	—	—
S51	-3.04	-1.86	-3.09	-2.37	-2.43	-3.05
L52	-5.78	-0.56	-1.73	-1.00	-1.21	-1.75
V53	-3.62	-0.44	-1.72	-0.91	-1.19	-1.81
L54	-4.24	0.22	-1.04	-0.20	-0.58	-1.18
K55	-3.15	-0.36	-1.60	-0.82	-1.09	-1.67
F56	-3.59	-0.55	-1.76	-0.98	-1.23	-1.82
H57	-3.98	-1.71	-2.90	-2.15	-2.26	-2.90
T58	-4.28	-1.58	-2.79	-2.07	-2.16	-2.76
V59	-4.09	0.45	-0.79	-0.02	-0.35	-0.88
R60	-2.06	0.11	-1.13	-0.29	-0.66	-1.27
D61	-0.69	-0.04	-1.31	-0.46	-0.82	-1.45
E62	-0.81	-2.37	-3.53	-2.84	-2.83	-3.44
E63	-1.88	-0.86	-2.09	-1.31	-1.53	-2.14
C64	-2.52	-0.56	-1.80	-0.98	-1.26	-1.89
S65	-1.41	-1.04	-2.23	-1.48	-1.66	-2.26
E66	-2.18	-0.05	-1.27	-0.50	-0.79	-1.34
L67	-0.55	-0.44	-1.68	-0.86	-1.16	-1.78
S68	-2.37	-0.92	-2.13	-1.38	-1.56	-2.15
M69	-0.63	-0.53	-1.75	-0.99	-1.22	-1.79

Continued on next page

Table 7.5.4 – continued from previous page

	$R_i^{DD/DD}$	$R_i^{CSA/CSA}$		$R_i^{CSA/CSA}$		
Model:		(a)	(b)	(c)	(d)	(e)
Residue	[s^{-1}]	[s^{-1}]	[s^{-1}]	[s^{-1}]	[s^{-1}]	[s^{-1}]
V70	-2.67	-0.24	-1.47	-0.71	-0.97	-1.54
A71	-2.22	0.72	-0.54	0.32	-0.13	-0.71
D72	-2.71	-0.70	-1.95	-1.13	-1.40	-2.04
K73	-3.29	-0.90	-2.15	-1.35	-1.58	-2.22
T74	-1.08	-2.00	-3.25	-2.47	-2.57	-3.25
E75	-0.77	—	—	—	—	—
K76	-2.30	-0.77	-2.04	-1.22	-1.48	-2.12
A77	-3.38	0.05	-1.20	-0.35	-0.72	-1.34
G78	-0.21	—	—	—	—	—
E79	-4.69	-0.19	-1.44	-0.69	-0.94	-1.48
Y80	-3.17	0.06	-1.16	-0.36	-0.69	-1.27
S81	-3.21	-1.52	-2.73	-2.01	-2.10	-2.70
V82	-5.08	-0.92	-2.15	-1.41	-1.58	-2.16
T83	-4.21	0.52	-0.76	0.08	-0.33	-0.92
Y84	-1.71	0.34	-0.88	-0.06	-0.44	-1.03
D85	2.01	0.90	-0.33	0.49	0.06	-0.49
G86	-3.29	-3.16	-4.31	-3.68	-3.53	-4.14
F87	-4.95	-0.35	-1.54	-0.81	-1.04	-1.58
N88	-3.22	-0.29	-1.53	-0.73	-1.02	-1.62
T89	-4.29	-1.94	-3.12	-2.41	-2.46	-3.07
F90	-4.07	-0.81	-2.08	-1.34	-1.52	-2.10
T91	-5.98	-2.17	-3.29	-2.65	-2.62	-3.19
I92	-5.92	-0.76	-1.97	-1.22	-1.42	-2.01
P93	-0.99	—	—	—	—	—

Continued on next page

Table 7.5.4 – continued from previous page

	$R_i^{DD/DD}$	$R_i^{CSA/CSA}$		$R_i^{CSA/CSA}$		
Model:		(a)	(b)	(c)	(d)	(e)
Residue	[s^{-1}]	[s^{-1}]	[s^{-1}]	[s^{-1}]	[s^{-1}]	[s^{-1}]
K94	-0.94	-2.38	-3.63	-2.89	-2.92	-3.58
T95	-4.00	-1.05	-2.25	-1.50	-1.68	-2.27
D96	-2.73	-1.39	-2.72	-1.81	-2.09	-2.84
Y97	-4.46	-2.46	-3.63	-2.85	-2.92	-3.62
D98	-1.41	-1.33	-2.56	-1.77	-1.96	-2.61
N99	-3.04	-1.37	-2.62	-1.86	-2.01	-2.63
F100	-4.80	-0.95	-2.19	-1.44	-1.62	-2.21
L101	-4.59	0.16	-1.05	-0.25	-0.59	-1.16
M102	-2.33	0.10	-1.12	-0.33	-0.66	-1.23
A103	-1.32	-0.26	-1.48	-0.70	-0.98	-1.55
H104	-3.07	-0.77	-1.99	-1.20	-1.44	-2.05
L105	-2.73	1.34	0.08	0.92	0.43	-0.10
I106	-3.85	0.13	-1.09	-0.29	-0.63	-1.20
N107	-3.84	0.39	-0.89	-0.04	-0.44	-1.04
E108	-2.77	0.09	-1.15	-0.37	-0.68	-1.25
K109	-1.42	-0.08	-1.31	-0.49	-0.83	-1.44
D110	-0.40	—	—	—	—	—
G111	-0.69	-3.05	-4.24	-3.58	-3.47	-4.10
E112	-4.62	-0.64	-1.85	-1.09	-1.31	-1.90
T113	-5.11	-1.47	-2.71	-1.93	-2.08	-2.73
F114	-2.10	-0.70	-1.92	-1.15	-1.37	-1.96
Q115	-5.07	-0.53	-1.69	-0.99	-1.18	-1.71
L116	-2.01	0.13	-1.11	-0.30	-0.65	-1.23
M117	-3.67	-0.04	-1.29	-0.48	-0.81	-1.40

Continued on next page

Table 7.5.4 – continued from previous page

	$R_i^{DD/DD}$	$R_i^{CSA/CSA}$		$R_i^{CSA/CSA}$		
Model:		(a)	(b)	(c)	(d)	(e)
Residue	[s^{-1}]	[s^{-1}]	[s^{-1}]	[s^{-1}]	[s^{-1}]	[s^{-1}]
G118	-3.97	-2.18	-3.42	-2.73	-2.73	-3.33
L119	-4.47	0.44	-0.76	-0.01	-0.33	-0.83
Y120	-4.37	0.30	-0.92	-0.12	-0.48	-1.04
G121	-4.08	-2.41	-3.63	-2.95	-2.92	-3.53
R122	-3.88	-0.48	-1.74	-0.94	-1.21	-1.82
E123	-3.03	-1.58	-2.80	-2.01	-2.17	-2.83
P124	-0.55	—	—	—	—	—
D125	-0.29	-1.54	-2.75	-2.02	-2.12	-2.73
L126	-1.95	-0.92	-2.12	-1.36	-1.56	-2.16
S127	-1.67	-1.79	-3.00	-2.27	-2.35	-2.98
S128	-2.36	—	—	—	—	—
D129	-4.43	—	—	—	—	—
I130	-4.44	-1.27	-2.56	-1.71	-1.94	-2.63
K131	-4.77	-1.47	-2.74	-1.92	-2.11	-2.78
E132	-3.89	-1.51	-2.79	-1.95	-2.15	-2.85
R133	-4.81	-1.39	-2.67	-1.83	-2.04	-2.73
F134	-4.42	-1.75	-3.02	-2.18	-2.36	-3.08
A135	-5.08	-0.51	-1.79	-0.96	-1.25	-1.89
Q136	-4.44	-2.17	-3.44	-2.62	-2.74	-3.45
L137	-3.60	-1.10	-2.39	-1.54	-1.79	-2.48
C138	-4.63	-1.97	-3.24	-2.41	-2.56	-3.28
E139	-5.24	-1.28	-2.53	-1.71	-1.92	-2.60
E140	-2.66	-1.84	-3.12	-2.25	-2.45	-3.20
H141	-1.50	-1.95	-3.17	-2.40	-2.51	-3.18

Continued on next page

Table 7.5.4 – continued from previous page

	$R_i^{DD/DD}$	$R_i^{CSA/CSA}$		$R_i^{CSA/CSA}$		
Model:		(a)	(b)	(c)	(d)	(e)
Residue	[s^{-1}]	[s^{-1}]	[s^{-1}]	[s^{-1}]	[s^{-1}]	[s^{-1}]
G142	-2.10	-2.51	-3.70	-3.04	-2.98	-3.58
I143	-5.69	-0.23	-1.48	-0.69	-0.98	-1.57
L144	-2.38	-0.06	-1.27	-0.48	-0.79	-1.37
R145	-1.79	-1.63	-2.90	-2.07	-2.25	-2.95
E146	-2.23	-2.01	-3.28	-2.48	-2.60	-3.30
N147	-1.81	-1.06	-2.29	-1.49	-1.70	-2.34
I148	-4.17	-0.65	-1.82	-1.10	-1.29	-1.84
I149	-3.38	0.19	-1.08	-0.22	-0.62	-1.24
D150	-4.43	0.41	-0.84	-0.02	-0.40	-0.97
L151	-0.01	0.10	-1.17	-0.29	-0.69	-1.34
S152	-2.43	-1.59	-2.84	-2.04	-2.20	-2.87
N153	-0.26	—	—	—	—	—
A154	-1.11	-0.37	-1.62	-0.82	-1.10	-1.70
N155	0.08	—	—	—	—	—
R156	-3.07	—	—	—	—	—
C157	-3.42	—	—	—	—	—

Chapter 8

Evidence of Slow Motions by Cross-Correlated Chemical Shift Modulations in Deuterated and Protonated Proteins

The experiment presented in this chapter allows one to monitor slow motions in proteins. The method exploits the fact that slow motions induce correlated fluctuations of neighbouring nuclei, in the present case of C^{α} and C^{β} carbons. The decays of double-quantum (DQC) $C^{\alpha}_{+}C^{\beta}_{+}$ and zero-quantum coherences (ZQC) $C^{\alpha}_{+}C^{\beta}_{-}$ are used as a probe to determine which residues are affected by slow motions. The main core of the text has been published in the *Journal of Biomolecular NMR*.

8.1 Introduction

Understanding internal dynamic processes in proteins is essential for elucidating various aspects of their biological function (Wand, 2001). Protein dynamics span a wide range of time-scales, and many complementary techniques are therefore necessary to characterise these processes (Palmer et al., 1996; Kay et al., 1998; Ishima and Torchia, 2000; Palmer et al., 2001; Frueh, 2002). Our laboratory has proposed a new approach for the investigation of slow motions on microsecond to millisecond time scales, which are much slower than the overall tumbling of the molecule, which occurs on a nanosecond timescale. The method is based on the fact that slow motions can induce correlated fluctuations of the isotropic chemical shifts of selected nuclei. An interesting feature of the method is that it can provide information on the existence of correlated and anticorrelated modulations. Specifically, the method has been applied to two-spin coherences involving C^{α} and C^{β} nuclei. The difference R^{AR} between the relaxation rates of DQC($C^{\alpha}_{+}C^{\beta}_{+}$) and ZQC($C^{\alpha}_{+}C^{\beta}_{-}$) indicates the presence of cross-correlated isotropic chemical shift modulations. The effect was found to be most pronounced for residues located in loops and near the end of β-strands and α-helices (Frueh et al., 2001). The experiments have originally been applied to protonated ^{15}N,^{13}C doubly enriched ubiquitin at pH 4.5. They have now been carried out with both protonated and deuterated ^{15}N,^{13}C triply labelled ubiquitin at pH 6.7. In deuterated proteins, deuterium-carbon dipolar cross-correlated relaxation (^{13}C-^{2}H/^{13}C-^{2}H) is almost negligible, so that it cannot mask the effects of cross-correlated chemical shift modulation.

8.2 The Experiment

8.2.1 The Pulse Sequence

The pulse sequence in figure 8.2.1 has been used to measure the relaxation rates of ZQC($C^{\alpha}_{+}C^{\beta}_{-}$) and DQC($C^{\alpha}_{+}C^{\beta}_{+}$) in the deuterated sample, see the work of Frueh (Frueh et al., 2001) for the sequence used for the protonated sample. The first part of the preparation period, up to point (a), is equivalent to that described in section 7.2.1. The magnetization is then transferred from the two-spin order term $2C'_zN_z$ to a three-spin order $4C'_zN_zC^{\alpha}_z$ at point (b). At this point, the carrier is shifted from the centre of the C' frequencies, 175 ppm, to the centre of the C^{α} and C^{β} frequencies, 43 ppm. The deuterons are selectively decoupled using a WALTZ-16 sequence (Shaka et al., 1983), avoiding the evolution under the scalar coupling $^1J(C^{ali},D^{ali})$ which would lead to anti-phase terms and thus complicate the analysis of the decays. The $4C'_zN_zC^{\alpha}_z$ coherence is converted into $8C'_zN_zC^{\alpha}_xC^{\beta}_z$ at point (c) following the evolution under the scalar coupling $^1J(C^{\alpha}C^{\beta})$. The successive 90° pulse creates the term $8C'_zN_zC^{\alpha}_xC^{\beta}_y$ that is a mixture of DQC and ZQC. These two components will be separated by phase cycling the three pulses prior to the relaxation period τ_m. Chemical shift evolution of the aliphatic carbons, C^{ali}, is refocused by a RE-BURP pulse (Geen and Freeman, 1991), as a result the effective scalar coupling between the DQC (or ZQC) and the aliphatic C^{γ} carbons is not averaged out and leads to a cosine modulation of the decays, see figure 8.4.1. At the end of the relaxation period, (d), the single quantum C^{α} magnetization is restored and successively converted back into $2H^N_zN_z$ (e) simultaneously with the chemical shift evolution of the nitrogen, in a semi-

constant fashion and finally converted to amide proton single quantum coherence and recorded.

Similar procedures have been followed to record the spectra for protonated ubiquitin: where the deuterium decoupling has been substituted by proton decoupling, for more details see the work of Frueh (Frueh et al., 2001).

During the relaxation time, several cross-correlated mechanisms are active: the desired $R^{CSM/CSM}_{C^\alpha C^\beta}$, and others that cannot be refocused such as $R^{CSA/CSA}_{C^\alpha C^\beta}$ and those involving the D^α and D^β deuterons, like $R^{DD/DD}_{C^\alpha D^\alpha, C^\beta D^\alpha}$, or $R^{DD/DD}_{C^\alpha D^\beta, C^\beta D^\beta}$.

8.2.2 Materials and Methods

Protonated and uniformly deuterated ^{15}N,^{13}C-enriched ubiquitin samples were obtained commercially (VLI). The samples were dissolved in 10% D_2O/ 90% H_2O and the pH adjusted to 6.7. The data were acquired at 303 K on a Bruker DMX-600 spectrometer equipped with a quadruple resonance TBI probe with triple axes gradients. Interscan delays of 1.5 and 3 s were used for the protonated and deuterated proteins, respectively. Each matrix consisted of 64 and 512 complex points in the t_1 and t_2 dimensions.

Uncertainties for DQC and ZQC rates were obtained by nonlinear regression analysis (Mosteller and Tukey, 1977). Errors of the relaxation rates R^{AR} and the scalar couplings $^2J_{C^\alpha C^\gamma}$ and $^2J_{C^\beta C^\gamma}$ were obtained by error propagation, see tables 8.5.1 and 8.5.2. The mixing time, τ_m, was of 1.5 (twice), 2, 4, 6, 8, 10, 12, 15, 17, 20, 25, 30, 45, 53 and 60 ms. All time points have been used in the first fitting where both

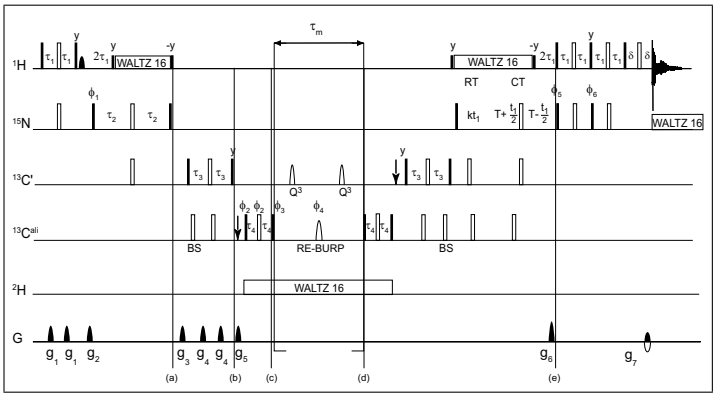

Figure 8.2.1: Pulse sequence for the measurement of C^{α}-C^{β} ZQC and DQC relaxation for a deuterated protein. Black and white rectangles indicate 90° and 180° pulses, respectively. The pulses are applied along the x axes, unless specified otherwise. The ^{1}H and ^{15}N carriers are positioned at 4.7 and 118 ppm, respectively. The ^{13}C carrier is initially at 175 ppm, then, at times indicated by arrows, moved to 43 ppm prior to the 90° pulse with phase ϕ_2 and back to 175 ppm just before the 90° pulse with phase y applied to ^{13}C'. Rectangular ^{13}C pulses have a strength of $\Delta/\sqrt{15}$ and $\Delta/\sqrt{3}$, for 90° and 180° pulses, respectively. When the carrier is positioned at 175 ppm, Δ is defined as the difference in Hz between the centres of the ^{13}C' and $^{13}C^{\alpha}$ regions, while Δ is defined as the difference between the centres of the ^{13}C' and $^{13}C^{ali}$ regions if the carrier is positioned at 43 ppm. Off-resonance pulses applied to $^{13}C^{\alpha}$ at 58 ppm are obtained by phase modulation while the carrier is at 175 ppm. Pulses introduced to compensate for Bloch-Siegert phase shifts (Emsley and Bodenhausen, 1990) are labelled with BS. During the mixing time τ_m, the ^{13}C' spins are inverted by Q^3 pulses (Emsley and Bodenhausen, 1992) of 300 ms duration. Chemical shift evolution of the MQC is refocused by a 500 ms RE-BURP pulse (Geen and Freeman, 1991) applied in the middle of the τ_m period. The delays are set to $\tau_1 = 2.7$ ms $\approx (4J_{NH})^{-1}$, $\tau_2 = 11$ ms $\approx (4J_{CN})^{-1}$, $\tau_3 = 4.3$ ms $\approx (4J_{C'C^{\alpha}})^{-1}$, $\tau_4 = 7.1$ ms $\approx (4J_{C^{\alpha}C^{\beta}})^{-1}$, and $\delta = 1.3$ ms. The ^{15}N magnetization evolves during a semi-constant time period indicated by RT (real time) and CT (constant time). Quadrature detection is obtained in t_1 by the enhanced-sensitivity pulsed field gradient method (Palmer et al., 1991; Kay et al., 1992) where for each value of t_1 separate data sets are recorded with (g_7, ϕ_6) and (-g_7, $\phi_6 + 180°$). A water flip-back pulse (Grzesiek and Bax, 1993) is used to improve water suppression. Proton, deuterium, and nitrogen decoupling are achieved by WALTZ-16 sequence (Shaka et al., 1983) with radio-frequency field-strengths of 7.3, 0.72, and 1.2 kHz, respectively. The phase cycle is ϕ_1 = 16(x, -x), ϕ_2 = 2[4(x), 4(y), 4(-x), 4(-y)], ϕ_4 = 8(x, y, -x, -y), ϕ_5 = 8[2(x), 2(-x)], ϕ_6 = 8(y, y, -y, -y). For selection of ZQC, ϕ_3 = 4(x), 4(y), 4(-x), 4(-y), 4(-x), 4(-y), 4(x), 4(y), and ϕ_{rec} = 4[4(x, -x, -x, x), 4(-x, x, x, -x)]; for selection of DQC, ϕ_3 = 2[4(x), 4(y), 4(-x), 4(-y)], and ϕ_{rec} = 4(x, -x, -x, x, -x, x, x, -x). All pulsed field gradients are of 1 ms duration with strengths g_1 = 6.5 G/cm, g_2 = 46.5 G/cm, g_3 = 27 G/cm, g_4 = - 6.5 G/cm, g_5 = -18.5 G/cm, g_6 = 40 G/cm, g_7 = 4.05 G/cm.

scalar couplings and relaxation rates have been fitted; this first interpolation gives the values of the scalar couplings that are kept constant in the second fitting where only the time points up to 30 ms have been included and only the relaxation rates allowed to vary. This procedure should minimize the influence of two-step relaxation rates.

8.3 Theory

Cross-correlated chemical shift modulation (CSM/CSM), along with cross-correlated chemical shift anisotropy (CSA/CSA) and dipole-dipole (DD/DD) mechanisms (Frueh et al., 2001) contribute to the difference R^{AR} between the autorelaxation rates of DQ and ZQ coherences in deuterated (eq. 8.3.1) and protonated (eq. 8.3.2) proteins:

$$R_D^{AR} = 2\sum_i R_{C^\alpha D^i/C^\beta D^i}^{DD/DD} + 2\sum R_{C^\alpha/C^\beta}^{CSA/CSA} + 2\sum R_{C^\alpha/C^\beta}^{CSM/CSM} \qquad (8.3.1)$$

$$R_H^{AR} = 2\sum_i R_{C^\alpha H^i/C^\beta H^i}^{DD/DD} + 2\sum R_{C^\alpha/C^\beta}^{CSA/CSA} + 2\sum R_{C^\alpha/C^\beta}^{CSM/CSM} \qquad (8.3.2)$$

Provided the static field is not too strong, the second terms are small since the CSA tensors of C^α and C^β nuclei are almost isotropic. In the dipolar terms $\sum_i R_{C^\alpha D^i/C^\beta D^i}^{DD/DD}$ and $\sum_i R_{C^\alpha H^i/C^\beta H^i}^{DD/DD}$, the summation runs over all neighbouring deuterons or protons, i = α, β_1, β_2, β_3. For a deuterated protein the dipolar contribution is reduced by a factor $(\gamma_H/\gamma_D)^2 = 16$ compared to a protonated protein. This facilitates the observation of the third term in eq. 8.3.1 which stems from cross-correlated modulations

of isotropic chemical shifts. This rate can thus be measured with enhanced precision and accuracy.

8.4 Results and Discussion

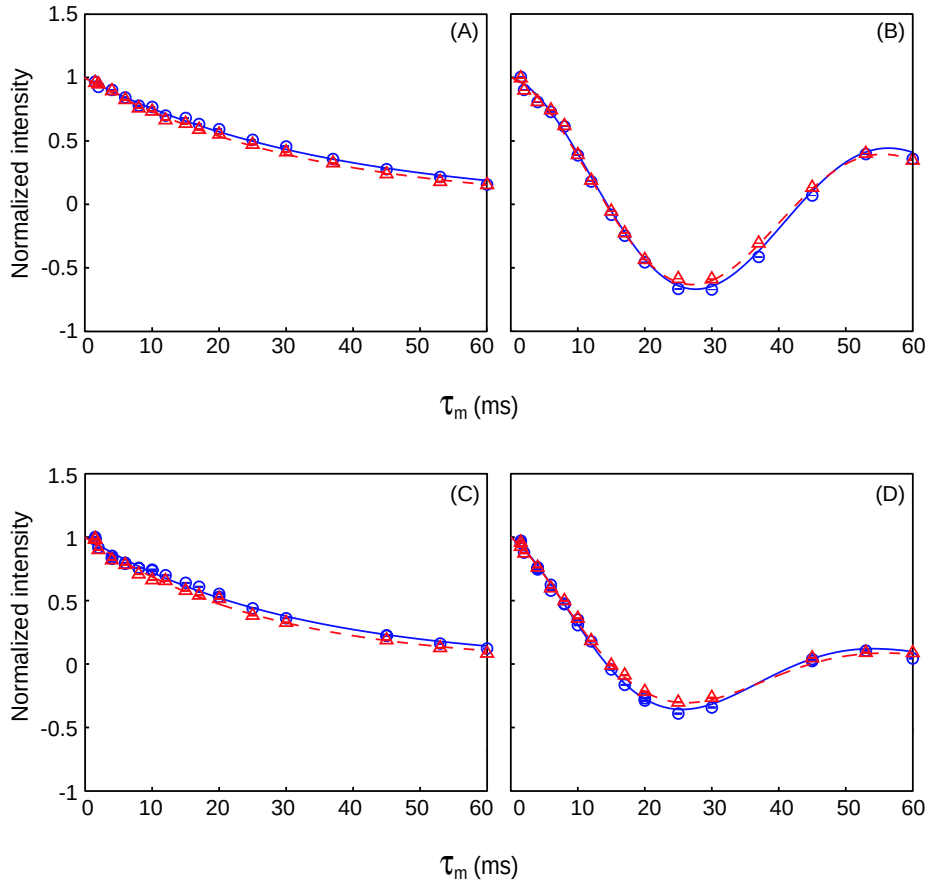

Figure 8.4.1: Examples of experimental decay curves for C^{α}-C^{β} ZQC and DQC for (A) residue Ser 65 of deuterated ubiquitin which has no aliphatic C^{γ} carbons, (B) residue Glu 16 of deuterated ubiquitin with one aliphatic C^{γ} carbon, and (C) for residue Asp 32 of protonated ubiquitin which has no aliphatic C^{γ} carbons, (D) residue Glu 16 of protonated ubiquitin with one aliphatic C^{γ} carbon. ZQC signals correspond to circles with solid lines and DQC signals to triangles with dashed lines.

Figure 8.4.1 displays some typical decay curves of DQC($C^{\alpha}_{+}C^{\beta}_{+}$) and ZQC($C^{\alpha}_{+}C^{\beta}_{-}$).

There are 60 detectable residues for deuterated and 64 for protonated ubiquitin. The additional residues are: Leu 8, Phe 45, Leu 73, and Arg 74. Four residues (Glu 24, Asn 25, Gly 47, Leu 71) were disregarded because of signal overlap in both samples. M1 was discarded in the deuterated protein due to very low signal intensity. All residues with two carbons C^{γ} and $C^{\gamma'}$ (Ile 3, Val 5, Ile 13, Val 17, Ile 23 Val 26, Ile 30, Ile 44, Ile 61, Val 70) were systematically excluded from the analysis because the effective couplings $[J(C^{\beta}\ C^{\gamma}) \pm J(C^{\alpha}\ C^{\gamma}\ )]$ and $[J(C^{\beta}\ C^{\gamma'}) \pm J(C^{\alpha}\ C^{\gamma'})]$ lead to an approximatly cosine-squared modulation of the relaxation curves. Residue Gln 31 in protonated ubiquitin had a relative error larger than 50% and was discarded. The fits were checked for variations in the apparent rates when the effective J-coupling constants were varied by ± 5 Hz from the best-fit value. Finally, 51 and 47 residues were retained for the subsequent analysis for protonated and deuterated proteins, respectively.

The carbon-deuterium DD/DD cross-correlation rates (^{13}C-^{2}H/^{13}C-^{2}H) are invariant to rotations about the dihedral angle χ_1 subtended between the two planes defined by the nuclei $C'C^{\alpha}C^{\beta}$ and $C^{\alpha}C^{\beta}C^{\gamma}$. An upper limit for the sum of the rates of eqs. 8.3.1 and 8.3.2 can be calculated for a rigid protein (i.e., with an order parameter S^2=1) that is tumbling isotropically. A lower limit can be estimated by accounting for the effects of fast isotropic internal motions with S^2 = 0.7 for $\sum_i R^{DD/DD}_{C^{\alpha}D^{\alpha}/C^{\beta}D^{\alpha}}$ and $\sum_i R^{DD/DD}_{C^{\alpha}H^{\alpha}/C^{\beta}H^{\alpha}}$ and S^2 = 0.4 for $\sum_i R^{DD/DD}_{C^{\alpha}D^{\beta}/C^{\beta}D^{\beta}}$ and $\sum_i R^{DD/DD}_{C^{\alpha}H^{\beta}/C^{\beta}H^{\beta}}$ (Lienin et al., 1998; Yang et al., 1998). In deuterated ubiquitin the ^{13}C-^{2}H/^{13}C-^{2}H dipole-dipole contributions range between 0.1 to 0.3 s^{-1}, while in protonated ubiquitin the ^{13}C-^{1}H/^{13}C-^{1}H contributions range between 5.6 to 12.0 s^{-1}.

The CSA/CSA cross-correlation rates depend on the dihedral angle χ_1 and hence are sensitive to conformational mobility. For ubiquitin with an isotropic correlation time τ_c= 4.1 ns, the CSA/CSA rates $R_{C^\alpha C^\beta}^{CSA/CSA}$ are expected to lie between 1.27 and -0.63 s^{-1}, if one assumes that the chemical shift tensors are axially symmetric and that the anisotropies are $\Delta\sigma_{max}(C^\alpha)$ = 43 ppm and $\Delta\sigma_{max}(C^\beta)$ = 45 ppm (Ye et al., 1993; Tjandra and Bax, 1997). The upper limit of $R_{C^\alpha C^\beta}^{CSA/CSA}$ = 1.27 s^{-1} is expected to be reached if the unique axes of the CSA tensors are parallel, and the lower limit of -0.63 s^{-1} if they are perpendicular.

Figure 8.4.2 shows a plot of the differences, R^{AR}, of experimental relaxation rates R^{DQC} and R^{ZQC} versus residue number for deuterated (A) and protonated (B) ubiquitin. The bands between the dashed lines correspond to contributions due to the sum of DD/DD and CSA/CSA mechanisms. The rates that lie outside the bands cannot be explained by these two mechanisms. These rates may therefore be attributed to the CSM/CSM mechanism, and the corresponding residues must be affected by slow motions. The DD/DD contributions are reduced by a factor $(\frac{\gamma_H}{\gamma_D})^2 \frac{S(S+1)}{I(I+1)}$ = 16 upon deuteration. Clearly, the contributions of the CSM/CSM mechanism are easier to determine accurately in the deuterated protein, because they are less masked by dipolar effects. As it can be seen from figure 8.4.2, 17 residues of the deuterated protein (Thr 7, Thr 9, Thr 12, Thr 14, Lys 27, Ala 28, Lys 29, Gln 31, Lys 33, Gln 41, Leu 43, Leu 50, Leu 56, Lys 63, Thr 66, Leu 69, Arg 72) but only 9 residues of the protonated protein (Lys 27, Ala 28, Lys 29, Leu 43, Ala 46, Leu 50, Tyr 59, Asn 60, His 68) reveal significant CSM/CSM contributions. Thr 12, Thr 14, Gln 41, Leu 43, Ala 46, Thr 66, His 68, Leu 69 are located in the β-sheets, Lys 27, Ala 28, Lys 29, Gln 31, Lys 33 are in

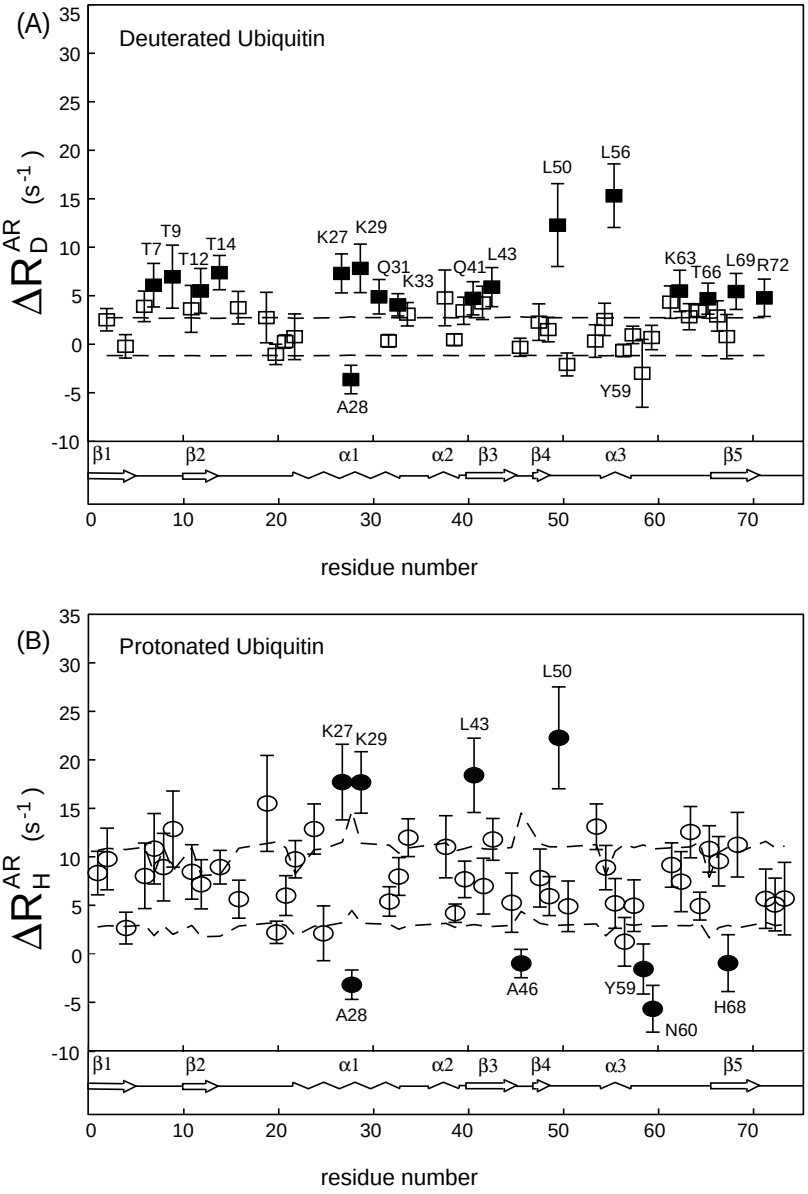

Figure 8.4.2: Relaxation rates R^{AR} corresponding to the difference between the experimental R^{DQC} and R^{ZQC} autorelaxation rates versus residue number. (A): deuterated and (B): protonated ubiquitin. The uncertainties were obtained from nonlinear regression analysis and error propagation. The band between the two dashed lines represents the range of rates that can be explained by DD/DD and CSA/CSA cross-correlated mechanisms, the former being scaled down by a factor 16 in (A), the latter being the same in both graphs. The rates that lie outside this band (filled symbols) feature cross-correlated chemical shift modulation.

the first α-helix, and Thr 7, Thr 9, Leu 50, Tyr 59, Asn 60, Lys 63, Arg 72 are located in loops or at the end of secondary structure elements. Out of 9 residues that exhibit CSM/CSM contributions in the protonated sample, five (Lys 27, Ala 28, Lys 29, Leu 43, Leu 50) also show CSM/CSM in the deuterated one. In the deuterated protein the rates of Ala 46, Tyr 59, Asn 60, and His 68 fall within the band predicted for DD/DD and CSA/CSA interactions. In the deuterated protein, twelve more residues exhibit rates that indicate CSM/CSM contributions. In the protonated protein, all of the corresponding rates, except for Gln 31, are within the band predicted for DD/DD and CSA/CSA interactions. Many residues in the first α-helix exhibit CSM/CSM contributions. This observation is in agreement with evidence for slow cooperative motions in the first α-helix (Carlomagno et al., 2000). In our previous work on protonated ubiquitin at pH 4.5 (Frueh et al., 2001) CSM/CSM contribution could be identified only for the residues in loops or at the ends of secondary structure regions. If we assume that CSA/CSA and CSM/CSM contributions of eq. 8.3.1 should be the same for protonated and deuterated ubiquitin, the differences in the experimental rates $\delta = \Delta\mathrm{R}_H^{AR} - \Delta\mathrm{R}_D^{AR}$ should give the differences of the DD/DD terms. Since the dipolar rates are almost negligible in the deuterated protein, the difference δ gives a measure of the DD/DD term $2\sum_i \mathrm{R}_{C^\alpha H^i/C^\beta H^i}^{DD/DD}$ in the protonated protein (figure 8.4.3). The two dashed lines represent the calculated upper and lower limits for the DD/DD term. The large error bars reflect the fact that δ is obtained from a difference between the two rates R^{AR}, which in turn stem from differences of DQ and ZQ autorelaxation rates. Most residues fall within the predicted band. For Ala 28, Ala 46, Leu 56, Asn 60, Ser 65, and His 68 the values are lower. This may indicate an underestimation of

the influence of dynamics on the DD/DD rates. For two residues, Gln 41 and Arg 54, the experimental values are higher than the predicted ones. At present, we do not have any explanation for these cases.

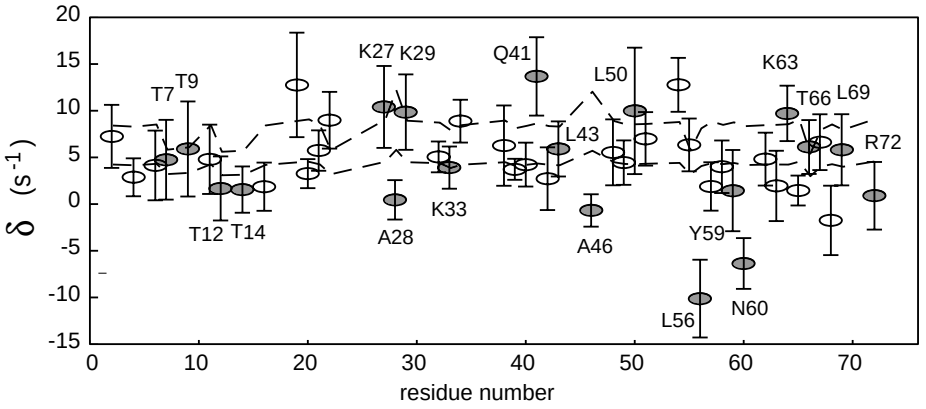

Figure 8.4.3: Differences in the experimental rates $\delta = \mathrm{R}_H^{AR}$-$\mathrm{R}_D^{AR}$ of the protonated and deuterated proteins. The band between the two dashed lines represents the expected range. The errors are obtained from the uncertainties in R^{AR} by error propagation

Depending on the details of $\mathrm{C}^{\alpha}/\mathrm{C}^{\beta}$ CSM/CSM interactions, they can exhibit either correlated or anti-correlated modulation, leading to positive or negative contributions to R^{AR}. Only Ala 28 shows anti-correlated modulations in both protonated and deuterated ubiquitin. In addition Ala 46, Tyr 59, Asn 60 and His 68 also exhibit anti-correlated CSM/CSM modulations in protonated ubiquitin. In the deuterated protein, the corresponding rates lie within the band predicted for DD/DD and CSA/CSA interactions. The results for both protonated and deuterated ubiquitin are summarized in the ribbon diagrams of figure 8.4.4, where the side chains are shown for all residues that feature significant CSM/CSM modulations.

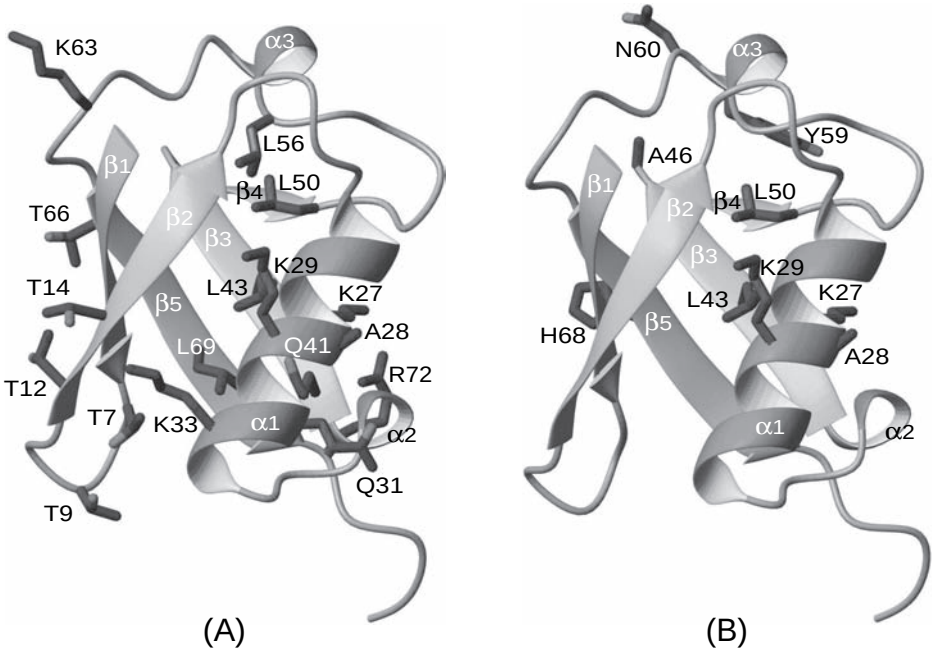

Figure 8.4.4: Ribbon representation of an X-ray structure of ubiquitin where side-chains are shown for residues that feature significant CSM/CSM contribution. (A) deuterated, (B) protonated ubiquitin.

8.5 Conclusions

Deuteration greatly reduces cross-correlated dipole-dipole contributions to the decay rates of C^{α}-C^{β} zero- and double-quantum coherences, thus facilitating the observation of subtle effects due to cross-correlated modulations of the isotropic chemical shifts. The CSM/CSM rates observed in deuterated ubiquitin reveal the presence of slow motions both in loops and in secondary structure elements. The number of amino

acids that were found to feature significant CSM/CSM effects increased from 9 to 17 upon deuteration. There is only a partial correlation of the residues that reveal modulations in the deuterated and protonated proteins. Further research is necessary before one could conclude that internal dynamics are affected by deuteration.

Table 8.5.1: Relaxation rates R_D and R_H computed from the experimentally observed decay rates R^{DQC} and R^{ZQC} as defined in eq. 8.3.1, with relative errors (303 K, 600 MHz).

Res	$R_D \pm \varepsilon_D$ [s^{-1}]	$R_H \pm \varepsilon_H$ [s^{-1}]	Res	$R_D \pm \varepsilon_D$ [s^{-1}]	$R_H \pm \varepsilon_H$ [s^{-1}]
M1	—	8.3 ± 2.2	R42	4.3 ± 1.7	7.0 ± 2.9
Q2	2.5 ± 1.2	9.8 ± 3.2	L43	5.9 ± 2.0	11.8 ± 2.2
F4	-0.2 ± 1.2	2.7 ± 1.6	F45	—	5.3 ± 3.1
K6	3.9 ± 1.6	8.0 ± 3.4	A46	-0.3 ± 0.9	-1.0 ± 1.5
T7	6.1 ± 2.2	10.8 ± 3.6	K48	2.3 ± 1.9	7.8 ± 3.0
L8	—	8.9 ± 3.5	Q49	1.5 ± 1.3	5.9 ± 2.0
T9	7.0 ± 3.2	12.9 ± 3.9	L50	12.3 ± 4.3	22.3 ± 5.3
K11	3.6 ± 2.4	8.4 ± 2.8	E51	-2.1 ± 1.2	4.9 ± 2.6
T12	5.5 ± 2.3	7.2 ± 2.5	R54	0.3 ± 1.7	13.1 ± 2.3
T14	7.4 ± 1.8	8.9 ± 1.7	T55	2.6 ± 1.7	8.9 ± 2.3
E16	3.8 ± 1.7	5.6 ± 2.0	L56	15.3 ± 3.3	5.2 ± 2.6
P19	2.7 ± 2.6	15.5 ± 5.0	S57	-0.6 ± 0.6	1.2 ± 2.5
S20	-1.0 ± 1.0	2.2 ± 1.2	D58	1.0 ± 0.9	5.0 ± 2.7
D21	0.3 ± 0.7	6.0 ± 2.1	Y59	-3.0 ± 3.5	-1.6 ± 2.6
T22	0.8 ± 2.4	9.7 ± 1.9	N60	0.7 ± 1.3	-5.7 ± 2.4
E24	—	12.9 ± 2.6	Q62	4.3 ± 1.7	9.2 ± 2.3
N25	—	2.1 ± 2.8	K63	5.5 ± 2.1	7.4 ± 3.1
K27	7.3 ± 2.0	17.7 ± 3.9	E64	2.8 ± 1.3	12.5 ± 2.6
A28	-3.6 ± 1.5	-3.2 ± 1.5	S65	3.5 ± 0.7	4.9 ± 1.4
K29	7.8 ± 2.5	17.7 ± 3.2	T66	4.7 ± 1.6	10.8 ± 2.4
Q31	4.9 ± 1.8	—	L67	2.9 ± 1.6	9.5 ± 2.5

Continued on next page

Table 8.5.1 – continued from previous page

Res	$R_D \pm \varepsilon_D$ [s^{-1}]	$R_H \pm \varepsilon_H$ [s^{-1}]	Res	$R_D \pm \varepsilon_D$ [s^{-1}]	$R_H \pm \varepsilon_H$ [s^{-1}]
D32	0.3 ± 0.6	5.4 ± 1.5	H68	0.8 ± 2.3	-1.0 ± 2.9
K33	4.1 ± 1.2	8.0 ± 1.9	L69	5.4 ± 1.9	11.3 ± 3.3
E34	3.1 ± 1.2	12.0 ± 1.9	L71	2.5 ± 1.6	—
P38	4.8 ± 2.9	11.0 ± 3.2	R72	4.8 ± 1.9	5.7 ± 3.1
D39	0.5 ± 0.6	4.2 ± 0.9	L73	—	5.1 ± 2.7
Q40	3.4 ± 1.4	7.7 ± 1.9	R74	—	5.7 ± 3.7
Q41	4.7 ± 1.7	18.4 ± 3.8			

Table 8.5.2: Coupling constants $^2J_{C^\alpha C^\gamma}$ and $^1J_{C^\beta C^\gamma}$ for deuterated and protonated ubiquitin with relative errors, as they results from the fitting of the whole experimental points (303 K and 600 MHz).

	Deuterated ubiquitin		Protonated ubiquitin	
Res	$^2J_{C^\alpha C^\gamma} \pm \varepsilon$ [Hz]	$^1J_{C^\beta C^\gamma} \pm \varepsilon$ [Hz]	$^2J_{C^\alpha C^\gamma} \pm \varepsilon$ [Hz]	$^1J_{C^\beta C^\gamma} \pm \varepsilon$ [Hz]
M1	—	—	-0.5 ± 0.4	39.4 ± 0.4
Q2	-0.2 ± 0.1	34.5 ± 0.1	-0.6 ± 0.8	35.0 ± 0.8
K6	0.1 ± 0.3	34.4 ± 0.3	-0.9 ± 0.4	33.6 ± 0.4
T7	-0.7 ± 0.3	33.1 ± 0.3	-1.1 ± 0.5	33.5 ± 0.5
L8	—	—	-1.1 ± 0.5	34.0 ± 0.5
T9	0.4 ± 0.5	39.1 ± 0.5	-2.0 ± 0.6	36.4 ± 0.6
K11	-0.2 ± 0.6	34.8 ± 0.6	-0.7 ± 0.4	34.1 ± 0.4
T12	2.6 ± 0.3	37.9 ± 0.3	1.5 ± 0.4	37.7 ± 0.4
T14	1.8 ± 0.3	37.3 ± 0.3	1.6 ± 0.3	38.9 ± 0.3
E16	0.2 ± 0.2	35.0 ± 0.2	-0.7 ± 0.3	34.2 ± 0.3
P19	-0.7 ± 0.4	30.2 ± 0.4	-1.8 ± 0.9	31.5 ± 0.9
T22	-0.9 ± 0.3	36.2 ± 0.3	-1.2 ± 0.4	37.7 ± 0.4
E24	—	—	-2.9 ± 0.9	35.6 ± 0.9
K27	-1.4 ± 0.5	34.2 ± 0.5	-3.2 ± 0.6	33.1 ± 0.6
K29	-1.0 ± 0.5	34.1 ± 0.5	-1.8 ± 0.4	34.4 ± 0.4
Q31	1.0 ± 0.3	35.8 ± 0.3	—	—
K33	-0.7 ± 0.3	34.5 ± 0.3	-1.3 ± 0.3	35.1 ± 0.3
E34	-1.0 ± 0.2	34.4 ± 0.2	-1.6 ± 0.2	34.5 ± 0.2
P38	0.1 ± 0.4	29.0 ± 0.4	-1.4 ± 0.4	29.6 ± 0.4
Q40	-0.6 ± 0.2	35.6 ± 0.2	-1.4 ± 0.3	35.1 ± 0.3

Continued on next page

Table 8.5.2 – continued from previous page

Res	Deuterated ubiquitin		Protonated ubiquitin	
	$^2J_{C^\alpha C^\gamma} \pm \varepsilon$ [Hz]	$^1J_{C^\beta C^\gamma} \pm \varepsilon$ [Hz]	$^2J_{C^\alpha C^\gamma} \pm \varepsilon$ [Hz]	$^1J_{C^\beta C^\gamma} \pm \varepsilon$ [Hz]
Q41	-0.7 ± 0.2	36.7 ± 0.2	-1.2 ± 0.5	36.6 ± 0.5
R42	-0.5 ± 0.3	34.7 ± 0.3	-0.6 ± 0.4	34.2 ± 0.4
L43	-0.8 ± 0.3	34.0 ± 0.3	-1.4 ± 0.3	35.2 ± 0.3
K48	-0.7 ± 0.3	34.1 ± 0.3	-1.2 ± 0.4	33.0 ± 0.4
Q49	0.5 ± 0.2	34.4 ± 0.2	0.0 ± 0.4	33.9 ± 0.4
L50	-0.4 ± 0.8	28.6 ± 0.8	-1.8 ± 0.8	26.0 ± 0.8
E51	-1.1 ± 0.2	34.6 ± 0.2	-1.7 ± 0.4	34.1 ± 0.4
R54	-1.7 ± 0.2	34.3 ± 0.2	-2.2 ± 0.3	34.2 ± 0.3
T55	-0.7 ± 0.2	37.0 ± 0.2	-1.5 ± 0.4	38.4 ± 0.4
L56	-0.4 ± 0.8	28.1 ± 0.8	-0.5 ± 0.5	25.9 ± 0.5
Q62	-1.3 ± 0.2	35.1 ± 0.2	-2.0 ± 0.4	34.2 ± 0.4
K63	-1.4 ± 0.5	34.0 ± 0.5	-2.4 ± 0.5	33.6 ± 0.5
E64	-0.8 ± 0.2	35.9 ± 0.2	-1.1 ± 0.4	35.4 ± 0.4
T66	3.0 ± 0.2	39.5 ± 0.2	2.0 ± 0.4	39.2 ± 0.4
L67	-1.5 ± 0.2	34.6 ± 0.2	-2.0 ± 0.3	34.1 ± 0.3
L69	0.7 ± 0.2	33.8 ± 0.2	0.4 ± 0.4	33.5 ± 0.4
L71	-1.1 ± 0.2	33.9 ± 0.2	—	—
R72	0.1 ± 0.3	34.9 ± 0.3	-0.3 ± 0.4	34.6 ± 0.4
L73	—	—	-1.6 ± 0.3	33.9 ± 0.3
R74	—	—	-1.3 ± 0.5	34.4 ± 0.5

Chapter 9

Appendix

k	q	F_k^q	A_k^q
0	0	$\frac{1}{\sqrt{4\pi}}$	$-\frac{1}{\sqrt{3}}\left[I_z S_z + \frac{1}{2}\left(I_+ S_- + I_- S_+\right)\right]$
1	0	$\sqrt{\frac{3}{4\pi}}\, cos\theta$	I_z
1	1	$\mp\sqrt{\frac{3}{8\pi}}\, sin\theta\, e^{\pm i\phi}$	$\mp\frac{1}{\sqrt{2}} I_\pm$
2	0	$\sqrt{\frac{5}{16\pi}}\, (3cos^2\theta - 1)$	$\frac{1}{\sqrt{6}}\left[2I_z S_z - \frac{1}{2}\left(I_+ S_- + I_- S_+\right)\right]$
2	1	$\mp\sqrt{\frac{15}{8\pi}}\, sin\theta\, cos\theta\, e^{\pm i\phi}$	$\mp\frac{1}{2}\left[I_z S_\pm + I_\pm S_z\right]$
2	2	$\sqrt{\frac{15}{32\pi}}\, sin^2\theta\, e^{\pm 2i\phi}$	$\frac{1}{2} I_\pm S_\pm$

Table 9.1: Spherical harmonics and irreducible tensor operators, the latter having been constructed with respect to an appropriate choice of tensors operators of rank 1 (Cohen-Tannoudji et al., 1992; Korzhnev et al., 2001).

Order	Modified Second-Order Spherical Harmonic Functions	
q	Y_2^q	Y_2^{*q}
0	$\frac{1}{2}(3cos^2\theta - 1)$	$\frac{1}{2}(3cos^2\theta - 1)$
1	$\sqrt{\frac{3}{2}}\, cos\theta\, sin\theta\, e^{i\phi}$	$\sqrt{\frac{3}{2}}\, cos\theta\, sin\theta\, e^{-i\phi}$
2	$\sqrt{\frac{3}{8}}\, sin^2\theta\, e^{i2\phi}$	$\sqrt{\frac{3}{8}}\, sin^2\theta\, e^{-i2\phi}$

Table 9.2: Modified spherical harmonic functions of second rank, $\tilde{\mathrm{Y}}_2^q = \sqrt{\frac{4\pi}{5}}\mathrm{Y}_2^q$, Cavanagh et al. (1996).

$\mathbf{E} = \begin{bmatrix} 1 & 0 \\ 0 & 1 \end{bmatrix}$	$\mathbf{I}_z = \frac{1}{2}\begin{bmatrix} 1 & 0 \\ 0 & -1 \end{bmatrix}$
$\mathbf{I}_x = \frac{1}{2}\begin{bmatrix} 0 & 1 \\ 1 & 0 \end{bmatrix}$	$\mathbf{I}_y = \frac{i}{2}\begin{bmatrix} 0 & -1 \\ 1 & 0 \end{bmatrix}$

Table 9.3: Products operators in the cartesian basis for a spin system.

$[A, B] = AB - BA$	$[AB, C] = A\,[B, C] + [A, C]\,B$
$[\mathrm{I}_x, \mathrm{I}_y] = i\mathrm{I}_z$	
$[\mathrm{I}_+, \mathrm{I}_x] = \mathrm{I}_z$	$[\mathrm{I}_-, \mathrm{I}_x] = -\mathrm{I}_z$
$[\mathrm{I}_+, \mathrm{I}_y] = i\mathrm{I}_z$	$[\mathrm{I}_-, \mathrm{I}_y] = i\mathrm{I}_z$
$[\mathrm{I}_z, \mathrm{I}_+] = \mathrm{I}_+$	$[\mathrm{I}_z, \mathrm{I}_-] = -\mathrm{I}_-$
$[\mathrm{I}_+, \mathrm{I}_-] = 2\mathrm{I}_z$	
$[\mathrm{I}_+, \mathrm{I}_\alpha] = -\mathrm{I}_+$	$[\mathrm{I}_-, \mathrm{I}_\alpha] = \mathrm{I}_-$
$[\mathrm{I}_+, \mathrm{I}_\beta] = \mathrm{I}_+$	$[\mathrm{I}_-, \mathrm{I}_\beta] = -\mathrm{I}_-$

Table 9.4: Commutator relationships for a spin-$\frac{1}{2}$.

$\mathrm{I}_+\mathrm{I}_- = \mathrm{I}_\alpha = \frac{1}{2}E + \mathrm{I}_z$	$\mathrm{I}_-\mathrm{I}_+ = \mathrm{I}_\beta = \frac{1}{2}E - \mathrm{I}_z$
$\mathrm{I}_z\mathrm{I}_\alpha = \mathrm{I}_\alpha\mathrm{I}_z = \frac{1}{2}\mathrm{I}_\alpha$	$\mathrm{I}_z\mathrm{I}_\beta = \mathrm{I}_\beta\mathrm{I}_z = \frac{1}{2}\mathrm{I}_\beta$
$\mathrm{I}_\alpha\mathrm{I}_\alpha = \mathrm{I}_\alpha$	$\mathrm{I}_\beta\mathrm{I}_\beta = \mathrm{I}_\beta$
$\mathrm{I}_+\mathrm{I}_\alpha = 0$	$\mathrm{I}_\alpha\mathrm{I}_+ = \mathrm{I}_+$
$\mathrm{I}_-\mathrm{I}_\alpha = \mathrm{I}_-$	$\mathrm{I}_\alpha\mathrm{I}_- = 0$
$\mathrm{I}_+\mathrm{I}_\beta = \mathrm{I}_+$	$\mathrm{I}_\beta\mathrm{I} = 0$
$\mathrm{I}_-\mathrm{I}_\beta = 0$	$\mathrm{I}_\beta\mathrm{I}_- = \mathrm{I}_-$
$\mathrm{I}_+\mathrm{I}_z = -\frac{1}{2}\mathrm{I}_+$	$\mathrm{I}_z\mathrm{I}_+ = \frac{1}{2}\mathrm{I}_+$
$\mathrm{I}_+\mathrm{I}_x = \frac{1}{2}\mathrm{I}_\alpha$	$\mathrm{I}_x\mathrm{I}_+ = \frac{1}{2}\mathrm{I}_\beta$
$\mathrm{I}_+\mathrm{I}_y = \frac{1}{2}i\mathrm{I}_\alpha$	$\mathrm{I}_y\mathrm{I}_+ = \frac{1}{2}i\mathrm{I}_\beta$
$\mathrm{I}_-\mathrm{I}_z = \frac{1}{2}\mathrm{I}_-$	$\mathrm{I}_z\mathrm{I}_- = -\frac{1}{2}\mathrm{I}_-$
$\mathrm{I}_-\mathrm{I}_x = \frac{1}{2}\mathrm{I}_\beta$	$\mathrm{I}_x\mathrm{I}_- = \frac{1}{2}\mathrm{I}_\alpha$
$\mathrm{I}_-\mathrm{I}_y = -\frac{1}{2}i\mathrm{I}_\beta$	$\mathrm{I}_y\mathrm{I}_- = -\frac{1}{2}i\mathrm{I}_\alpha$
$\mathrm{I}_-\mathrm{I}_- = \mathrm{I}_+\mathrm{I}_+ = 0$	$\mathrm{I}_\alpha\mathrm{I}_\alpha = \mathrm{I}_\beta\mathrm{I}_\beta = 0$
$\mathrm{I}_z\mathrm{I}_x = \frac{1}{2}i\mathrm{I}_y$	$\mathrm{I}_z\mathrm{I}_y = -\frac{1}{2}i\mathrm{I}_x$

Table 9.5: Multiplication properties for a spin-$\frac{1}{2}$.

Bibliography

F. Abbate, L. Franzoni, F. Löhr, C. Lücke, E. Ferrari, R. T. Sorbi, H. Rüterjans and A. Spisni: 'Letter to the editor: Complete ^{1}H, ^{15}N and ^{13}C assignment of a recombiant mouse urinary protein'. *J. Biomol. NMR* **15**, 187–188, 1999.

A. Abragam: *The Principles of Nuclear Magnetism*. Oxford University Press, 1961.

W. D. Arnold and E. Oldfield: 'The chemical nature of hydrogen bonding in proteins via NMR: J- couplings, chemical shifts, and AIM theory'. *J. Am. Chem. Soc.* **122**, 12835–12841, 2000.

P. W. Atkins: *Physical Chemistry*. Oxford University Press, 5 edition, 1994.

J. Beynon, Robert and L. Hurst, Jane: 'Urinary proteins and the modulation of chemical scents in mice and rats'. *Peptides* **25**, 1553–1563, 2004.

R. J. Beynon, C. Veggerby, C. E. Payne, D. H. L. Robertson, S. J. Gaskell, R. E. Humphries and J. L. Hurst: 'Polymorphism in Major Urinary Proteins: Molecular Heterogeneity in a Wild Mouse Population'. *J. Chem. Ecol.* **28**, 1429–1446, 2002.

R. J. Bingham, J. B. C. Findlay, S.-Y. Hsieh, A. P. Kalverda, A. Kjellberg, C. Perazzolo, S. E. V. Phillips, K. Seshadri, C. H. Trinh, W. B. Turnbull, G. Bodenhausen and S. W. Homans: 'Thermodynamics of Binding of 2-Methoxy-3-isopropylpyrazine and 2-Methoxy-3-isobutylpyrazine to the Major Urinary Protein'. *J. Am. Chem. Soc.* **126**, 1675 – 1681, 2004.

M. J. Blandamer: *Biocalorimetry: Applications of Calorimetry in the Biological Sciences*. Wiley, 1998.

F. Bloch: 'Nuclear Induction'. *Phys. Rev.* **70**, 460–474, 1946.

N. Bloembergen, E. M. Purcell and P. R. V.: 'Relaxation Effects in Nuclear Magnetic Resonance Absorption'. *Phys. Rev.* **73**, 679–712, 1948.

D. Bytchenkoff, P. Pelupessy and G. Bodenhausen: 'Anisotropic Local Motions and Location of Amide Protons in Proteins'. *J. Am. Chem. Soc.* **127**, 5180–5185, 2005.

T. Carlomagno, M. Maurer, M. Hennig and C. Griesinger: 'Ubiquitin Backbone Motion Studied via NH^N-C'C^a Dipolar-Dipolar and C'-C'C^a/NH^N CSA-Dipolar Cross-Correlated Relaxation'. *J. Am. Chem. Soc.* **122**, 5105–5113, 2000.

J. P. Carver and R. E. Richards: 'A General Two-Site Solution for the Chemical Exchange Produced Dependence of T_2 Upon the Carr-Purcell Pulse Separation'. *J. Magn. Res.* **6**, 89–105, 1972.

J. Cavanagh, W. J. Fairbrother, A. G. Palmer and N. J. Skelton: *Protein NMR Spectroscopy Principles and Practice*. Academic Press, San Diego, 1996.

C. Cohen-Tannoudji, B. Diu and F. Laloë: *Quantum Mechanics*. John Wiley & Sons, Ltd, 2nd ed. edition, 1992.

F. Delaglio, S. Grzesiek, G. W. Vuister, G. Zhu, J. Pfeifer and A. Bax: 'Nmrpipe - a Multidimensional Spectral Processing System Based On Unix Pipes'. *J. Biomol. NMR* **6**, 277–293, 1995.

J. Dittmer and G. Bodenhausen: 'Evidence for slow motion in proteins by multiple refocusing of heteronuclear nitrogen/proton multiple quantum coherences in NMR'. *J. Am. Chem. Soc.* **126**, 1314–1315, 2004.

L. Emsley and G. Bodenhausen: 'Phase Shifts Induced by Transient Bloch-Siegert Effects in NMR'. *Chem. Phys. Lett.* **168**, 297–303, 1990.

L. Emsley and G. Bodenhausen: 'Optimization of shaped selective pulses for NMR using a quaternion description of their overall propagators'. *J. Magn. Reson.* **97**, 135–148, 1992.

R. R. Ernst, G. Bodenhausen and A. Wokaun: *Principles of Nuclear Magnetic Resonance in One and Two Dimensions*. Clarendon Press, Oxford, 1987.

D. R. Flower: 'The lipocalin protein family: structural and function'. *Biochem. J.* **318**, 1–14, 1996.

D. R. Flower, A. C. T. North and C. E. Sansom: 'The lipocalin protein family: structural and sequence overview'. *Biochimica et Biophysica Acta* **1482**, 9–24, 2000.

D. Frueh: 'Internal motions in proteins and interference effects in nuclear magnetic resonance'. *Progr. NMR Spectrosc.* **41**, 305–324, 2002.

D. Frueh, J. R. Tolman, G. Bodenhausen and C. Zwahlen: 'Cross-correlated chemical shift modulation: A signature of slow internal motions in proteins'. *J. Am. Chem. Soc.* **123**, 4810–4816, 2001.

H. Geen and R. Freeman: 'Band-selective radiofrequency pulses'. *J. Magn. Reson.* **93**, 93–141, 1991.

M. Goldman: 'Interference Effects in the Relaxation of a Pair of Unlike Spin-1/2 Nuclei'. *J. Magn. Reson.* **60**, 437–452, 1984.

M. Goldman: *Quantum Description of High-Resolution NMR in Liquids*, volume 1. Oxford University Press, Oxford, 1998.

S. Grzesiek and A. Bax: 'Correlating Backbone Amide and Side-Chain Resonances In Larger Proteins By Multiple Relayed Triple Resonance NMR'. *J. Am. Chem. Soc.* **114**, 6291–6293, 1992.

S. Grzesiek and A. Bax: 'The importance of not saturating H_2O in protein NMR. Application to sensitivity enhancement and NOE measurements'. *J. Am. Chem. Soc.* **115**, 12593–12594, 1993.

G. A. Holdgate: 'Making cool drugs hot: Isothermal titration calorimetry as a tool to study binding energetics'. *BioTechniques* **31**, 164–184, 2001.

D. D. Hu and M. R. Eftink: 'Thermodynamic studies of the interaction of trp aporepressor with tryptophan analogs.' *Biophys. Chem.* **49**, 233–239, 1994.

P. S. Hubbard: 'Some Properties of Correlation Functions of Irreducible Tensor Operators'. *Phys. Rev.* **180**, 319–326, 1969.

R. Ishima and D. A. Torchia: 'Estimating the Time Scale of Chemical Exchange of Proteins from Measurments of Transverse Relaxation Rates in Solution'. *J. Biomolec. NMR* **14**, 369–372, 1999.

R. Ishima and D. A. Torchia: 'Protein dynamics from NMR'. *Nature Str. Biol.* **7**, 740–743, 2000.

M. Karplus: 'Contact Electron-Spin Coupling of Nuclear Magnetic Moments'. *J. Chem. Phys.* **30**, 11–15, 1959.

L. E. Kay, P. Keifer and T. Saarinen: 'Pure Absorption Gradient Enhanced Heteronuclear Single Quantum Correlation Spectroscopy with Improved Sensitivity'. *J. Am. Chem. Soc.* **114**, 10663–10665, 1992.

L. E. Kay, D. R. Muhandiram, G. Wolf, S. E. Shoelson and J. D. Forman-Kay: 'Correlation between binding and dynamics at SH2 domain interfaces'. *Nature Str. Biol.* **5**, 156–163, 1998.

R. G. Khalifah, F. Zhang, J. S. Parr and E. S. Rowe: 'Thermodynamic of binding of the CO_2-competitive inhibitor imidazole and related compounds to human carbonic anhydrase I: an isothermal titration calorimetry approach to study weak binding by displacement with strong inhibitors.' *Biochemistry* **32**, 3058–3066, 1993.

R. Koradi, M. Billeter and K. Wüthrich: 'MOLMOL: A program for display and analysis of macromolecular structures'. *J. Mol. Graph.* **14**, 51, 1996.

D. M. Korzhnev, M. Billeter, A. S. Arseniev and V. Y. Orekhov: 'NMR Studies of Brownian tumbling and internal motions in proteins'. *Prog. NMR Spectrosc.* **38**, 197–266, 2001.

P. J. Kraulis: 'Protein three-dimensional structure determination and sequence-specific assignment of ^{13}C and ^{15}N-separated NOE data. A novel real-space ab initio approach'. *J. Mol. Biol.* **243**, 696–718, 1994.

P. Kuser, L. Franzoni, E. Ferrari, A. Spisni and I. Polikarpov: 'The X-ray structure of a recombinant major urinary protein at 1.75 resolution. A comparative study of X-ray and NMR-derived structures'. *Acta Cryst.* **D57**, 1863–1869, 2001.

S. F. Lienin, T. Bremi, B. Brutscher, R. Brüschweiler and R. R. Ernst: 'Anisotropic Intramolecular Backbone Dynamics of Ubiquitin Characterized by NMR Relaxation and MD Computer Simulation'. *J. Am. Chem. Soc.* **120**, 9870–9879, 1998.

T. M. Logan, E. T. Olejniczak, R. X. Xu and S. W. Fesik: 'A General Method for Assigning NMR Spectra of Denatured Proteins Using 3D HC(CO)NH-TOCSY Triple Resonance Experiments'. *J. Biomolec. NMR* **3**, 225, 1993.

K. Loth, P. Pelupessy and G. Bodenhausen: 'Chemical Shift Anisotropy Tensors of Carbonyl, Nitrogen, and Amide Proton Nuclei in Proteins through Cross-Correlated Relaxation in NMR Spectroscopy'. *J. Am. Chem. Soc.* **127**, 6062–6068, 2005.

C. Lücke, L. Franzoni, F. Abbate, F. Löhr, E. Ferrari, R. T. Sorbi, H. Rüterjans and A. Spisni: 'Solution structure of a recombiant mouse urinary protein'. *Eur. J. Biochem.* **266**, 1210–1218, 1999.

Z. Luz and S. Meiboom: 'Nuclear Magnetic Resonance Study of the Protolysis of Trimethylammonium Ion in Aqueous Solution — Order of the Reaction with Respect to Solvent'. *J. Chem. Phys.* **39**, 366–370, 1963.

A. M. Mandel, M. Akke and A. G. Palmer: 'Dynamics of ribonuclease H: Temperature dependence of motions on multiple time scales'. *Biochemistry* **35**, 16009–16023, 1996.

O. Millet, J. P. Loria, C. D. Kroenke, M. Pons and A. G. Palmer: 'The Static Magnetic Field Dependence of Chemical Exchange Linebroadening Defines the NMR Chemical Shift Time Scale'. *J. Am. Chem. Soc.* **122**, 2867–2877, 2000.

F. Mosteller and J. W. Tukey: *Analysis and Regression: A Second Course in Statistics*. Addison-Wisley, Reading, M.A., 1st ed. edition, 1977.

R. O'Brian, J. E. Ladbury and B. Z. Chowdhry: *Protein-Ligand Interactions: Hydrodynamics and Calorimetry. A Practical Approach*. Oxford University Press: Oxford, 2001.

C. Pace, B. Shirley, M. McNutt and K. Gajiwala: 'Forces contributing to the conformational stability of proteins'. *FASEB J.* **10**, 75–83, 1996.

A. G. Palmer, J. Cavanagh, P. E. Wright and M. Rance: 'Sensitivity Improvement in Proton-Detected Two-Dimensional Heteronuclear Correlation NMR Spectroscopy'. *J. Magn. Reson.* **93**, 151–170, 1991.

A. G. Palmer, C. D. Kroenke and J. P. Loria: 'Nuclear magnetic resonance methods for quantifying microsecond-to-millisecond motions in biological macromolecules'. *Methods Enzymol.* **339**, 204–238, 2001.

A. G. Palmer, J. Williams and A. McDermott: 'Nuclear magnetic resonance studies of biopolymer dynamics'. *J. Phys. Chem.* **100**, 13293–13310, 1996.

E. M. Purcell, H. C. Torrey and P. R. V.: 'Resonance Absorption by Nuclear Magnetic Moments in a Solid'. *Phys. Rev.* **69**, 37?38, 1946.

A. G. Redfield: 'The Theory of Relaxation Processes'. *Adv. Magn. Reson.* (pages 1–32), 1965.

A. J. Shaka, J. Keeler, T. Frenkiel and R. Freeman: 'An improved sequence for broadband decoupling: WALTZ-16'. *J. Magn. Reson.* **52**, 335–338, 1983.

A. Sivaprasadarao and J. B. C. Findlay: 'Structure-Function Studies on Human Retinol-Binding Protein Using Site-Directed Mutagenesis'. *Biochem. J.* **300**, 437–442, 1994.

O. W. Sørensen, M. Rance and R. R. Ernst: 'Z-Filters for Purging Phase- or Multiplet-Distorted Spectra'. *J. Magn. Reson.* **56**, 527–534, 1984.

N. Tjandra and A. Bax: 'Large Variations in $^{13}C^{\alpha}$ Chemical Shift Anisotropy in Proteins Correlate with Secondary Structure'. *J. Am. Chem. Soc.* **119**, 9576–9577, 1997.

N. Tjandra, S. Feller, R. Pastor and A. Bax: 'Rotational Diffusion Anisotropy of Human Ubiquitin from ^{15}N NMR Relaxation'. *J. Am. Chem. Soc.* **117**, 12562–12566, 1995.

M. Tollinger, N. R. Skrynnikov, F. A. A. Mulder, J. D. Forman-Kay and L. E. Kay: 'Slow Dynamics in Folded and Unfolded States of an SH3 Domain'. *J. Am. Chem. Soc.* **123**, 11341–11352, 2001.

W. B. Turnbull and A. H. Daranas: 'On the Value of c: Can Low Affinity Systems Be Studied by Isothermal Titration Calorimetry?' *J. Am. Chem. Soc.* **125**, 14859 – 14866, 2003.

L. Žídek, M. V. Novotny and M. J. Stone: 'Increased protein backbone conformational entropy upon hydrophobic ligand binding'. *Nature Str. Biol.* **6**, 1118–1121, 1999.

A. J. Wand: 'Dynamic activation of protein function: A view emerging from NMR spectroscopy'. *Nat. Struct. Biol.* **8**, 926–931, 2001.

R. K. Wangsness and F. Bloch: 'The Dynamical Theory of Nuclear Induction'. *Phys. Rev.* **89**, 728–739, 1953.

L. G. Werbelow and D. M. Grant: 'Intramolecular dipolar relaxation in multispin systems'. *Adv. Magn. Reson.* **9**, 189–299, 1977.

T. Wiseman, S. Williston, J. F. Brands and L. N. Lin: 'Rapid Measurement of binding Constants and Heats of Binding Using a New Titration Calorimeter'. *Anal. Biochem.* **179**, 131–137, 1989.

J. Wist, C. Perazzolo and G. Bodenhausen: 'Slow Motion in Non-deuterated Proteins: Correlated Chemical Shift Modulations'. *Appl. Magn. Reson.* **29**, 251–259, 2005.

D. Yang, A. Mittermaier, Y. K. Mok and L. E. Kay: 'A study of protein side-chain dynamics from new ^{2}H auto-correlation and ^{13}C cross-correlation NMR experiments: application to the N-terminal SH3 domain from drk'. *J. Mol. Biol.* **276**, 939–954, 1998.

C. Ye, F. Riqiang, J. Hu, L. Hou and S. Ding: 'Carbon-13 chemical shift anisotropies of solid amino acids'. *Magn. Reson. Chem.* **31**, 699–704, 1993.

K. Yoshinori, M. Totsuka, A. Ametani and S. Kaminogawa: 'Tryptophan-19 of β-lactoglobulin, the only residue completely conserved in the lipocalin superfamily, is not essential for binding retinol, but relevant to stabilizing bound retinol and maintaining its structure'. *Biochim. Biophys. Acta* **1207**, 58–67, 1994.

Curriculum Vitæ

Chiara Perazzolo
Date of birth: 30th of April, 1975
Place of birth: San Bonifacio, Verona, Italy
Nationality: Italian

Education

06/2002–present	Preparation of a Ph.D. in Nuclear Magnetic Resonance (NMR) applied to biomolecules under the supervision of Prof. G. Bodenhausen at the École Polytechnique Fédérale de Lausanne, Switzerland.
08/1994–07/2000	Laurea in Chemistry 110/110 *cum laude* at the University of Padova, Italy.
	Thesis: *Application of Diffusion Based NMR Techniques in the Study of Drug-Receptor Interactions.*
	Supervisor: Prof. S. Mammi, S. Davalli.
09/1999–12/1999	Erasmus Fellowship, Trondheim University (Norway), under supervision of Prof. J. Bakke.
09/1989–06/1994	High School Graduate at ITIS G. Silva- Legnago (Italy).

Work

10/2003	Organisation of the *15th Swiss Symposium on NMR Spectroscopy*
	Lausanne, Switzerland.
05/2001–05/2002	Fellowship in NMR and Molecular Modelling at the Goodman's laboratory at University of California, San Diego.
08/2000-03/2001	Junior Researcher, Spectroscopy Lab. Computational, Analytical and Structural Sciences
	GlaxoSmithKline Research Centre.
1993–1999	Several periods as waitress in restaurant/pizzeria.

Languages

- Italian: mother tongue
- English: fluent
- French: fluent

Publications

1. *Effect of Protein-Pheromone Complexation on Correlated Chemical Shift Modulations*
   C. Perazzolo, J. Wist, K. Loth, L. Poggi, S. W. Homans and G. Bodenhausen
   J. Biomol. NMR **33**: 233-242, 2005.

2. *Slow Motions in Non-Deuterated Proteins: Concerted Chemical Shift Modulations of Backbone Nuclei*
   J. Wist, C. Perazzolo and G. Bodenhausen
   Appl. Magn. Reson. **29**: 251-259, 2005.

3. *Thermodynamics of Binding of 2-Methoxy-3-isopropylpyrazine and 2-Methoxy-3-isobutylpyrazine to the Major Urinary Protein*
   R. J. Bingham, J. B. C. Findlay, S.-Y. Hsieh, A. P. Kalverda, A. Kjellberg, C. Perazzolo, S. E. V. Phillips, K. Seshadri, C. H. Trinh, W. B. Turnbull, G. Bodenhausen, and S. W. Homans
   J. Am. Chem. Soc. **126**: 1675-1681, 2004.

4. *Evidence of Slow Motions by Cross-Correlated Chemical Shift Modulation in Deuterated and Protonated Proteins*
   L. Vugmeyster, C. Perazzolo, J. Wist, D. Frueh and G. Bodenhausen
   Journal of Biomolecular NMR **28**: 173-177, 2004.

Conferences

1. *NMR: a tool for Biology VII*
   Pasteur Institute, Paris, France, January 30-February 1, 2006.

2. *16th Swiss Symposium on NMR Spectroscopy*
   Bern, Switzerland, October 21, 2005.

3. *Swiss Chemical Society - Fall Meeting 2005*
   École Polytechnique Fédérale de Lausanne, Switzerland, October 13, 2005.
   Oral Presentation: **Effects of Protein-Pheromone Complexation on Correlated Chemical Shift Modulations**

4. *2nd European School on Solid State NMR and 3rd International Summer School*,
   Organiser: The Working Party on NMR-Spectroscopy (AG-NMR) of the Austrian Chemical Society (GÖCH) and The Institute of Organic Chemistry, Johannes Kepler University, Linz, Austria, September 18-23, 2005.
   Course title: **Solid State NMR for Liquid State NMR Spectroscopists**

5. *Protein Science Ph.D. School*,
   Organiser: Protein Science School of the University of Copenhagen, June 20-July 1.
   Course title: **Protein NMR. Recording, Structure Calculation and Evaluation**
   Equivalent to 10 ECTS points.

6. *17th EENC/ 32th AMPERE*
   Lille, France, September 6-11, 2004.
   Poster title: **Temperature dependence of cross-correlation: a probe for protein-ligand interactions**

7. *NMR: a tool for Biology VI*
   Pasteur Institute, Paris, France, February 2-4, 2004.

8. *15th Swiss Symposium on NMR Spectroscopy*
   Lausanne, Switzerland, October 3, 2003.

9. *44th ENC*,
   Savannah, Georgia, USA, March 30, April 4, 2003.
   Poster title: **Investigation of Slow Motion by Cross-Correlated Chemical Shift Modulation in Deuterated Human Ubiquitin**

10. *Merrifield Satellite Symposium*,
    San Diego, CA, USA, June 15, 2001.

11. *2nd International Peptide Symposium and 17th American Peptide Symposium*,
    San Diego, CA, USA, June 9-14, 2001.